Electronic Supporting Information

Reactions of $[(dmpe)_2MnH(C_2H_4)]$: synthesis and characterization of manganese(I) borohydride and hydride complexes

Jeffrey S. Price,[a] Declan M. DeJordy,[a] David J. H. Emslie,*[a] and James F. Britten[b]

a. Department of Chemistry, McMaster University, 1280 Main Street West, Hamilton, Ontario, L8S 4M1, Canada. Fax: (905)-522-2509; Tel: (905)-525-9140 x23307
b. McMaster Analytical X-ray Diffraction Facility (MAX), McMaster University, 1280 Main Street West, Hamilton, Ontario, L8S 4M1.

E-mail: emslied@mcmaster.ca

Website: https://emsliegroup.mcmaster.ca/

The supplemental file *Cartesian_coordinates_for_calculated_structures.xyz* contains the computed Cartesian coordinates of all of the molecules reported in this study. The file may be opened as a text file to read the coordinates, or opened directly by a structure visualization program such as Mercury (version 3.3 or later, http://www.ccdc.cam.ac.uk/pages/Home.aspx).

Contents **Pages**

Computational Methods····S2
Figures Showing Calculated Structures with AIM Bond Paths and Critical Points····S3
Figures Showing Superimposed Calculated and X-ray Structures····S3
Tables of Selected Calculated and Crystallographically Determined Bond Lengths and Angles, Mayer Bond Orders, and AIM Properties····S4-S5
Tables of Crystal Data and Crystal Structure Refinement····S6-S12
Selected NMR Spectra for Complexes **3**-**8**····S13-S48
Selected NMR Spectra for Deuteration of $[(dmpe)_2Mn(\mu\text{-}H)_2BH_2]$ (**3**)····S49-S50
Experimental Details and Selected NMR Spectra of Intermediates in the Reactions of $[(dmpe)_2MnH(C_2H_4)]$ (**1**) with 9-BBN or $HBMes_2$····S51
Experimental Details and Selected NMR Spectra of Solutions Generated by Hydroboration of Ethylene by HBR_2····S52-S58
Selected NMR Spectra for Determining the Mechanism of the Reaction of $[(dmpe)_2MnH(C_2H_4)]$ (**1**) with $HBMes_2$····S59
References····S60

Selected Abbreviations:

dmpe = 1,2-bis(dimethylphosphino)ethane

9-BBN = 9-borabicyclo(3.3.1)nonane (HBC_8H_{14})

Mes = Mesityl (2,4,6-trimethylphenyl)

AIM = Atoms in Molecules

Computational Methods

Geometry optimization calculations were conducted with the ADF DFT package (SCM, version 2017.207).[1] Calculations were performed in the gas phase within the generalized gradient approximation using the 1996 Perdew-Burke-Ernzerhof exchange and correlation functional (PBE),[2] using the scalar zeroth-order approximation (ZORA)[3] for relativistic effects, and Grimme's DFT-D3-BJ dispersion correction.[4] Preliminary geometry optimizations were conducted with frozen cores corresponding to the configuration of the preceding noble gas (core = medium) using double-ζ basis sets with one polarization function (DZP), a Voronoi grid with an integration value of 5, and default convergence criteria for energy and gradients. These structures were further refined using all-electron triple-ζ basis sets with two polarization functions (TZ2P) and fine integration grids (Becke[5] verygood-quality). Analytical frequency calculations[6] were conducted to ensure that the geometry optimization led to an energy minimum. For **3** and **4**, slightly negative frequencies (frequency range from –11 to –42 cm^{-1}) were observed but were shown to be spurious imaginary frequencies using the SCANFREQ command.[7] Atoms in Molecules (AIM)[8] properties were obtained using the QTAIM keyword in SCM version 2019.301[1] with an analysis level of Full.[9]

Figures Showing Calculated Structures with AIM Bond Paths and Critical Points

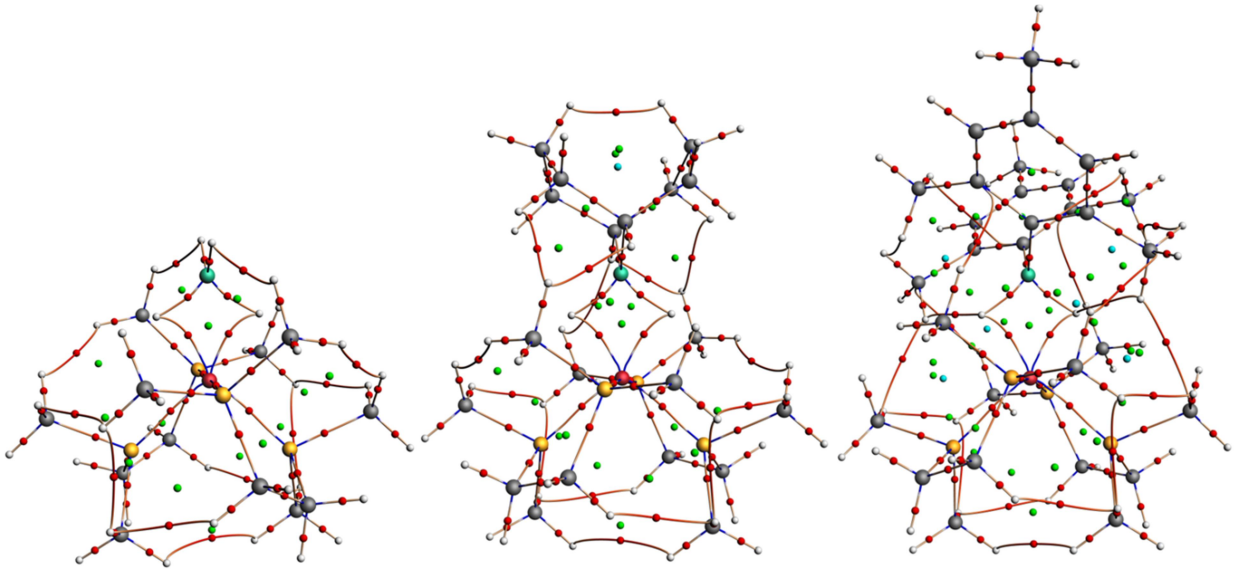

Figure S1. Calculated structures of, from left to right, $[(dmpe)_2Mn(\mu\text{-}H)_2BH_2]$ (**3**), $[(dmpe)_2Mn(\mu\text{-}H)_2BC_8H_{14}]$ (**4**), and $[(dmpe)_2Mn(\mu\text{-}H)_2BMes_2]$ (**5**), with AIM bond paths, bond critical points (small red spheres), ring critical points (small green spheres), cage critical points (small blue spheres). Atoms labelled by colour; Mn = red, B = turquoise, C = grey, H = white.

Figures Showing Superimposed Calculated and X-ray Structures

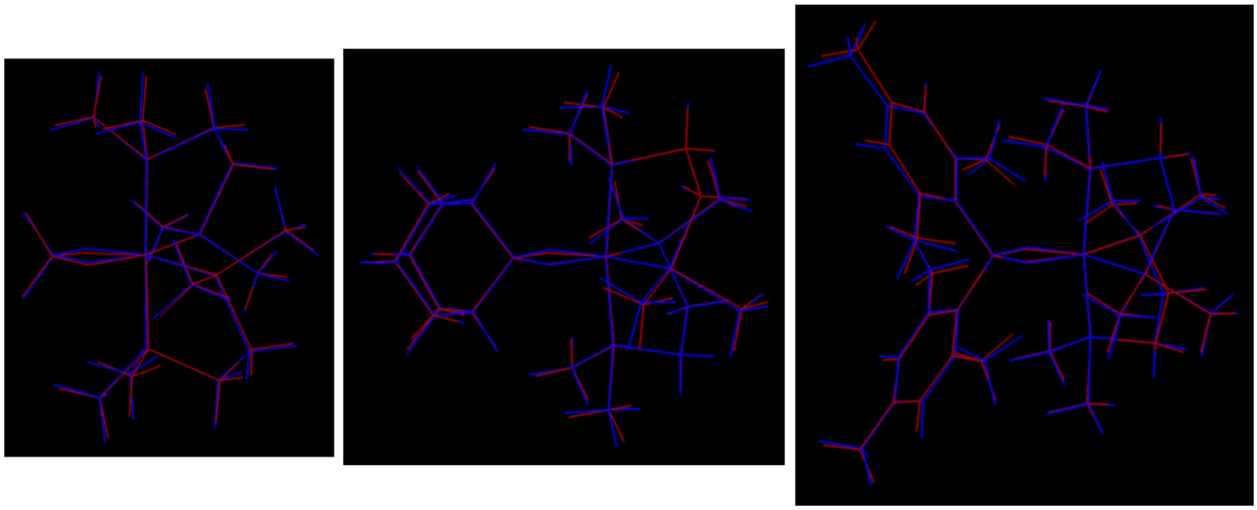

Figure S2. Superposition of calculated (blue) and X-ray (red) structures of, from left to right, $[(dmpe)_2Mn(\mu\text{-}H)_2BH_2]$ (**3**), $[(dmpe)_2Mn(\mu\text{-}H)_2BC_8H_{14}]$ (**4**), and $[(dmpe)_2Mn(\mu\text{-}H)_2BMes_2]$ (**5**).

Tables of Selected Calculated and Crystallographically Determined Bond Lengths and Angles, Mayer Bond Orders, and AIM Properties

Table S1. Selected calculated and crystallographically determined bond lengths (Å), Mayer bond orders, and AIM properties for borohydride complexes $[(dmpe)_2Mn(\mu\text{-}H)_2BH_2]$ (**3**), $[(dmpe)_2Mn(\mu\text{-}H)_2BC_8H_{14}]$ (**4**), and $[(dmpe)_2Mn(\mu\text{-}H)_2BMes_2]$ (**5**). b.o. = bond order, δ = bond delocalization index, bpl = bond path length, ρ = electron density, $\nabla^2\rho$ = Laplacian of the electron density, *G* = gradient kinetic energy density, *V* = potential energy density, *H* = total energy density of Cremer and Kraka, ε = ellipticity. H_b refers to the Mn*H*$_2$B environments.

			3	4	5
Mn–H_b		d(XRD)	1.76(4), 1.78(4)	1.66(3), 1.71(2)	1.69(4), 1.72(4)
		d(DFT)	1.69, 1.70	1.68, 1.68	1.71, 1.71
		Mayer b.o.	0.48, 0.48	0.54, 0.54	0.45, 0.45
	bond critical point properties	δ	0.476, 0.477	0.494, 0.496	0.452, 0.453
		bpl	1.81, 1.81	1.75, 1.76	1.78, 1.78
		ρ	0.0833, 0.0836	0.0842, 0.0834	0.0782, 0.0782
		$\nabla^2\rho$	0.225, 0.228	0.242, 0.248	0.237, 0.237
		G (au)	0.0831, 0.0839	0.0860, 0.0878	0.0806, 0.0806
		V (au)	–0.110, –0.111	–0.112, –0.114	–0.102, –0.102
		H (au)	–0.0268, –0.0269	–0.0256, –0.0257	–0.0213, –0.0213
		ε	1.00, 1.01	0.578, 0.584	0.482, 0.482
B–H_b		d(XRD)	1.31(4), 1.34(4)	1.25(2), 1.31(2)	1.19(4), 1.24(3)
		d(DFT)	1.32, 1.32	1.34, 1.34	1.32, 1.32
		Mayer	0.55, 0.55	0.44, 0.44	0.48, 0.48
	bond critical point properties	δ	0.418, 0.419	0.389, 0.393	0.396, 0.396
		bpl	1.34, 1.34	1.36, 1.36	1.33, 1.33
		ρ	0.127, 0.127	0.122, 0.122	0.126, 0.126
		$\nabla^2\rho$	–0.152, –0.152	–0.151, –0.153	–0.156, –0.156
		G (au)	0.0664, 0.0665	0.0603, 0.0607	0.0655, 0.0655
		V (au)	–0.171, –0.171	–0.159, –0.159	–0.170, –0.170
		H (au)	–0.104, –0.105	–0.0985, –0.0986	–0.104, –0.104
		ε	0.121, 0.121	0.121, 0.124	0.123, 0.123
B–$H_{terminal}$		d(XRD)	1.18(4), 1.19(5)	–	–
		d(DFT)	1.21, 1.22	–	–
		Mayer	0.81, 0.81	–	–
	bond critical point properties	δ	0.592, 0.593	–	–
		bpl	1.21, 1.22	–	–
		ρ	0.169, 0.169	–	–
		$\nabla^2\rho$	–0.336, –0.337	–	–
		G (au)	0.0923, 0.0923	–	–
		V (au)	–0.269, –0.269	–	–
		H (au)	–0.176, –0.177	–	–
		ε	0.0940, 0.0948	–	–
Mn–B		d(XRD)	2.170(4)	2.206(2)	2.245(3)
		d(DFT)	2.13	2.17	2.22
		Mayer	0.43	0.43	0.35
		δ	0.230	0.213	0.188
Mn(μ-H)$_2$B	ring critical point properties	ρ	0.0789	0.0752	0.0702
		$\nabla^2\rho$	0.134	0.138	0.147
		G (au)	0.0640	0.0614	0.0587
		V (au)	–0.0945	–0.0884	–0.0808
		H (au)	–0.0305	–0.0270	–0.0221
		ε	–4.27	–3.09	–2.65

Table S2. Selected calculated and crystallographically determined angles (°). cent.BR_2 = centroid between the two terminal substituents on boron.

			3	**4**	**5**
Angles	H_b–Mn–H_b	XRD	75(2)	70(1)	65(2)
		DFT	76.4	76.5	73.0
	H_b–B–H_b	XRD	109(2)	99(1)	97(2)
		DFT	105.3	101.7	100.3
	Mn–B–R	XRD	120(2), 127(2)	126.9(1), 128.2(1)	123.2(2), 124.1(2)
		DFT	124.0, 124.4	127.1, 127.6	123.6, 123.6
	Mn–B–(cent.BR_2)	XRD	173.6	178.7	179.4
		DFT	179.7	179.3	180.0
	plane(H_b–Mn–H_b)/ plane(H_b–B–H_b)	XRD	8.3	3.5	0.2
		DFT	0.5	0.4	0.0

Tables of Crystal Data and Crystal Structure Refinement

Table S3. Crystal and structure refinement data for $[(dmpe)_2Mn(\mu\text{-}H)_2BH_2]$ (**3**).

Identification code	MnBH4
Empirical formula	$C_{12}H_{36}BMnP_4$
Formula weight	370.04
Temperature/K	100
Crystal system	orthorhombic
Space group	Pbca
a/Å	11.8683(5)
b/Å	11.8704(5)
c/Å	28.4192(14)
α/°	90
β/°	90
γ/°	90
Volume/Å^3	4003.7(3)
Z	8
ρ_{calc}g/cm^3	1.228
μ/mm^{-1}	0.965
F(000)	1584.0
Crystal size/mm^3	0.47 × 0.383 × 0.144
Radiation	MoKα (λ = 0.71073)
2Θ range for data collection/°	3.432 to 60.978
Index ranges	-16 ≤ h ≤ 15, -16 ≤ k ≤ 16, -40 ≤ l ≤ 35
Reflections collected	35368
Independent reflections	6389 [R_{int} = 0.0507, R_{sigma} = 0.0424]
Data/restraints/parameters	6389/2/184
Goodness-of-fit on F^2	1.201
Final R indexes [I>=2σ (I)]	R_1 = 0.0557, wR_2 = 0.1282
Final R indexes [all data]	R_1 = 0.0596, wR_2 = 0.1299
Largest diff. peak/hole / e Å^{-3}	1.29/-0.56

Table S4. Crystal and structure refinement data for $[(dmpe)_2Mn(\mu\text{-}H)_2BC_8H_{14}]$ (**4**).

Identification code	MnH_9BBN
Empirical formula	$C_{20}H_{48}BMnP_4$
Formula weight	478.21
Temperature/K	100
Crystal system	monoclinic
Space group	$P2_1/n$
a/Å	11.3252(7)
b/Å	14.1954(9)
c/Å	16.8724(10)
α/°	90
β/°	103.169(3)
γ/°	90
Volume/Å^3	2641.2(3)
Z	4
ρ_{calc}g/cm^3	1.203
μ/mm^{-1}	0.746
F(000)	1032.0
Crystal size/mm^3	0.456 × 0.372 × 0.22
Radiation	MoKα (λ = 0.71073)
2Θ range for data collection/°	5.74 to 65.55
Index ranges	-17 ≤ h ≤ 16, 0 ≤ k ≤ 21, 0 ≤ l ≤ 25
Reflections collected	9679
Independent reflections	9679 [R_{int} = ?, R_{sigma} = 0.0401]
Data/restraints/parameters	9679/0/243
Goodness-of-fit on F^2	1.047
Final R indexes [I>=2σ (I)]	R_1 = 0.0337, wR_2 = 0.0713
Final R indexes [all data]	R_1 = 0.0490, wR_2 = 0.0775
Largest diff. peak/hole / e Å^{-3}	0.48/-0.38

Table S5. Crystal and structure refinement data for $[(dmpe)_2Mn(\mu\text{-}H)_2BMes_2]$ (**5**).

Identification code	MnH_BMes2
Empirical formula	$C_{30}H_{56}BMnP_4$
Formula weight	606.37
Temperature/K	100
Crystal system	triclinic
Space group	P-1
a/Å	10.068(3)
b/Å	12.286(3)
c/Å	13.967(3)
α/°	90.611(4)
β/°	101.870(5)
γ/°	104.056(5)
Volume/$Å^3$	1636.7(7)
Z	2
$\rho_{calc}g/cm^3$	1.230
μ/mm^{-1}	0.617
F(000)	652.0
Crystal size/mm^3	0.198 × 0.164 × 0.072
Radiation	MoKα (λ = 0.71073)
2Θ range for data collection/°	2.986 to 56.87
Index ranges	-13 ≤ h ≤ 12, -16 ≤ k ≤ 16, 0 ≤ l ≤ 18
Reflections collected	7863
Independent reflections	7863 [R_{int} = ?, R_{sigma} = 0.0562]
Data/restraints/parameters	7863/0/348
Goodness-of-fit on F^2	1.045
Final R indexes [I>=2σ (I)]	R_1 = 0.0468, wR_2 = 0.0885
Final R indexes [all data]	R_1 = 0.0798, wR_2 = 0.0995
Largest diff. peak/hole / e $Å^{-3}$	0.55/-0.44

Table S6. Crystal and structure refinement data for *trans*,*trans*-[{(dmpe)$_2$MnH}$_2$(μ-dmpe)] (***trans*,*trans*-6**).

Identification code	MnHdmpe_bridging_trans
Empirical formula	$C_{30}H_{82}Mn_2P_{10}$
Formula weight	862.53
Temperature/K	100
Crystal system	monoclinic
Space group	$P2_1/c$
a/Å	13.8329(9)
b/Å	14.9650(10)
c/Å	11.0995(7)
α/°	90
β/°	102.760(3)
γ/°	90
Volume/Å^3	2241.0(3)
Z	2
ρ_{calc}g/cm^3	1.278
μ/mm^{-1}	0.940
F(000)	924.0
Crystal size/mm^3	0.437 × 0.361 × 0.238
Radiation	MoKα (λ = 0.71073)
2Θ range for data collection/°	5.444 to 80.486
Index ranges	-25 ≤ h ≤ 25, -27 ≤ k ≤ 27, -20 ≤ l ≤ 20
Reflections collected	106256
Independent reflections	14051 [R_{int} = 0.0441, R_{sigma} = 0.0286]
Data/restraints/parameters	14051/0/204
Goodness-of-fit on F^2	1.034
Final R indexes [I>=2σ (I)]	R_1 = 0.0278, wR_2 = 0.0612
Final R indexes [all data]	R_1 = 0.0418, wR_2 = 0.0672
Largest diff. peak/hole / e Å^{-3}	0.61/-0.33

Table S7. Crystal and structure refinement data for *cis*,*cis*-[{(dmpe)$_2$MnH}$_2$(μ-dmpe)] (***cis*,*cis*-6**).

Identification code	MnHdmpe_bridging_cis
Empirical formula	$C_{30}H_{82}Mn_2P_{10}$
Formula weight	862.53
Temperature/K	100
Crystal system	monoclinic
Space group	$P2_1/n$
a/Å	15.392(2)
b/Å	10.4309(14)
c/Å	28.529(4)
α/°	90
β/°	98.652(2)
γ/°	90
Volume/Å^3	4528.2(10)
Z	4
ρ_{calc}g/cm^3	1.265
μ/mm^{-1}	0.931
F(000)	1848.0
Crystal size/mm^3	0.27 × 0.143 × 0.125
Radiation	MoKα (λ = 0.71073)
2Θ range for data collection/°	2.676 to 58.4
Index ranges	-21 ≤ h ≤ 21, -14 ≤ k ≤ 14, -39 ≤ l ≤ 38
Reflections collected	56722
Independent reflections	12351 [R_{int} = 0.0898, R_{sigma} = 0.0918]
Data/restraints/parameters	12351/870/486
Goodness-of-fit on F^2	1.019
Final R indexes [I>=2σ (I)]	R_1 = 0.1092, wR_2 = 0.2817
Final R indexes [all data]	R_1 = 0.1648, wR_2 = 0.3234
Largest diff. peak/hole / e Å^{-3}	2.30/-1.35

Table S8. Crystal and structure refinement data for *trans*-[(dmpe)$_2$MnH(κ$_1$-dmpe)] (***trans*-7**).

Identification code	MnHdmpe3_trans
Empirical formula	$C_{18}H_{49}MnP_6$
Formula weight	506.36
Temperature/K	100
Crystal system	monoclinic
Space group	$P2_1$
a/Å	20.562(4)
b/Å	9.4569(18)
c/Å	28.035(5)
α/°	90
β/°	90.843(4)
γ/°	90
Volume/Å^3	5451.0(18)
Z	8
ρ_{calc}g/cm^3	1.234
μ/mm^{-1}	0.839
F(000)	2176.0
Crystal size/mm^3	0.020 × 0.020 × 0.020
Radiation	MoKα (λ = 0.71073)
2Θ range for data collection/°	3.492 to 56.508
Index ranges	-27 ≤ h ≤ 27, -12 ≤ k ≤ 12, -37 ≤ l ≤ 37
Reflections collected	85573
Independent reflections	26856 [R_{int} = 0.2398, R_{sigma} = 0.5649]
Data/restraints/parameters	26856/910/959
Goodness-of-fit on F^2	0.644
Final R indexes [I>=2σ (I)]	R_1 = 0.0888, wR_2 = 0.0771
Final R indexes [all data]	R_1 = 0.2458, wR_2 = 0.1006
Largest diff. peak/hole / e Å^{-3}	0.98/-0.78
Flack parameter	0.46(3)

Table S9. Crystal and structure refinement data for *trans*-[(dmpe)$_2$MnH(PMe$_3$)] (***trans*-8**).

Identification code	MnHPMe3_trans
Empirical formula	$C_{15}H_{42}MnP_5$
Formula weight	432.27
Temperature/K	100
Crystal system	triclinic
Space group	P-1
a/Å	9.2251(10)
b/Å	9.4251(10)
c/Å	15.1932(16)
α/°	91.032(3)
β/°	106.889(3)
γ/°	113.056(3)
Volume/Å^3	1150.0(2)
Z	2
ρ_{calc}g/cm^3	1.248
μ/mm^{-1}	0.916
F(000)	464.0
Crystal size/mm^3	0.02 × 0.02 × 0.01
Radiation	MoKα (λ = 0.71073)
2Θ range for data collection/°	2.834 to 52.618
Index ranges	-11 ≤ h ≤ 11, -11 ≤ k ≤ 11, -18 ≤ l ≤ 18
Reflections collected	19746
Independent reflections	4659 [R_{int} = 0.1174, R_{sigma} = 0.1203]
Data/restraints/parameters	4659/0/205
Goodness-of-fit on F^2	1.034
Final R indexes [I>=2σ (I)]	R_1 = 0.0674, wR_2 = 0.1023
Final R indexes [all data]	R_1 = 0.1237, wR_2 = 0.1159
Largest diff. peak/hole / e Å^{-3}	0.85/-0.75

Selected NMR Spectra for Complexes 3-8

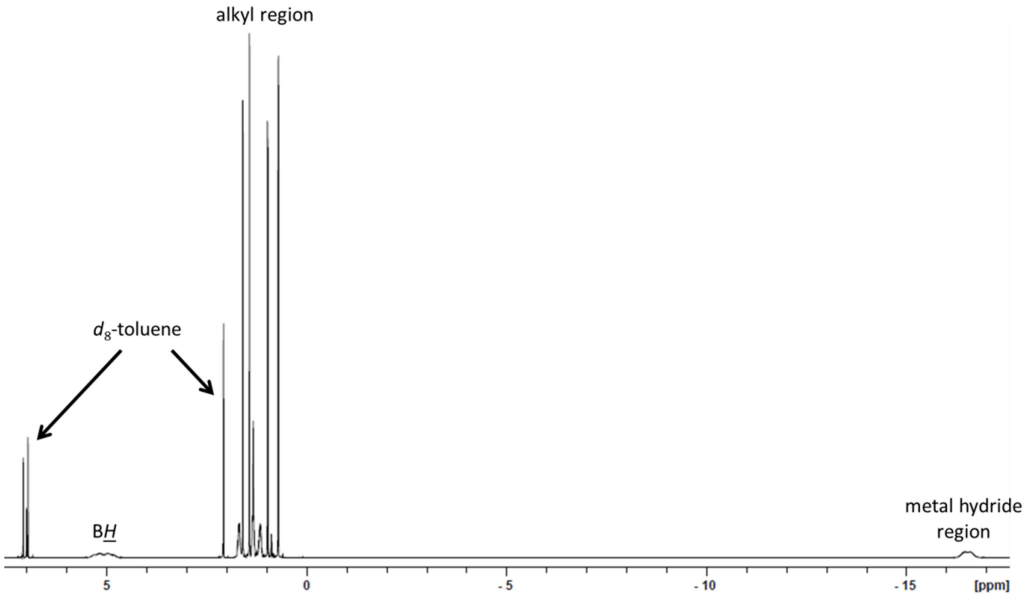

Figure S3. ^{1}H NMR spectrum of [(dmpe)$_2$Mn(μ-H)$_2$BH$_2$] (**3**) in d_8-toluene (600 MHz, 298 K).

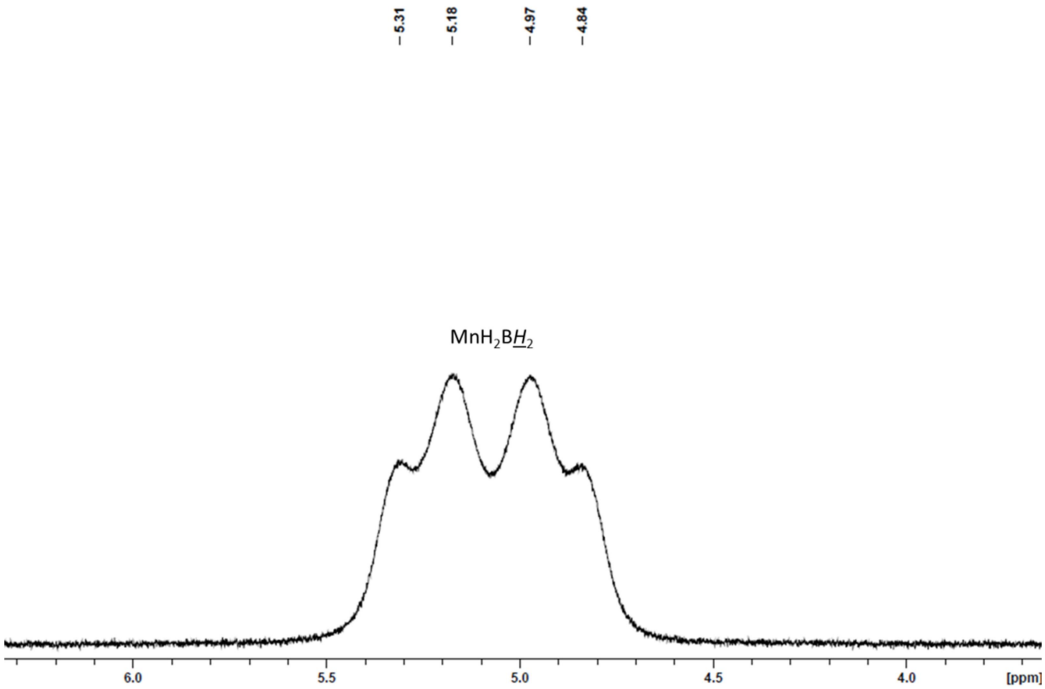

Figure S4. Expanded B*H* region of the ^{1}H NMR spectrum of [(dmpe)$_2$Mn(μ-H)$_2$BH$_2$] (**3**) in d_8-toluene (600 MHz, 298 K).

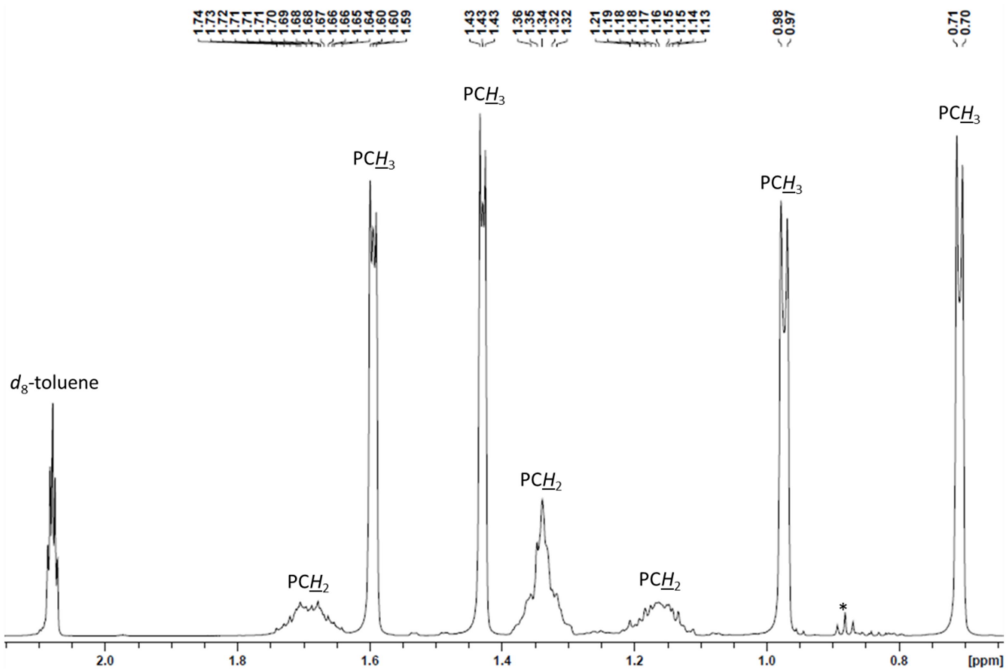

Figure S5. Expanded alkyl region of the ^{1}H NMR spectrum of [(dmpe)$_2$Mn(μ-H)$_2$BH$_2$] (**3**) in d_8-toluene (600 MHz, 298 K). * indicates a peak from *n*-hexane.

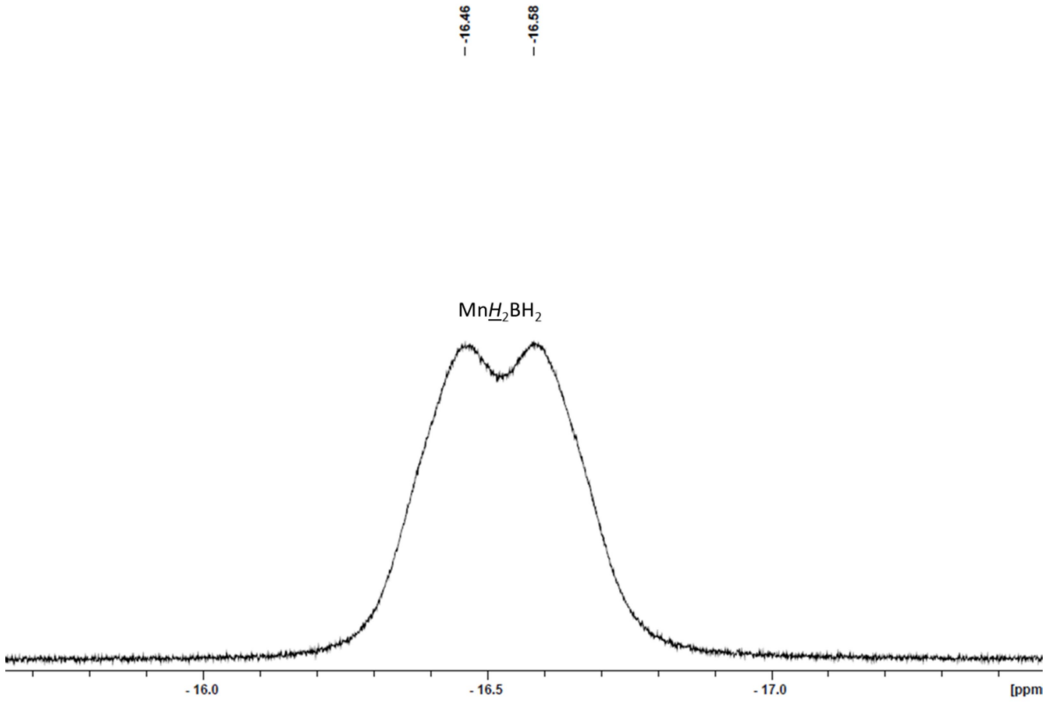

Figure S6. Expanded Mn*H* region of the ^{1}H NMR spectrum of [(dmpe)$_2$Mn(μ-H)$_2$BH$_2$] (**3**) in d_8-toluene (600 MHz, 298 K).

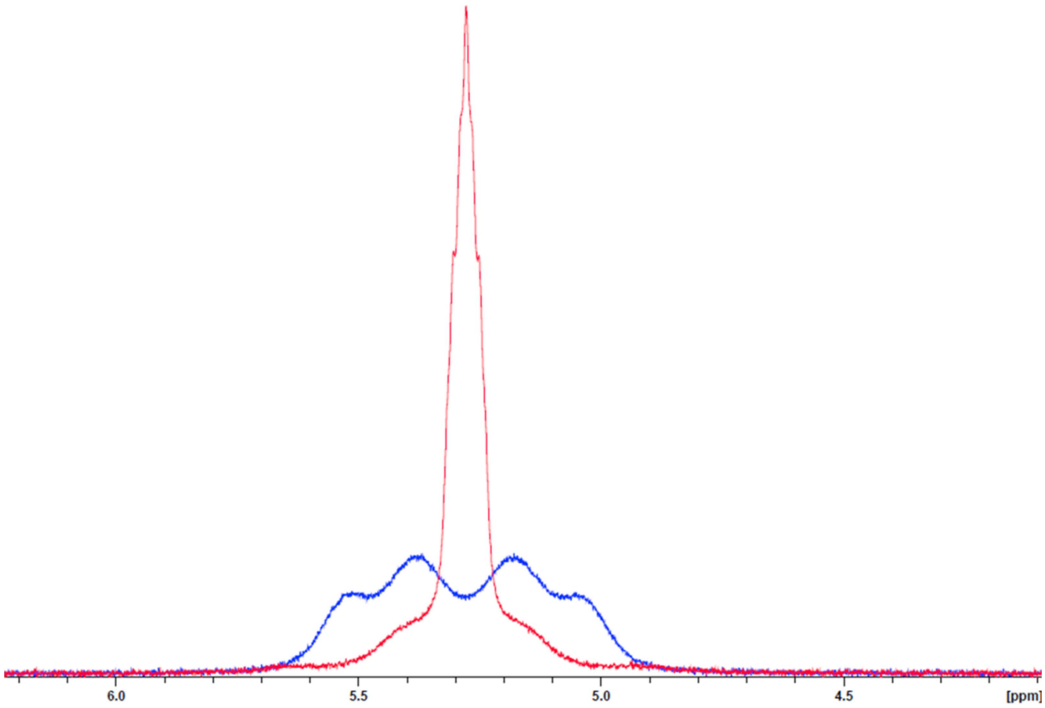

Figure S7. Expanded B*H* region of an overlay of the ^{1}H (blue) and $^{1}H\{^{11}B\}$ (red) NMR spectra of $[(dmpe)_2Mn(\mu\text{-}H)_2BH_2]$ (**3**) in C_6D_6 (600 MHz, 298 K).

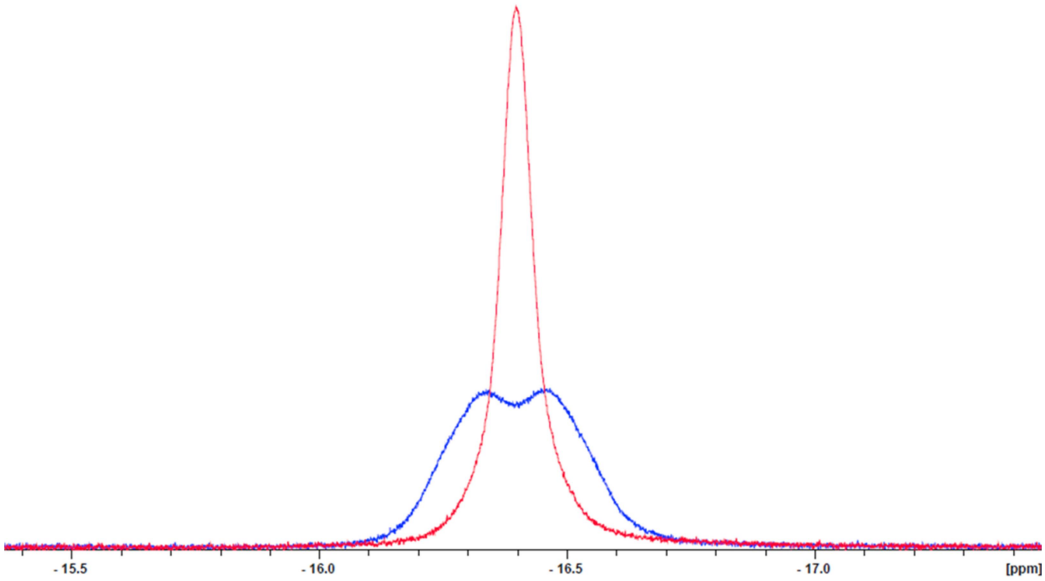

Figure S8. Expanded Mn*H* region of an overlay of the ^{1}H (blue) and $^{1}H\{^{11}B\}$ (red) NMR spectra of $[(dmpe)_2Mn(\mu\text{-}H)_2BH_2]$ (**3**) in C_6D_6 (600 MHz, 298 K).

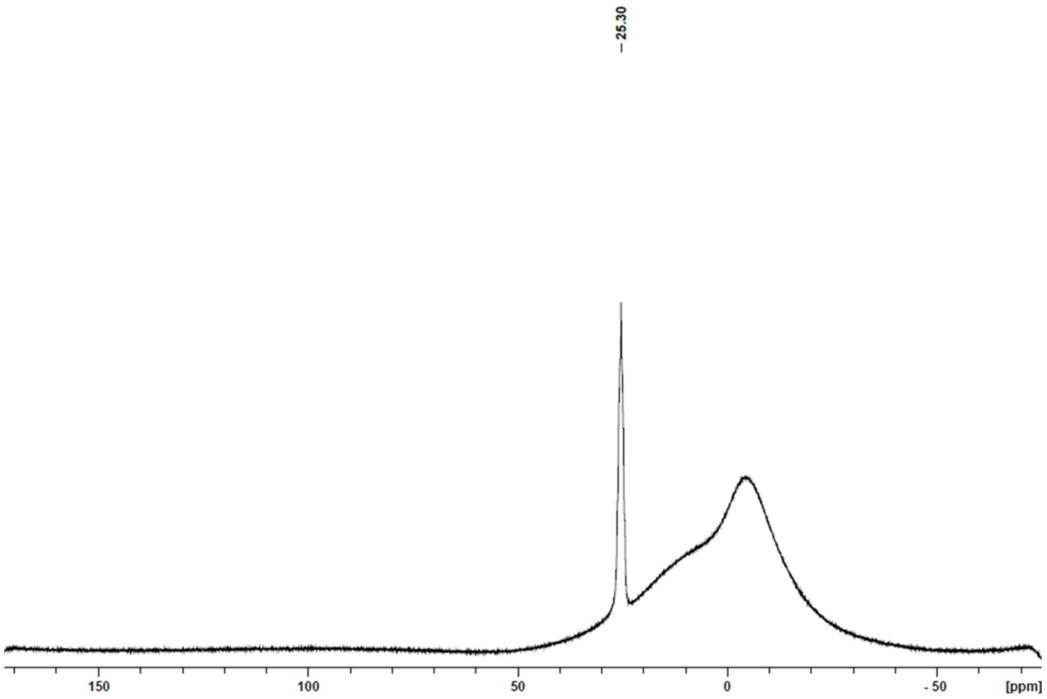

Figure S9. $^{11}B\{^{1}H\}$ NMR spectrum of $[(dmpe)_2Mn(\mu\text{-}H)_2BH_2]$ (**3**) in d_8-toluene (192 MHz, 298 K).

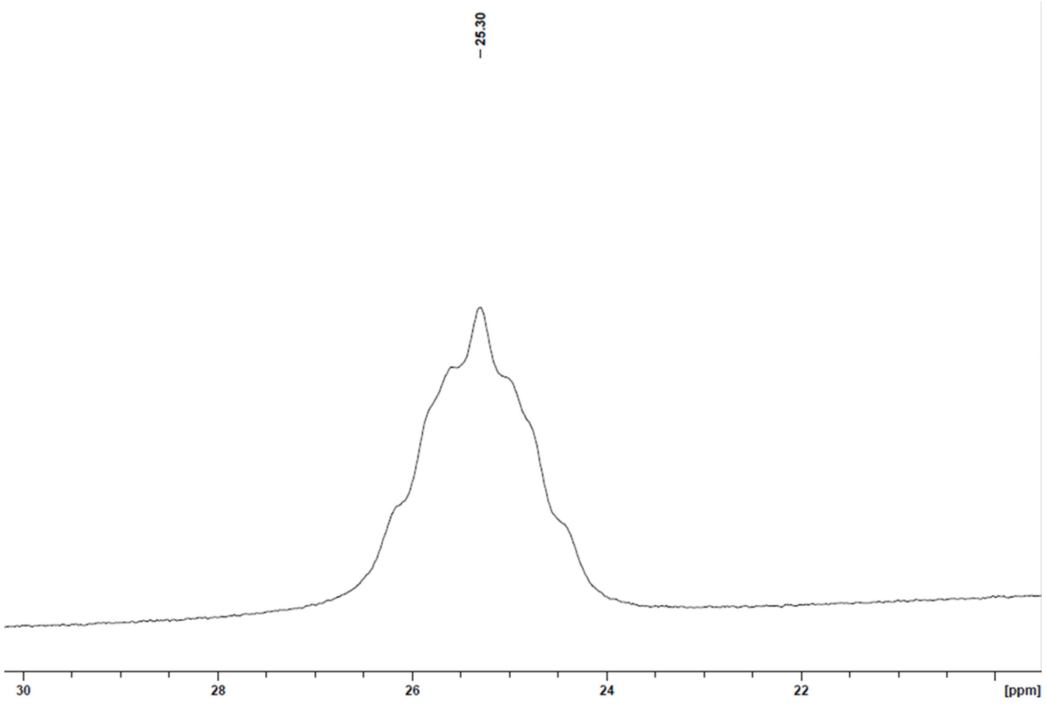

Figure S10. Expanded signal-containing region of the $^{11}B\{^{1}H\}$ NMR spectrum of $[(dmpe)_2Mn(\mu\text{-}H)_2BH_2]$ (**3**) in d_8-toluene (192 MHz, 298 K).

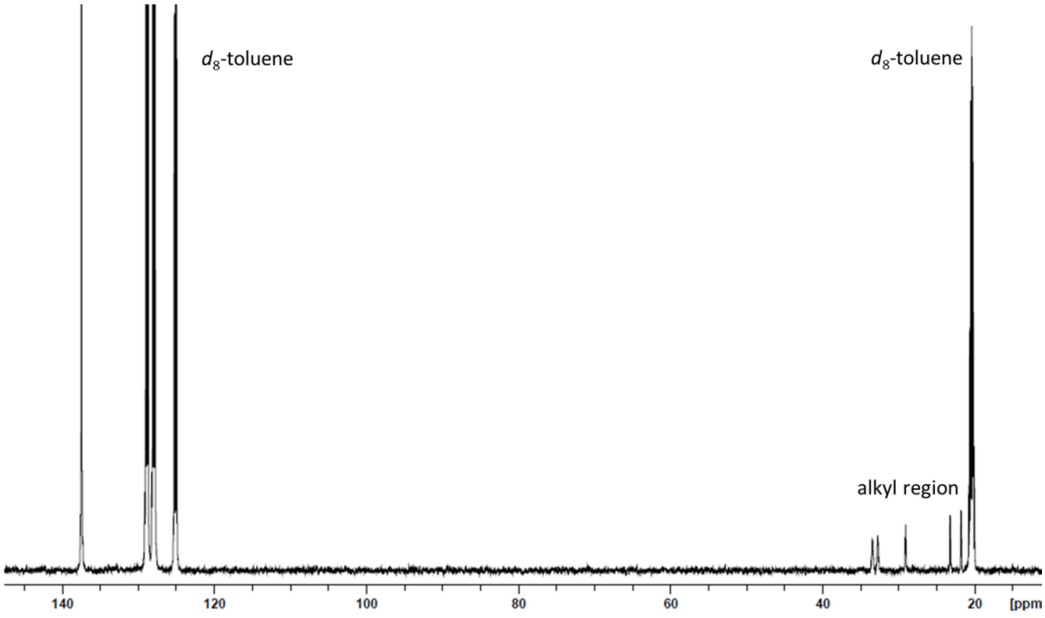

Figure S11. $^{13}C\{^1H\}$ NMR spectrum of $[(dmpe)_2Mn(\mu\text{-}H)_2BH_2]$ (**3**) in d_8-toluene (151 MHz, 298 K).

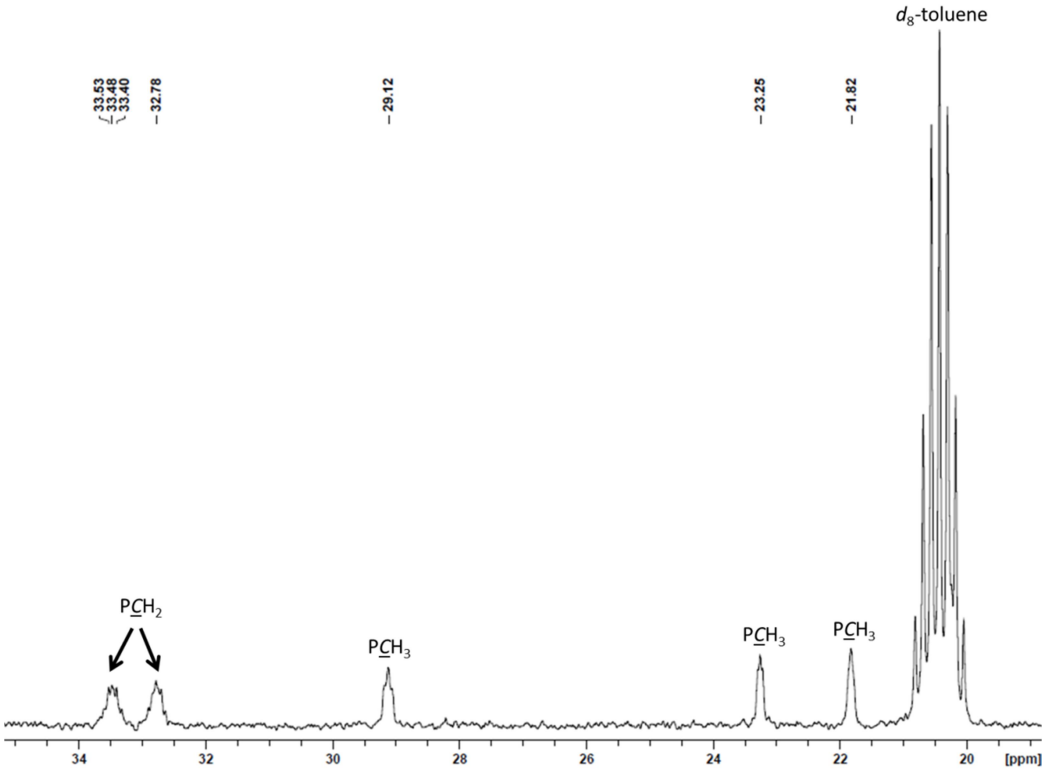

Figure S12. Expanded alkyl region of the $^{13}C\{^1H\}$ NMR spectrum of $[(dmpe)_2Mn(\mu\text{-}H)_2BH_2]$ (**3**) in d_8-toluene (151 MHz, 298 K).

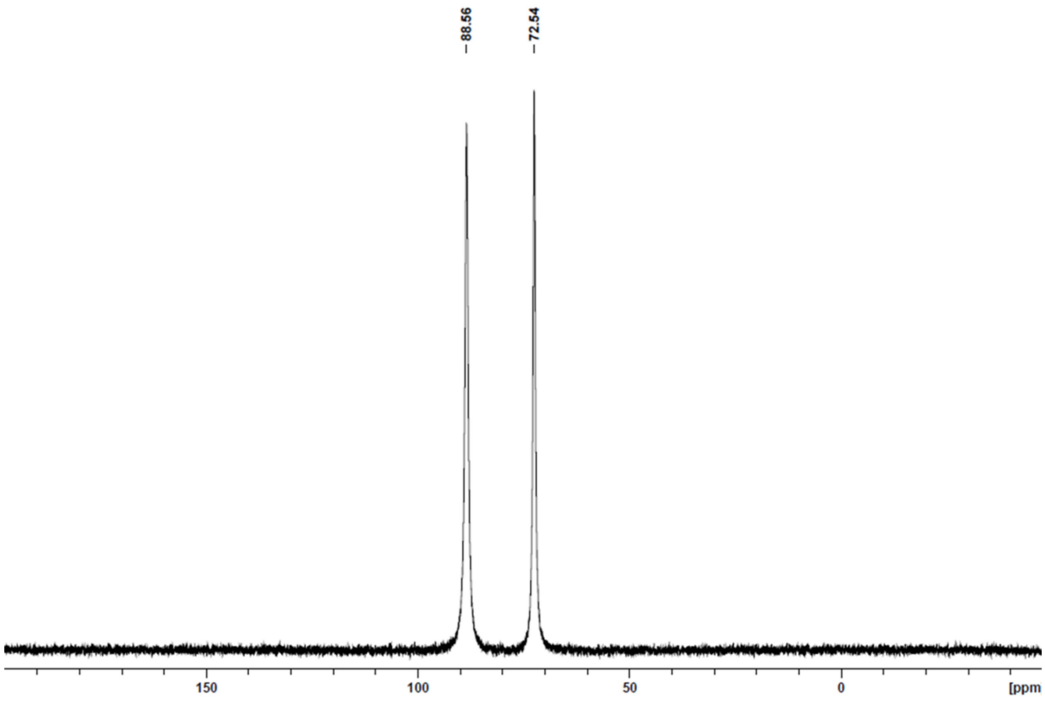

Figure S13. $^{31}P\{^{1}H\}$ NMR spectrum of $[(dmpe)_2Mn(\mu\text{-}H)_2BH_2]$ (**3**) in d_8-toluene (243 MHz, 298 K).

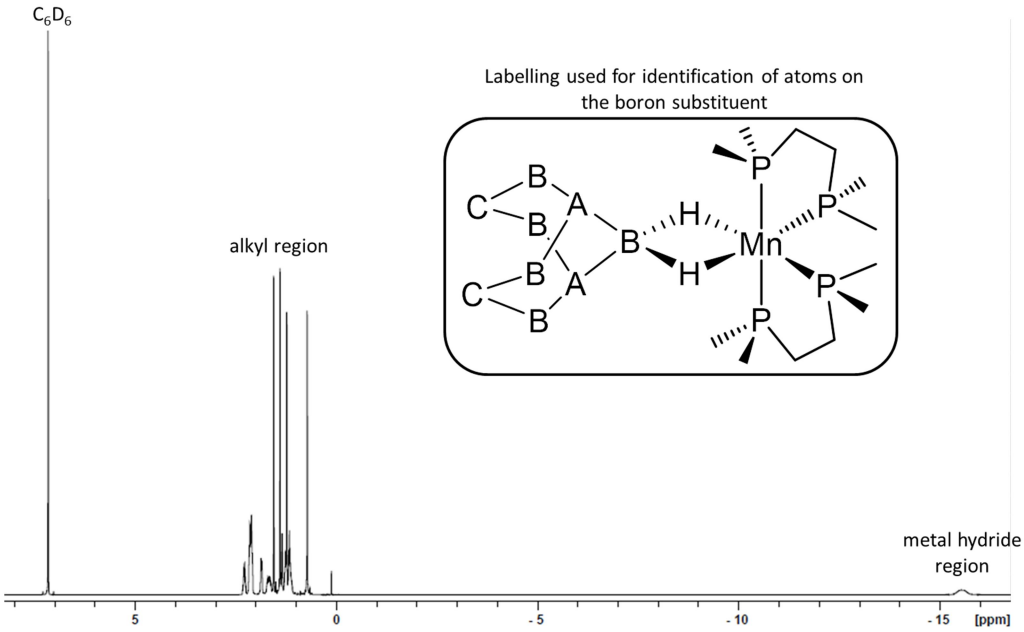

Figure S14. ^{1}H NMR spectrum of $[(dmpe)_2Mn(\mu\text{-}H)_2BC_8H_{14}]$ (**4**) in C_6D_6 (600 MHz, 298 K).

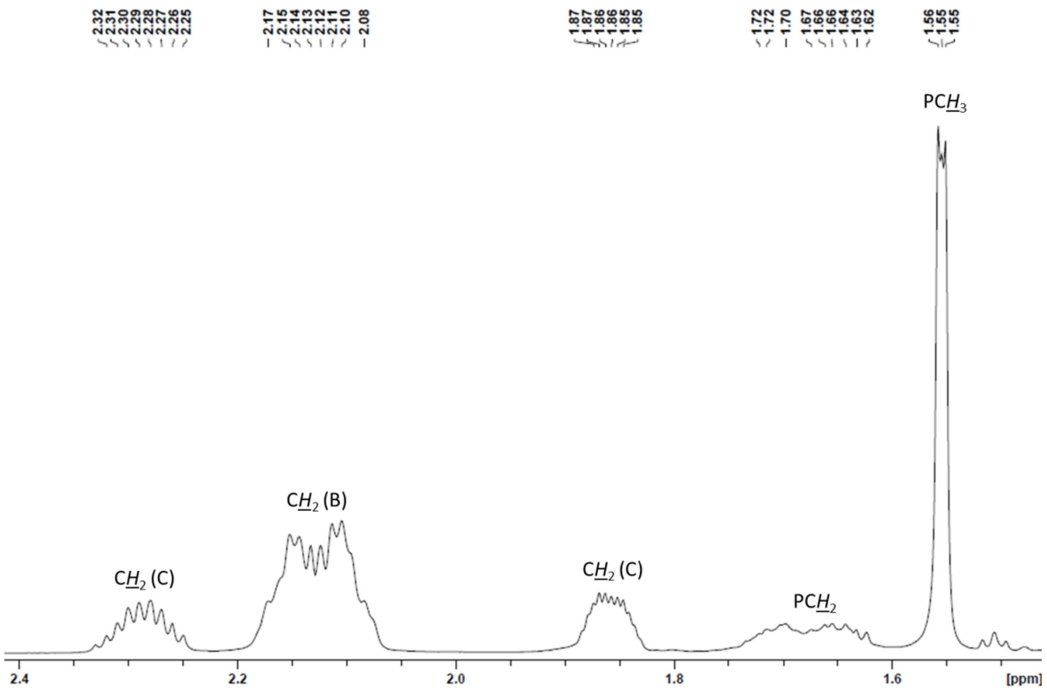

Figure S15. Expanded high frequency portion of the alkyl region of the ^{1}H NMR spectrum of $[(dmpe)_2Mn(\mu\text{-}H)_2BC_8H_{14}]$ (**4**) in C_6D_6 (600 MHz, 298 K).

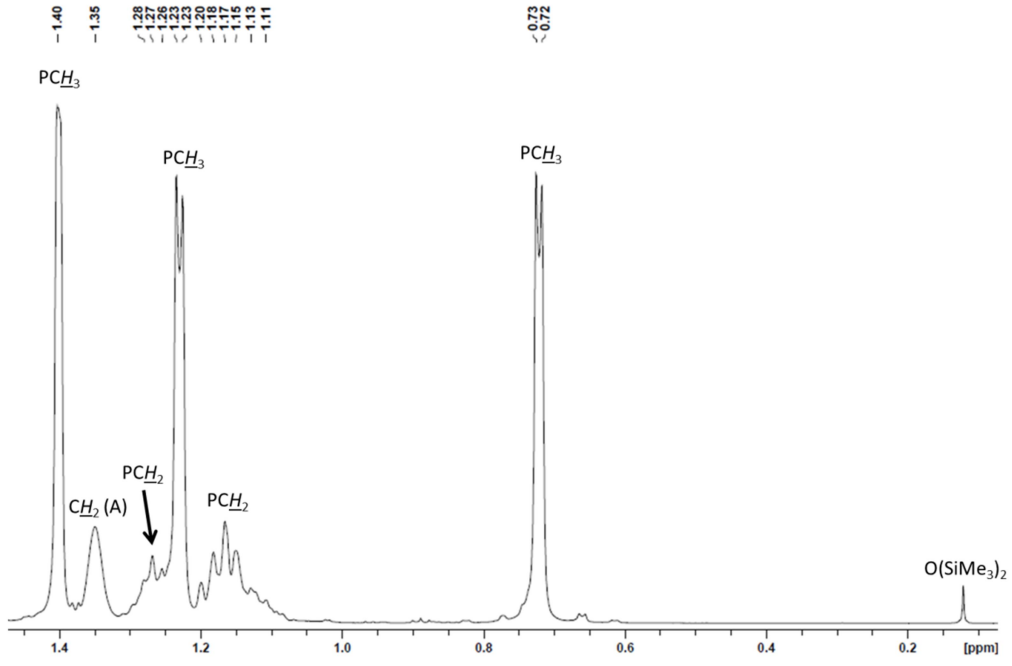

Figure S16. Expanded low frequency portion of the alkyl region of the ^{1}H NMR spectrum of $[(dmpe)_2Mn(\mu\text{-}H)_2BC_8H_{14}]$ (**4**) in C_6D_6 (600 MHz, 298 K).

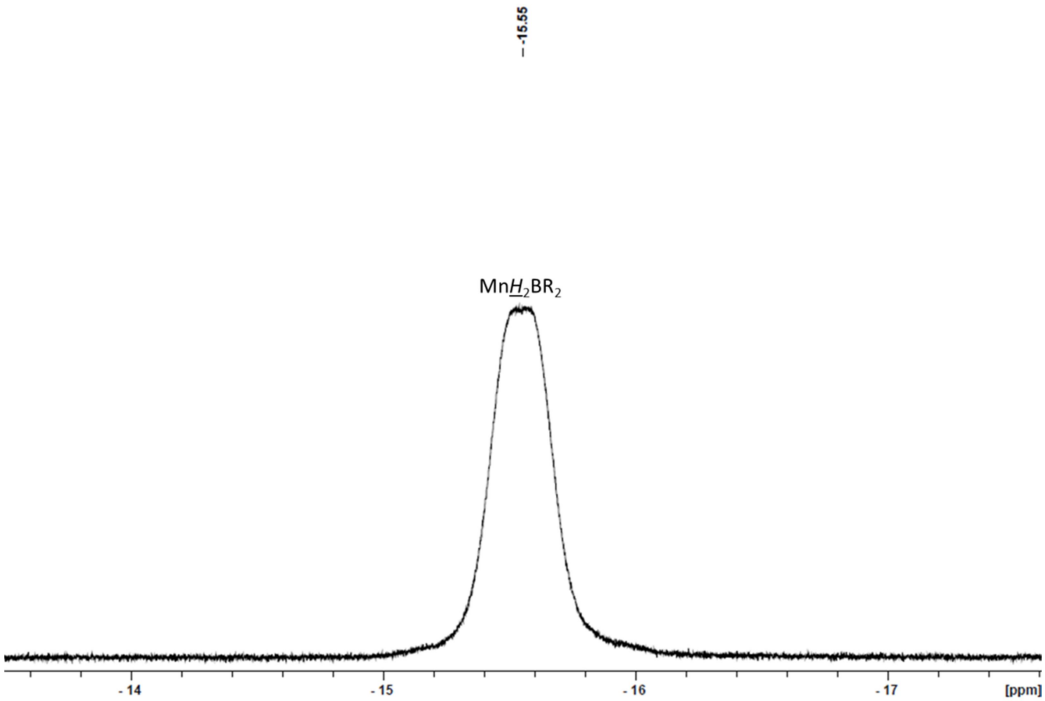

Figure S17. Expanded Mn*H* region of the ^{1}H NMR spectrum of [(dmpe)$_2$Mn(μ-H)$_2$BC$_8$H$_{14}$] (**4**) in C$_6$D$_6$ (600 MHz, 298 K).

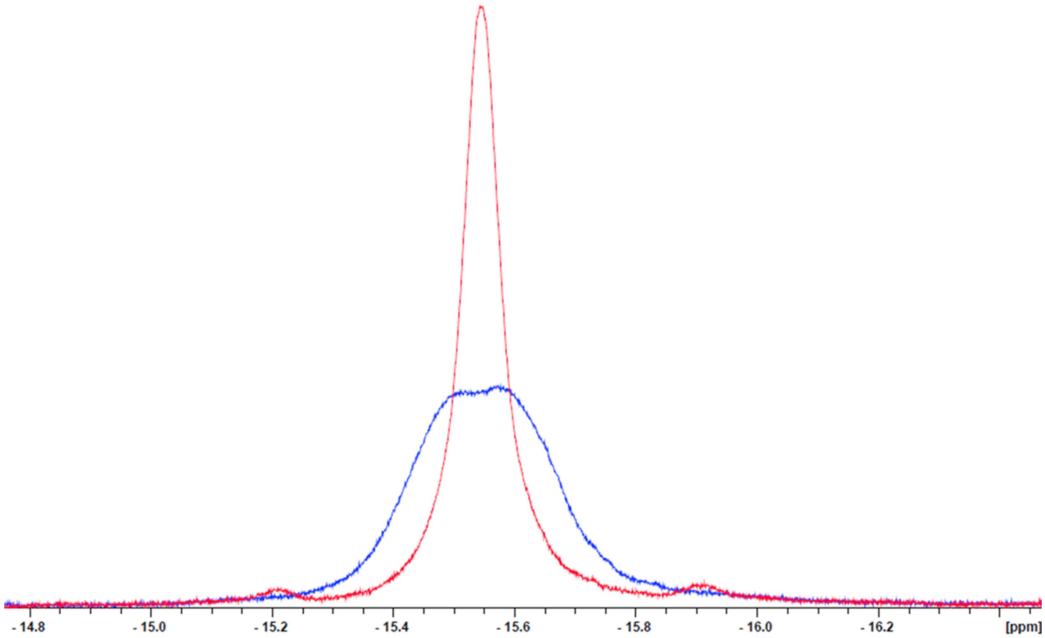

Figure S18. Expanded Mn*H* region of an overlay of the ^{1}H (blue) and ^{1}H{^{11}B} (red) NMR spectra of [(dmpe)$_2$Mn(μ-H)$_2$BC$_8$H$_{14}$] (**4**) in C$_6$D$_6$ (600 MHz, 298 K).

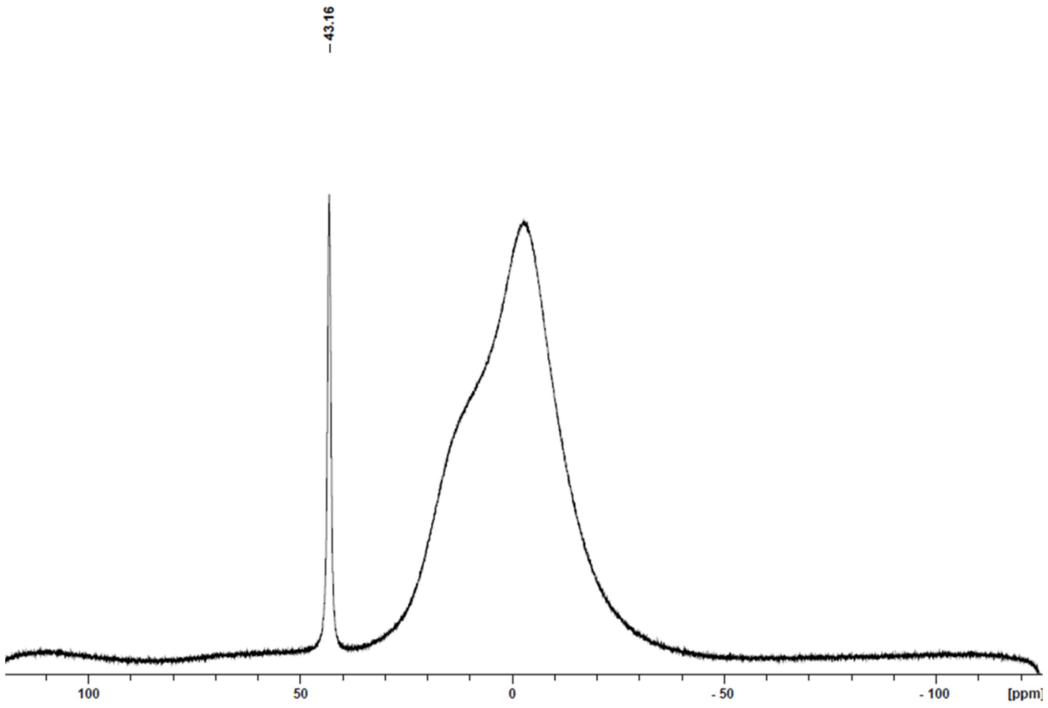

Figure S19. $^{11}B\{^{1}H\}$ NMR spectrum of $[(dmpe)_2Mn(\mu\text{-}H)_2BC_8H_{14}]$ (**4**) in C_6D_6 (192 MHz, 298 K).

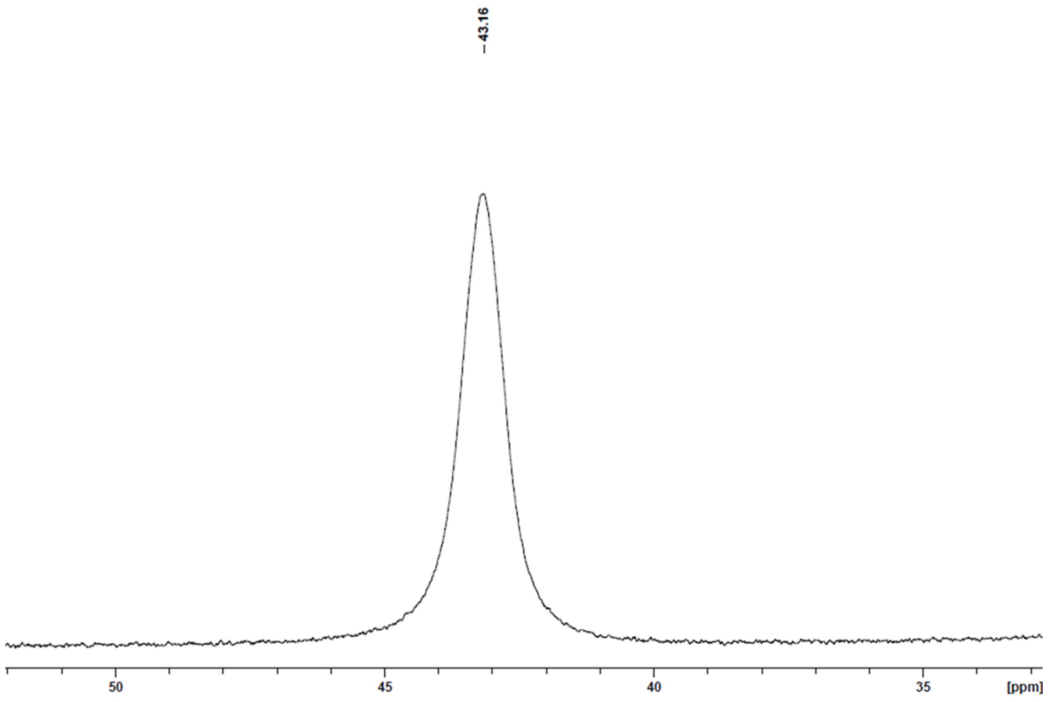

Figure S20. Expanded signal-containing region of the $^{11}B\{^{1}H\}$ NMR spectrum of $[(dmpe)_2Mn(\mu\text{-}H)_2BC_8H_{14}]$ (**4**) in C_6D_6 (192 MHz, 298 K).

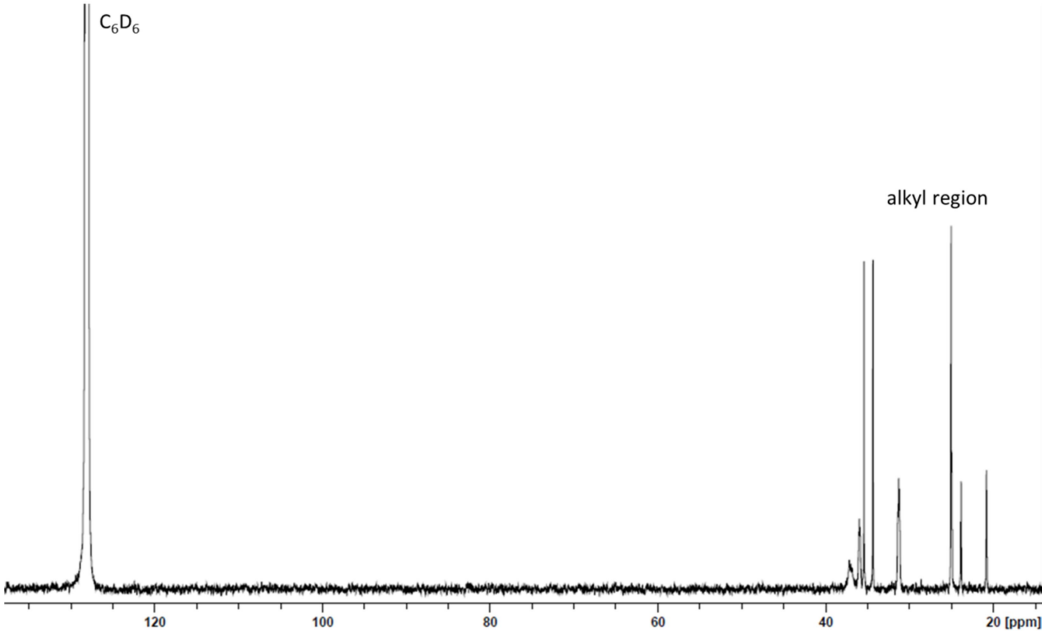

Figure S21. $^{13}C\{^{1}H\}$ NMR spectrum of $[(dmpe)_2Mn(\mu\text{-}H)_2BC_8H_{14}]$ (**4**) in C_6D_6 (151 MHz, 298 K).

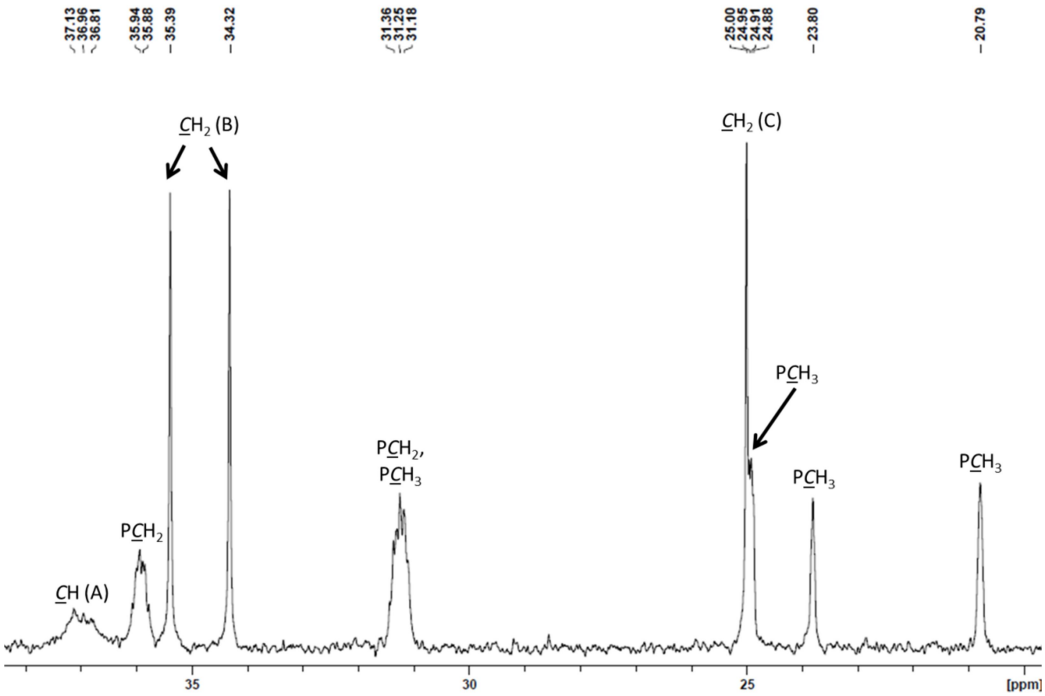

Figure S22. Expanded alkyl region of the $^{13}C\{^{1}H\}$ NMR spectrum of $[(dmpe)_2Mn(\mu\text{-}H)_2BC_8H_{14}]$ (**4**) in C_6D_6 (151 MHz, 298 K).

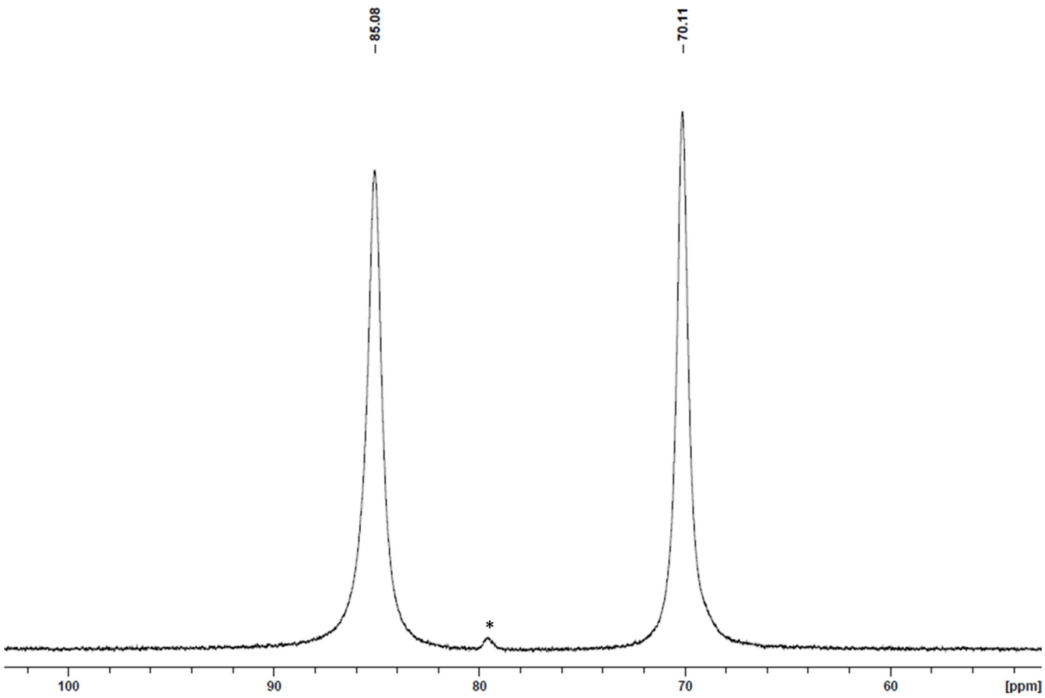

Figure S23. $^{31}P\{^{1}H\}$ NMR spectrum of $[(dmpe)_2Mn(\mu\text{-}H)_2BC_8H_{14}]$ (**4**) in C_6D_6 (243 MHz, 298 K). * indicates a signal from an impurity.

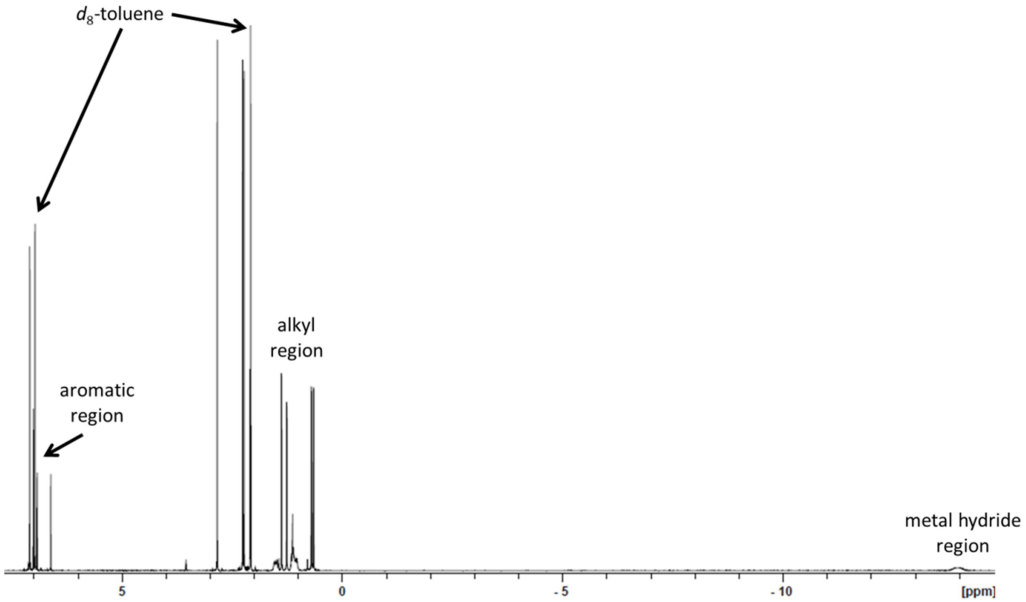

Figure S24. ^{1}H NMR spectrum of $[(dmpe)_2Mn(\mu\text{-}H)_2BMes_2]$ (**5**) in d_8-toluene (600 MHz, 298 K).

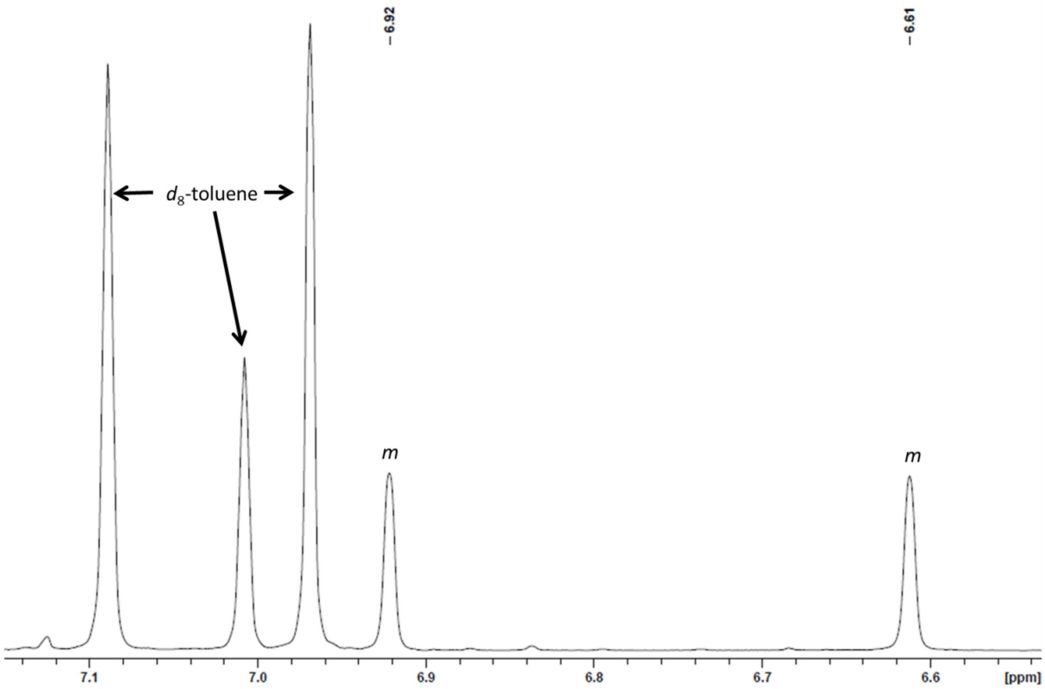

Figure S25. Expanded aromatic region of the ^{1}H NMR spectrum of [(dmpe)$_2$Mn(μ-H)$_2$BMes$_2$] (**5**) in d_8-toluene (600 MHz, 298 K).

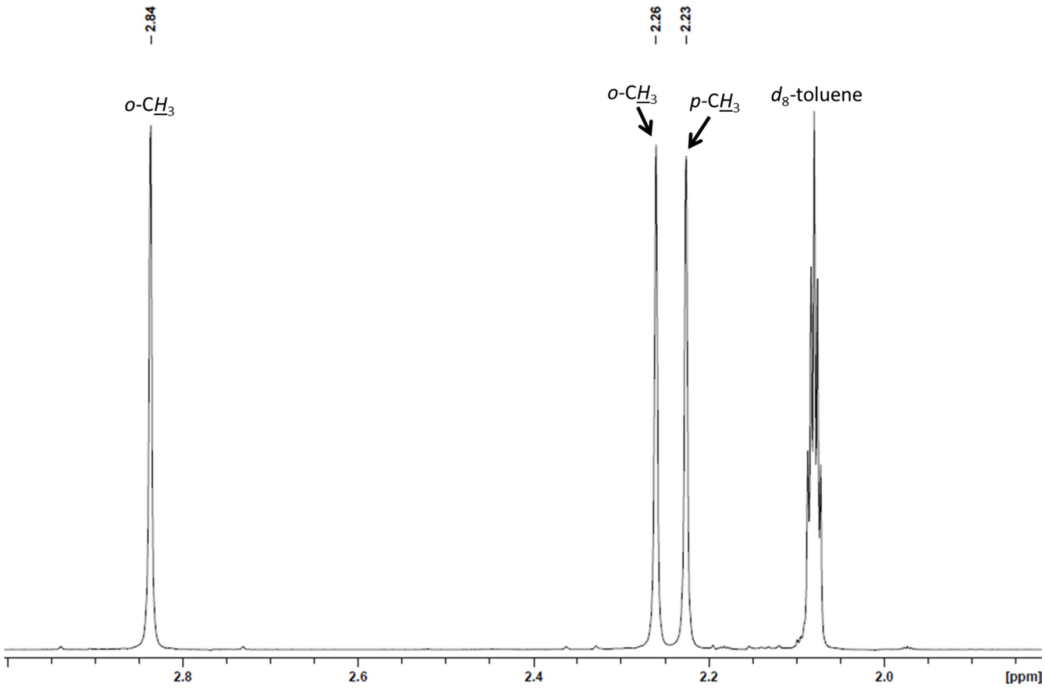

Figure S26. Expanded high frequency portion of the alkyl region of the ^{1}H NMR spectrum of [(dmpe)$_2$Mn(μ-H)$_2$BMes$_2$] (**5**) in d_8-toluene (600 MHz, 298 K).

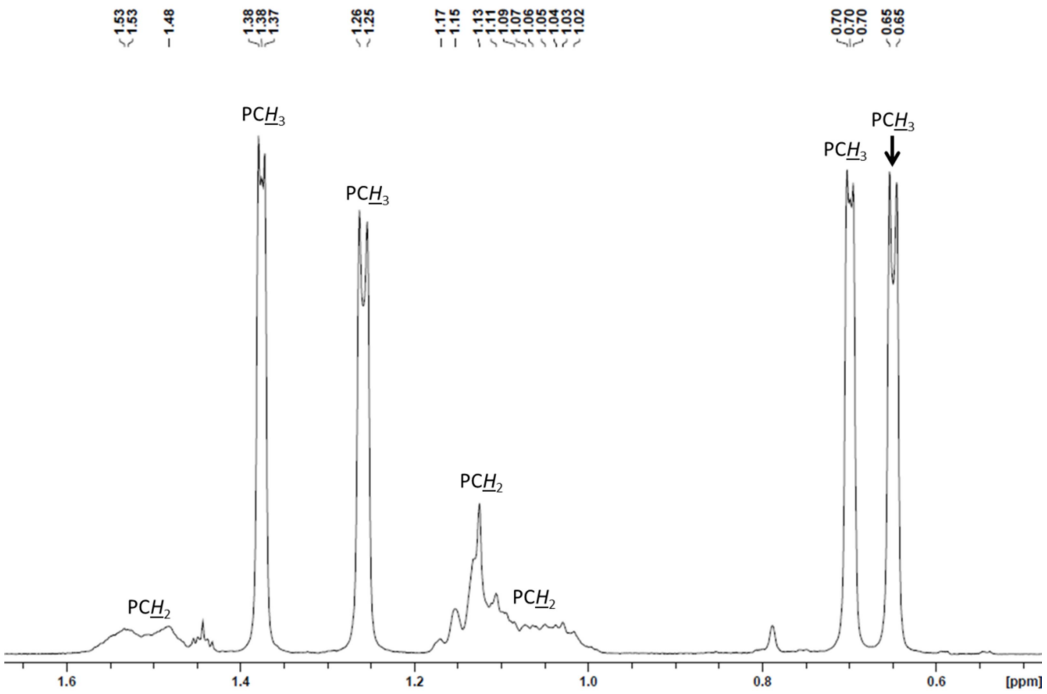

Figure S27. Expanded low frequency portion of the alkyl region of the ^{1}H NMR spectrum of [(dmpe)$_2$Mn(μ-H)$_2$BMes$_2$] (**5**) in d_8-toluene (600 MHz, 298 K).

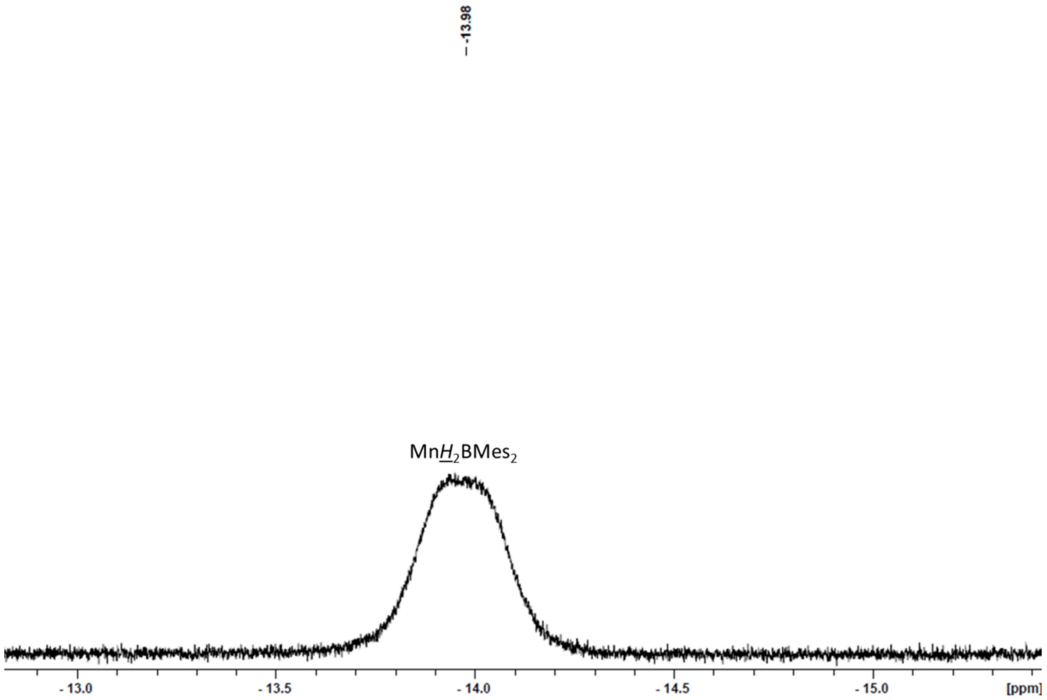

Figure S28. Expanded Mn*H* region of the ^{1}H NMR spectrum of [(dmpe)$_2$Mn(μ-H)$_2$BMes$_2$] (**5**) in d_8-toluene (600 MHz, 298 K).

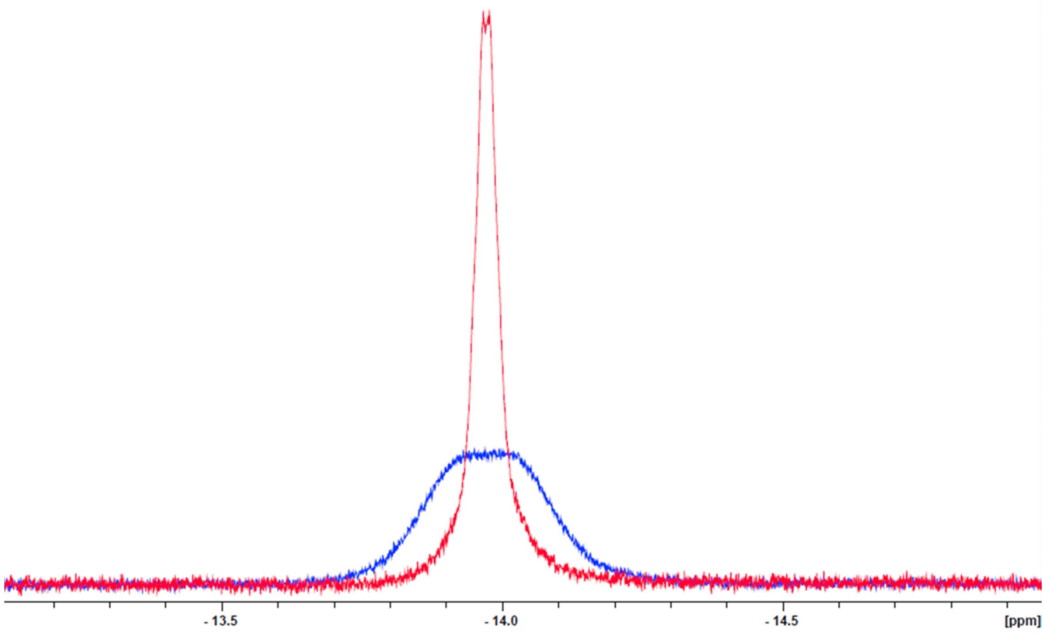

Figure S29. Expanded Mn*H* region of an overlay of the ^{1}H (blue) and $^{1}H\{^{11}B\}$ (red) NMR spectra of $[(dmpe)_2Mn(\mu\text{-}H)_2BMes_2]$ (**5**) in d_8-toluene (600 MHz, 298 K).

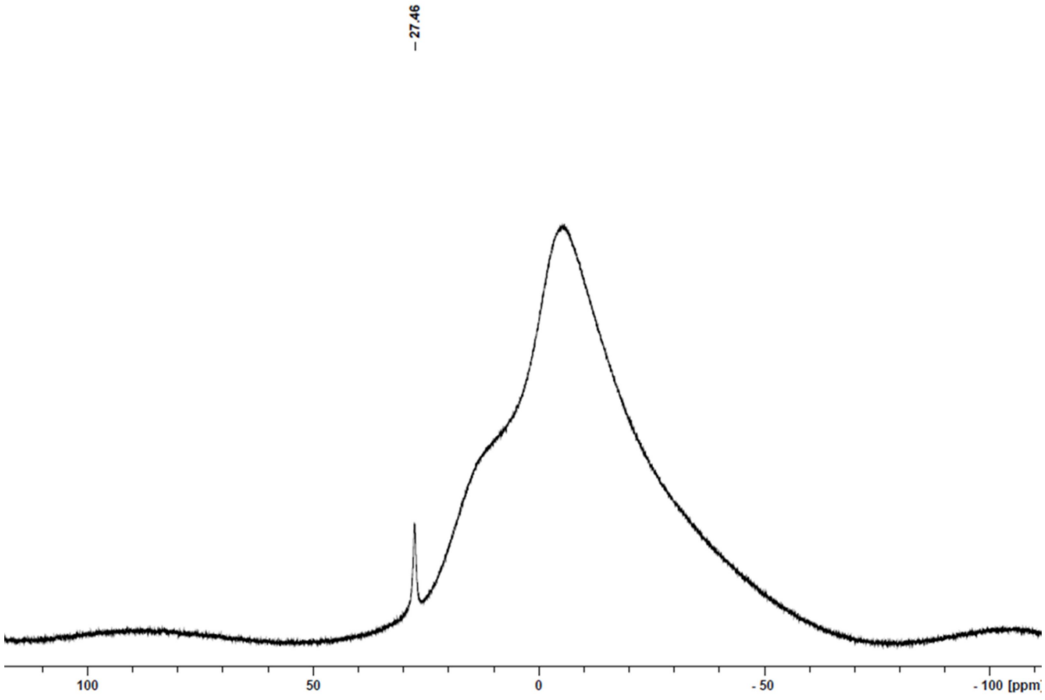

Figure S30. $^{11}B\{^{1}H\}$ NMR spectrum of $[(dmpe)_2Mn(\mu\text{-}H)_2BMes_2]$ (**5**) in d_8-toluene (192 MHz, 298 K).

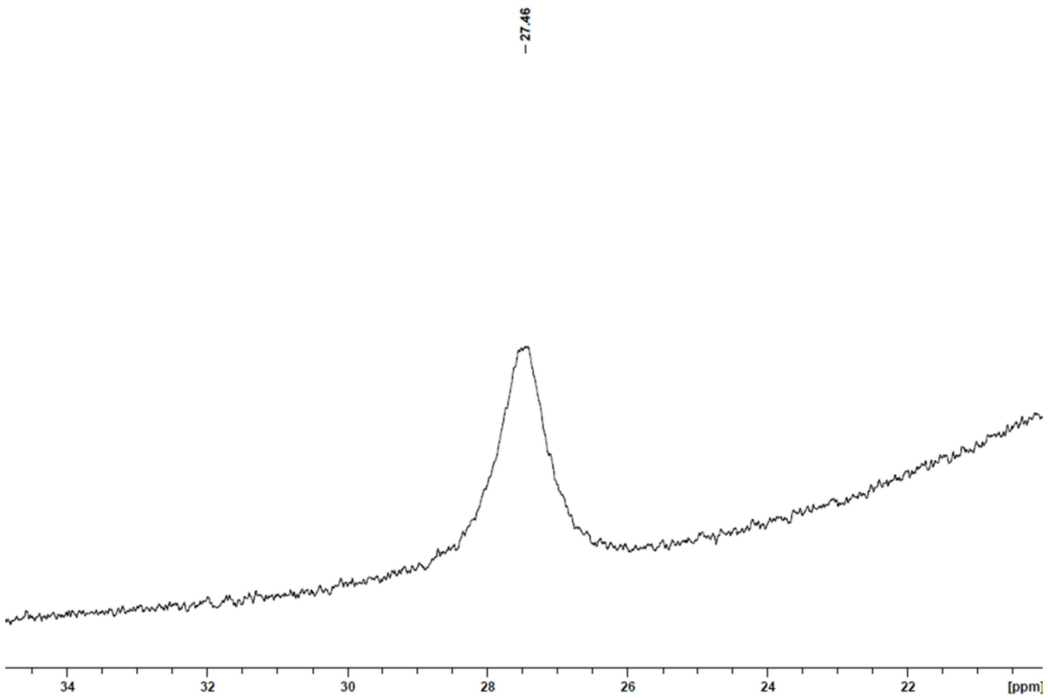

Figure S31. Expanded signal-containing region of the $^{11}B\{^1H\}$ NMR spectrum of $[(dmpe)_2Mn(\mu\text{-}H)_2BMes_2]$ (**5**) in d_8-toluene (192 MHz, 298 K).

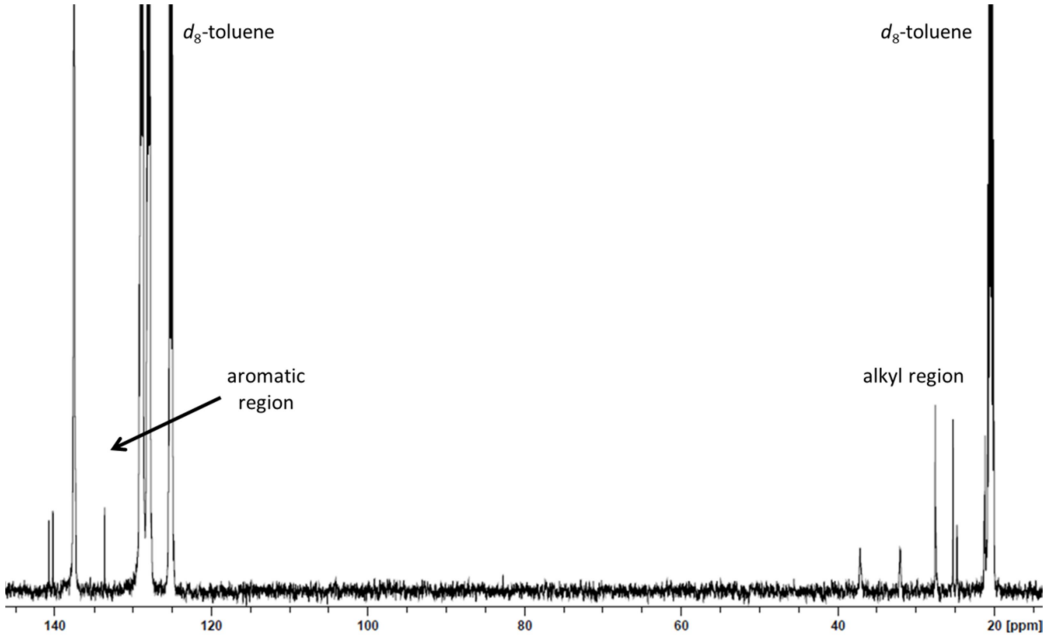

Figure S32. $^{13}C\{^1H\}$ NMR spectrum of $[(dmpe)_2Mn(\mu\text{-}H)_2BMes_2]$ (**5**) in d_8-toluene (151 MHz, 298 K).

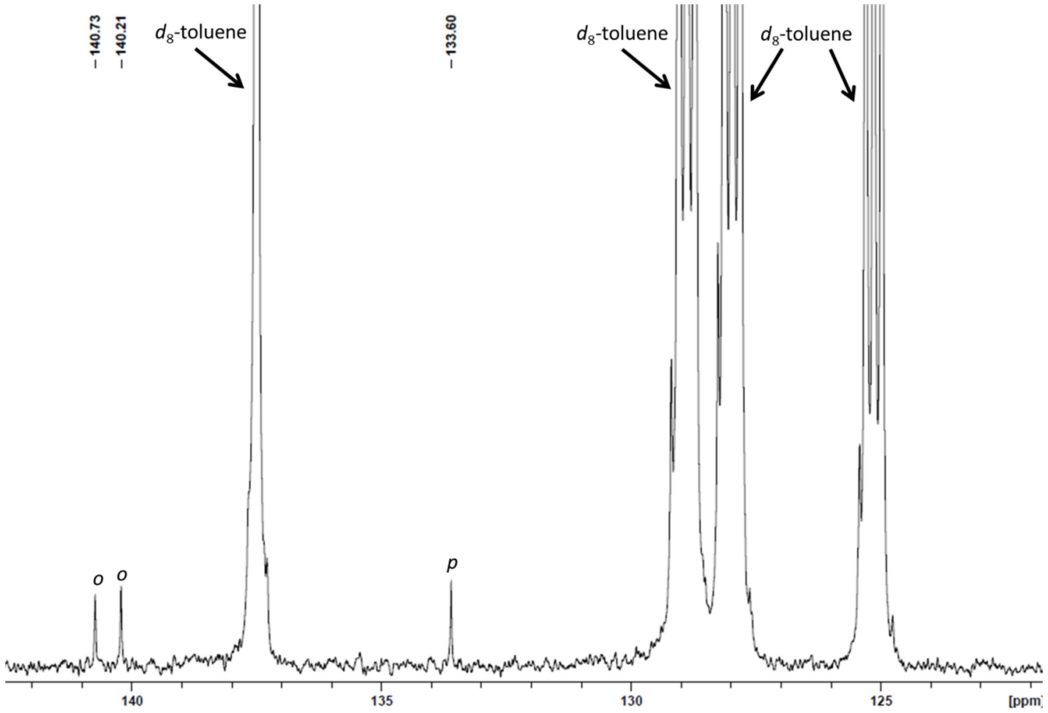

Figure S33. Expanded aromatic region of the $^{13}C\{^1H\}$ NMR spectrum of $[(dmpe)_2Mn(\mu\text{-}H)_2BMes_2]$ (**5**) in d_8-toluene (151 MHz, 298 K).

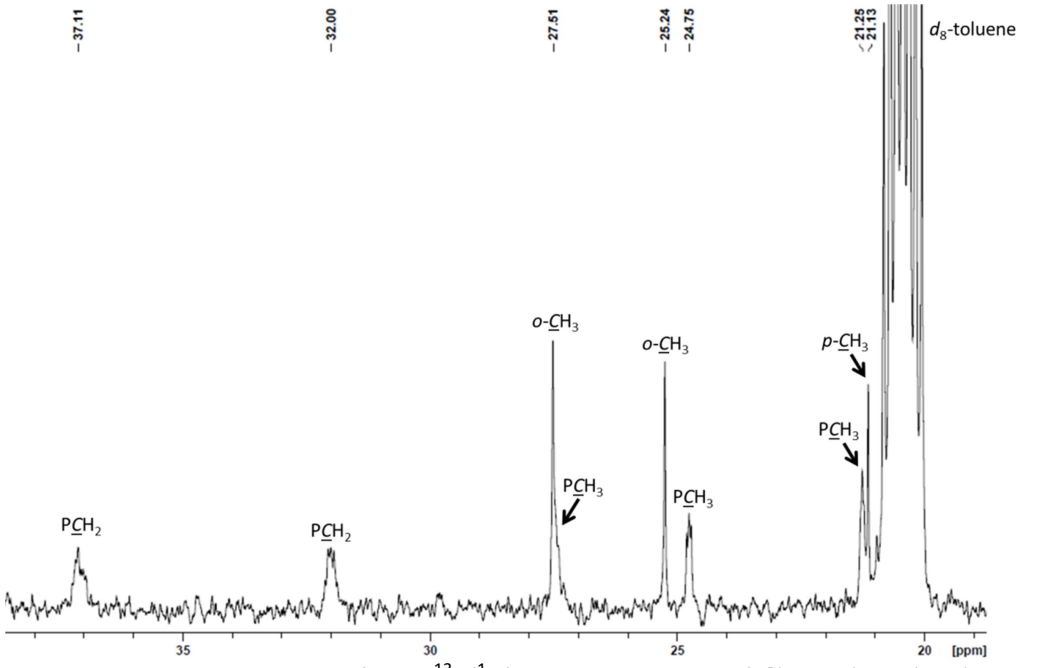

Figure S34. Expanded alkyl region of the $^{13}C\{^1H\}$ NMR spectrum of $[(dmpe)_2Mn(\mu\text{-}H)_2BMes_2]$ (**5**) in d_8-toluene (151 MHz, 298 K).

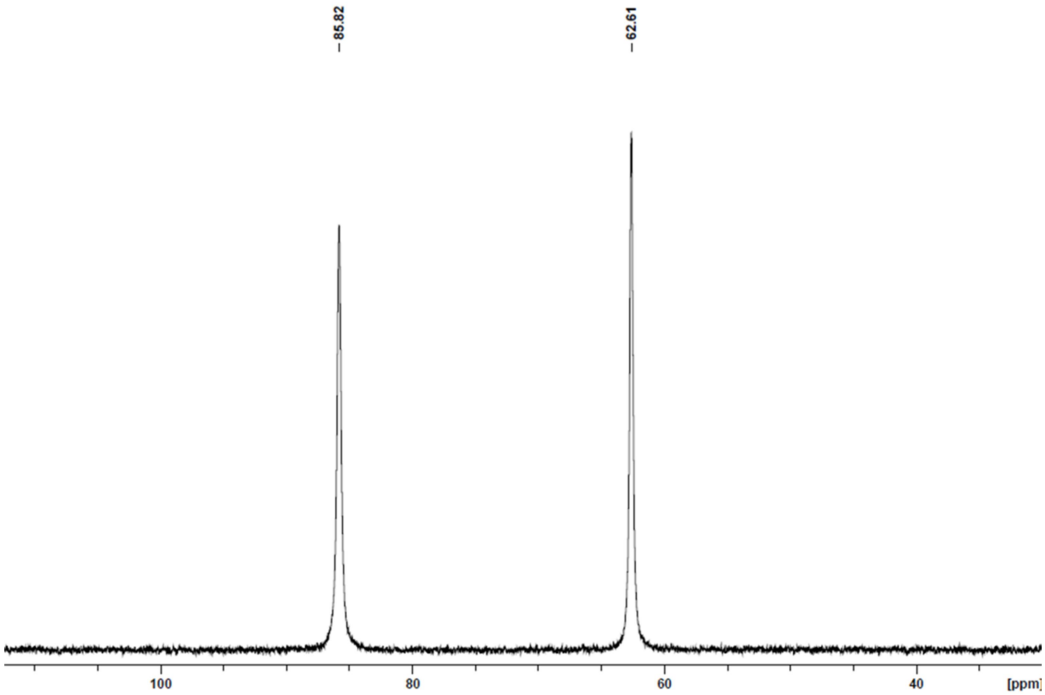

Figure S35. $^{31}P\{^{1}H\}$ NMR spectrum of $[(dmpe)_2Mn(\mu\text{-}H)_2BMes_2]$ (**5**) in d_8-toluene (243 MHz, 298 K).

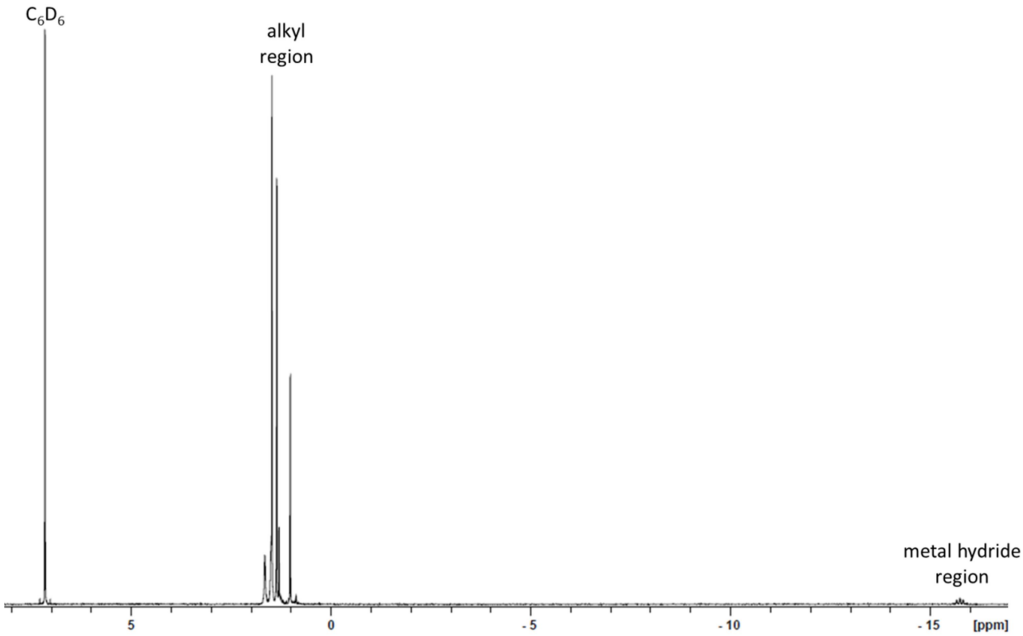

Figure S36. ^{1}H NMR spectrum of *trans*,*trans*-[{$(dmpe)_2MnH\}_2$(μ-dmpe)] (***trans*,*trans*-6**) in C_6D_6 (600 MHz, 298 K).

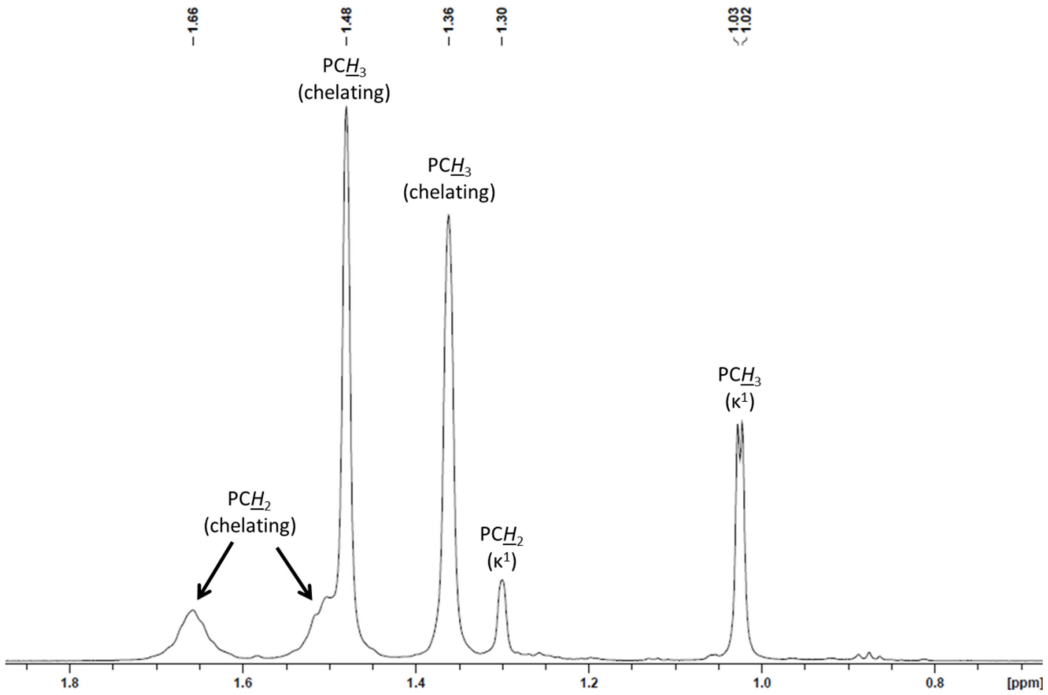

Figure S37. Expanded alkyl region of the ^{1}H NMR spectrum of *trans*,*trans*-[{(dmpe)$_2$MnH}$_2$(μ-dmpe)] (***trans*,*trans*-6**) in C_6D_6 (600 MHz, 298 K).

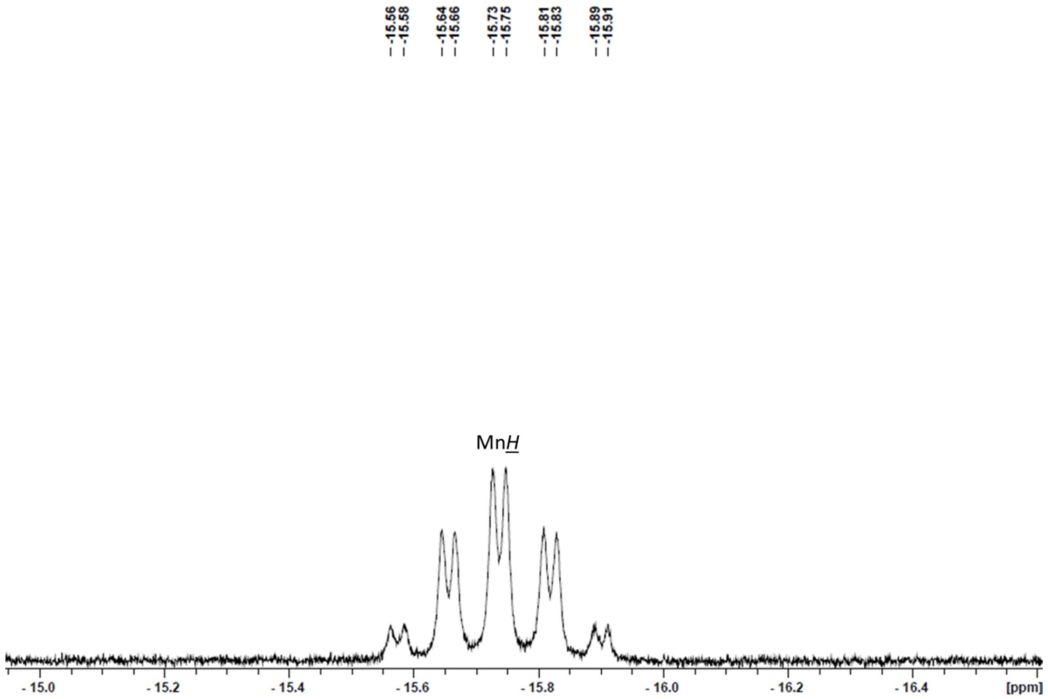

Figure S38. Expanded Mn*H* region of the ^{1}H NMR spectrum of *trans*,*trans*-[{(dmpe)$_2$MnH}$_2$(μ-dmpe)] (***trans*,*trans*-6**) in C_6D_6 (600 MHz, 298 K).

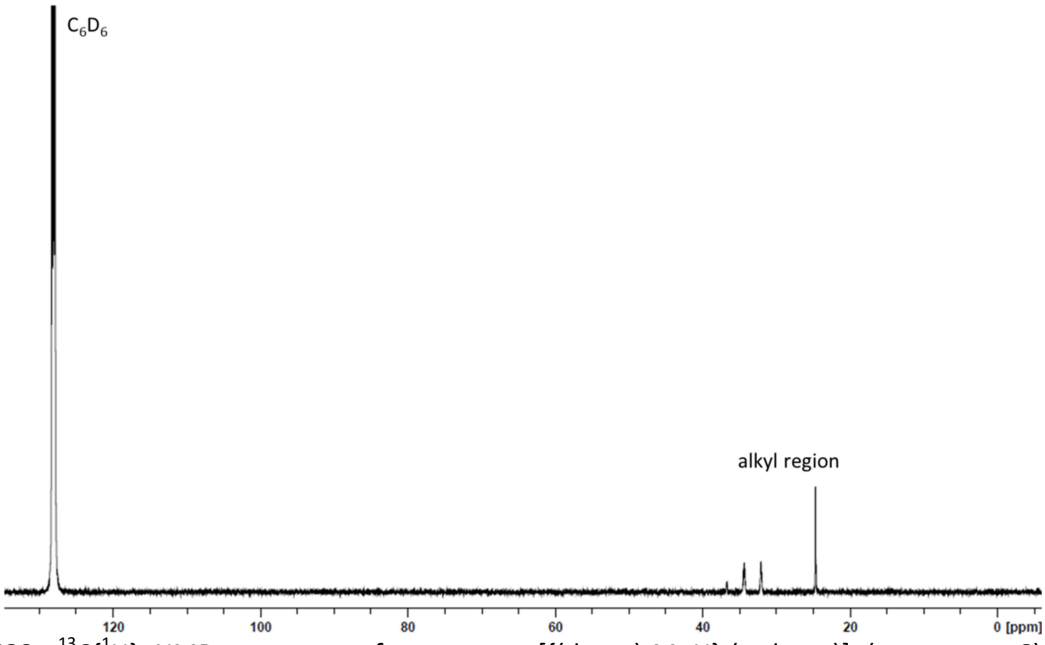

Figure S39. $^{13}C\{^{1}H\}$ NMR spectrum of *trans,trans*-[{(dmpe)$_2$MnH}$_2$(μ-dmpe)] (***trans,trans*-6**) in C_6D_6 (126 MHz, 298 K).

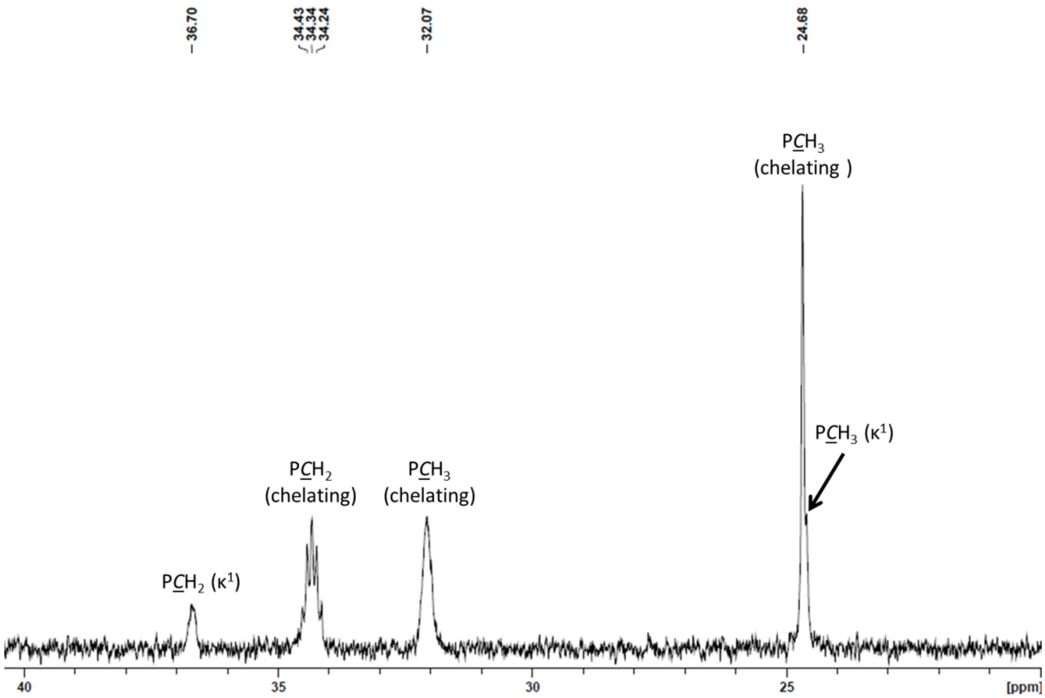

Figure S40. Expanded alkyl region of the $^{13}C\{^{1}H\}$ NMR spectrum of *trans,trans*-[{(dmpe)$_2$MnH}$_2$(μ-dmpe)] (***trans,trans*-6**) in C_6D_6 (126 MHz, 298 K).

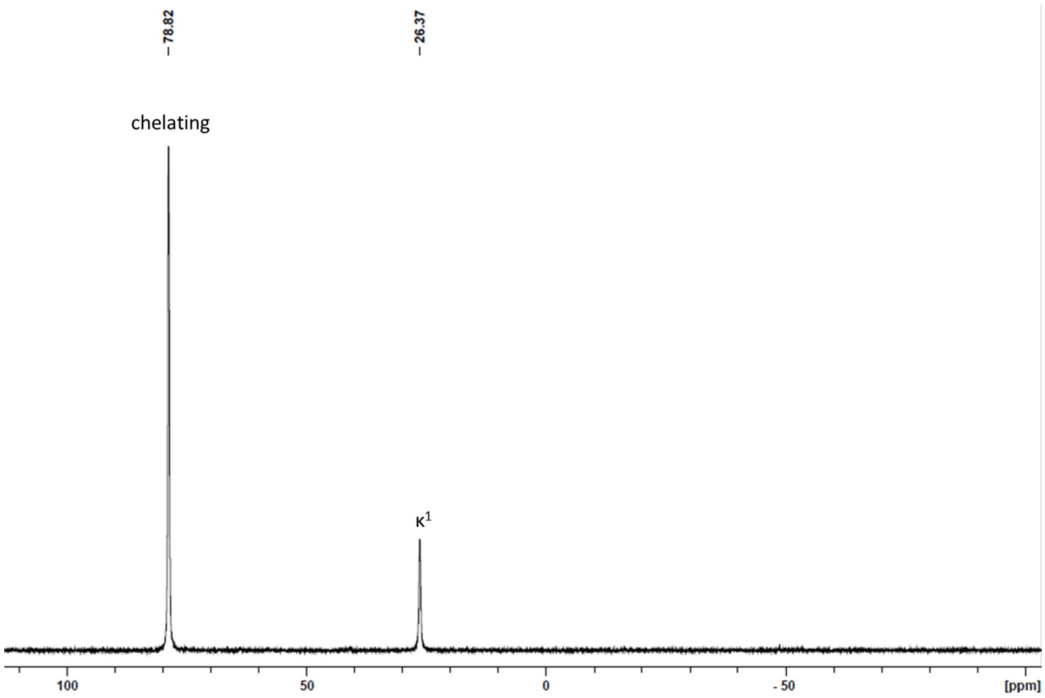

Figure S41. $^{31}P\{^{1}H\}$ NMR spectrum of *trans*,*trans*-[{(dmpe)$_2$MnH}$_2$(μ-dmpe)] (***trans*,*trans*-6**) in C_6D_6 (243 MHz, 298 K).

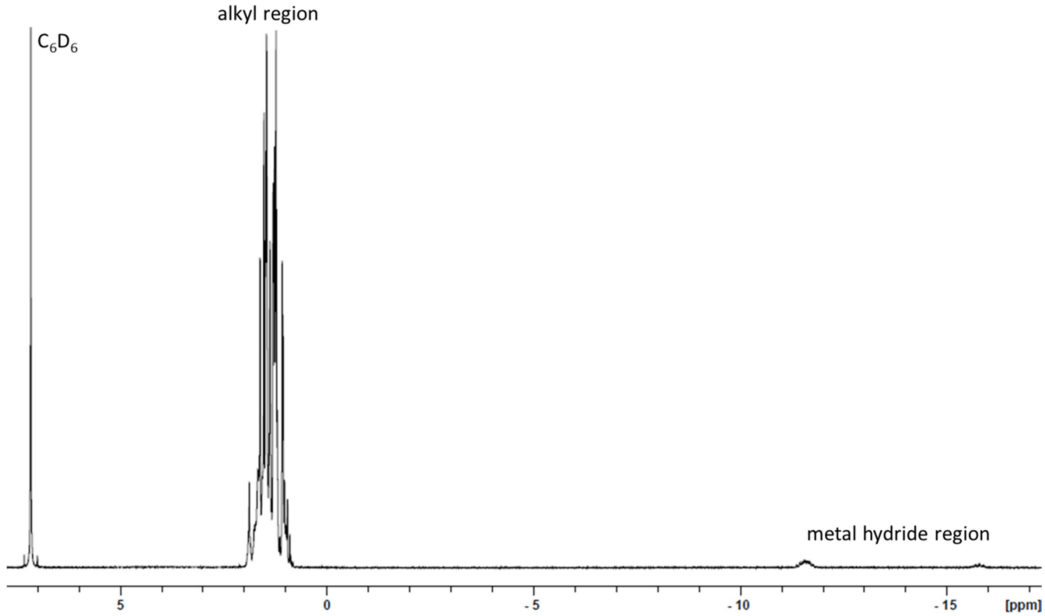

Figure S42. ^{1}H NMR spectrum of a solution containing *cis*-containing [{(dmpe)$_2$MnH}$_2$(μ-dmpe)] (***cis*-containing 6**) generated by exposing a solution of *trans*,*trans*-[{(dmpe)$_2$MnH}$_2$(μ-dmpe)] (***trans*,*trans*-6**) in C_6D_6 to light at room temperature for 25 hours (500 MHz, 298 K).

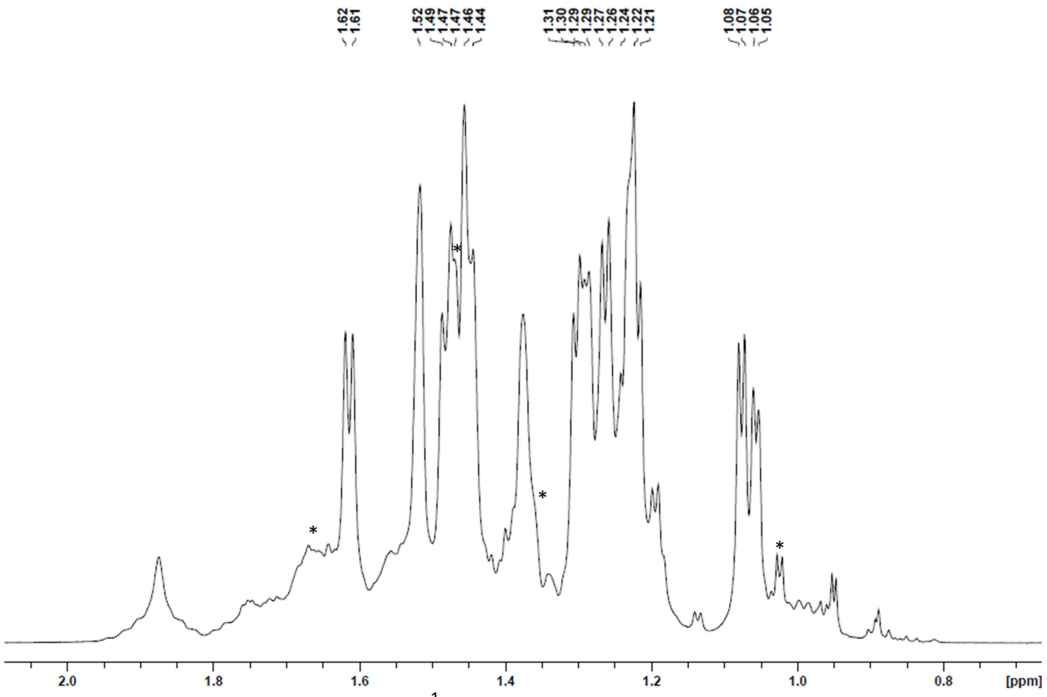

Figure S43. Expanded alkyl region of the ^{1}H NMR spectrum of a solution containing *cis*-containing [{(dmpe)$_2$MnH}$_2$(μ-dmpe)] (***cis*-containing 6**) generated by exposing a solution of *trans*,*trans*-[{(dmpe)$_2$MnH}$_2$(μ-dmpe)] (***trans*,*trans*-6**) in C_6D_6 to light at room temperature for 25 hours (500 MHz, 298 K). * indicates peaks from ***trans*,*trans*-6**.

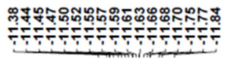

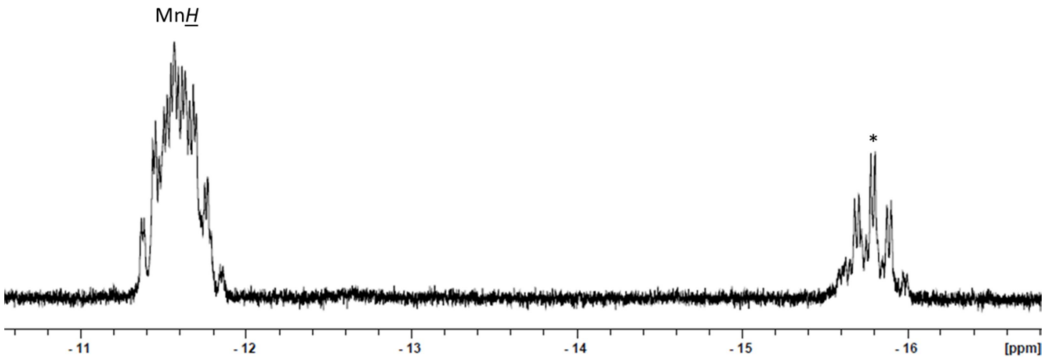

Figure S44. Expanded Mn*H* region of the ^{1}H NMR spectrum of a solution containing *cis*-containing [{(dmpe)$_2$MnH}$_2$(μ-dmpe)] (***cis*-containing 6**) generated by exposing a solution of *trans*,*trans*-[{(dmpe)$_2$MnH}$_2$(μ-dmpe)] (***trans*,*trans*-6**) in C_6D_6 to light at room temperature for 25 hours (500 MHz, 298 K). Mn*H* indicates a peak from ***cis*-containing 6**, and * indicates a peak from ***trans*,*trans*-6**.

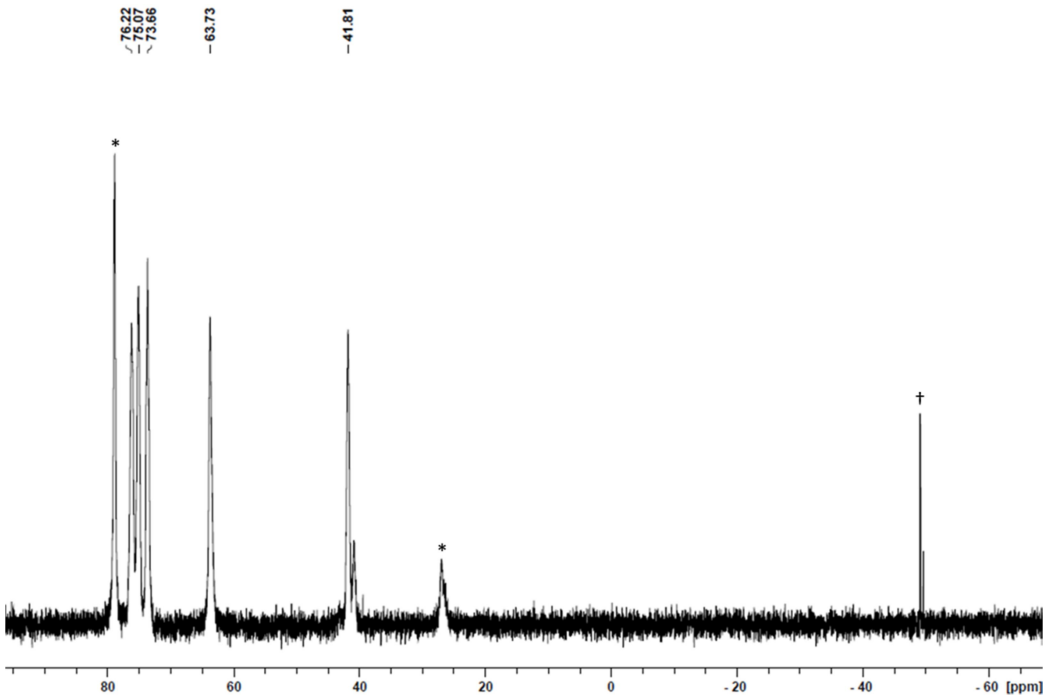

Figure S45. $^{31}P\{^{1}H\}$ NMR spectrum of a solution containing *cis*-containing $[\{(dmpe)_2MnH\}_2(\mu\text{-dmpe})]$ (***cis*-containing 6**) generated by exposing a solution of *trans*,*trans*-$[\{(dmpe)_2MnH\}_2(\mu\text{-dmpe})]$ (***trans*,*trans*-6**) in C_6D_6 to light at room temperature for 25 hours (202 MHz, 298 K). * indicates peaks from ***trans*,*trans*-6**, and † indicates a peak from an impurity of ***trans*-7**.

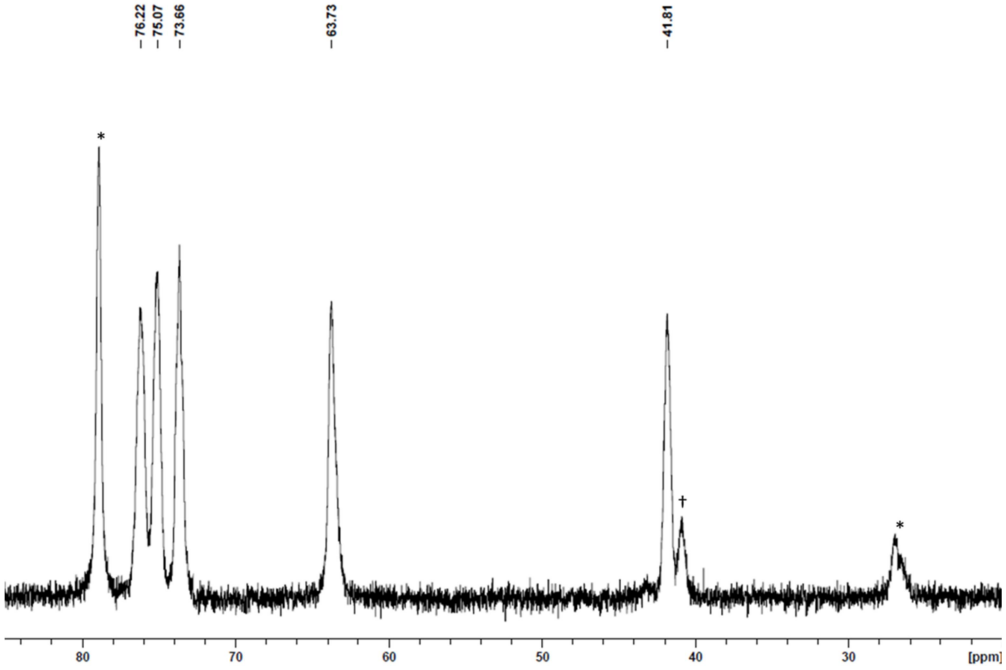

Figure S46. Zoomed in $^{31}P\{^{1}H\}$ NMR spectrum of a solution *cis*-containing $[\{(dmpe)_2MnH\}_2(\mu\text{-dmpe})]$ (***cis*-containing 6**) generated by exposing a solution of *trans*,*trans*-$[\{(dmpe)_2MnH\}_2(\mu\text{-dmpe})]$ (***trans*,*trans*-6**) in C_6D_6 to light at room temperature for 25 hours (202 MHz, 298 K). * indicates peaks from ***trans*,*trans*-6**, and † indicates a peak from an unidentified impurity.

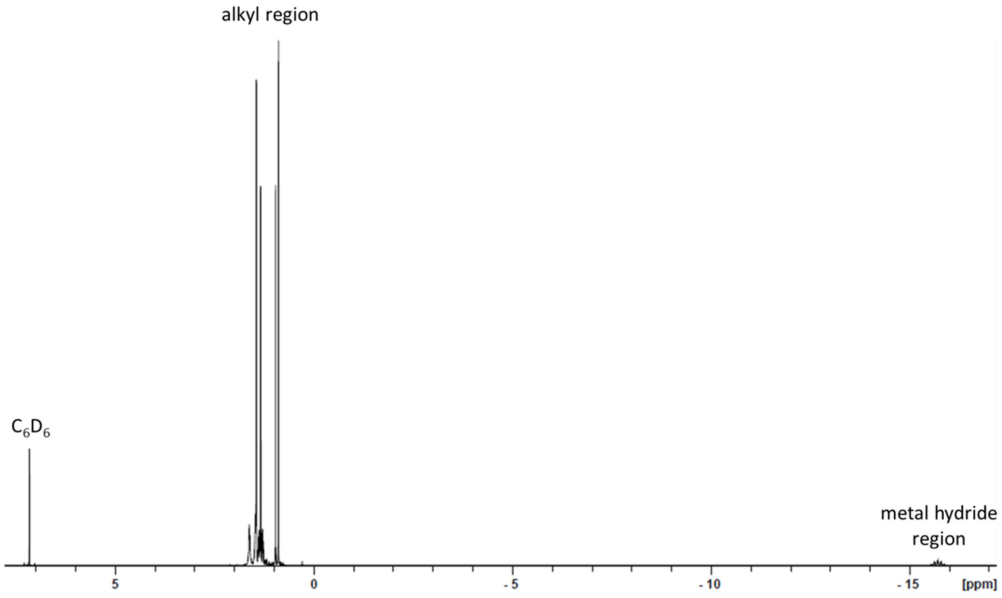

Figure S47. ^{1}H NMR spectrum of *trans*-[(dmpe)$_2$MnH(κ$_1$-dmpe)] (***trans*-7**) in C_6D_6 (600 MHz, 298 K).

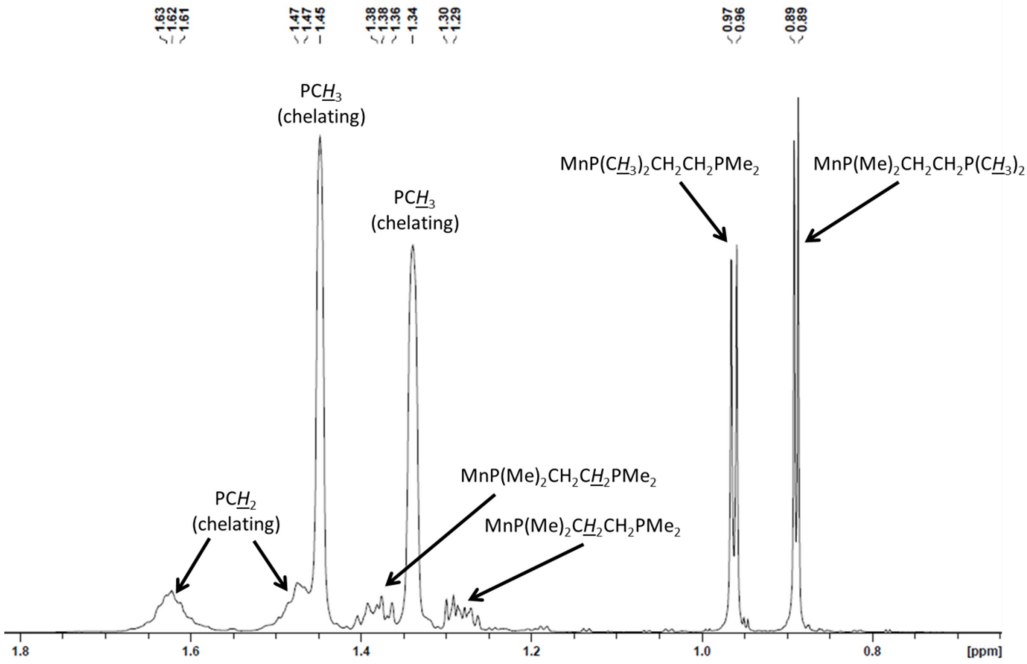

Figure S48. Expanded alkyl region of the ^{1}H NMR spectrum of *trans*-[(dmpe)$_2$MnH(κ$_1$-dmpe)] (***trans*-7**) in C_6D_6 (600 MHz, 298 K).

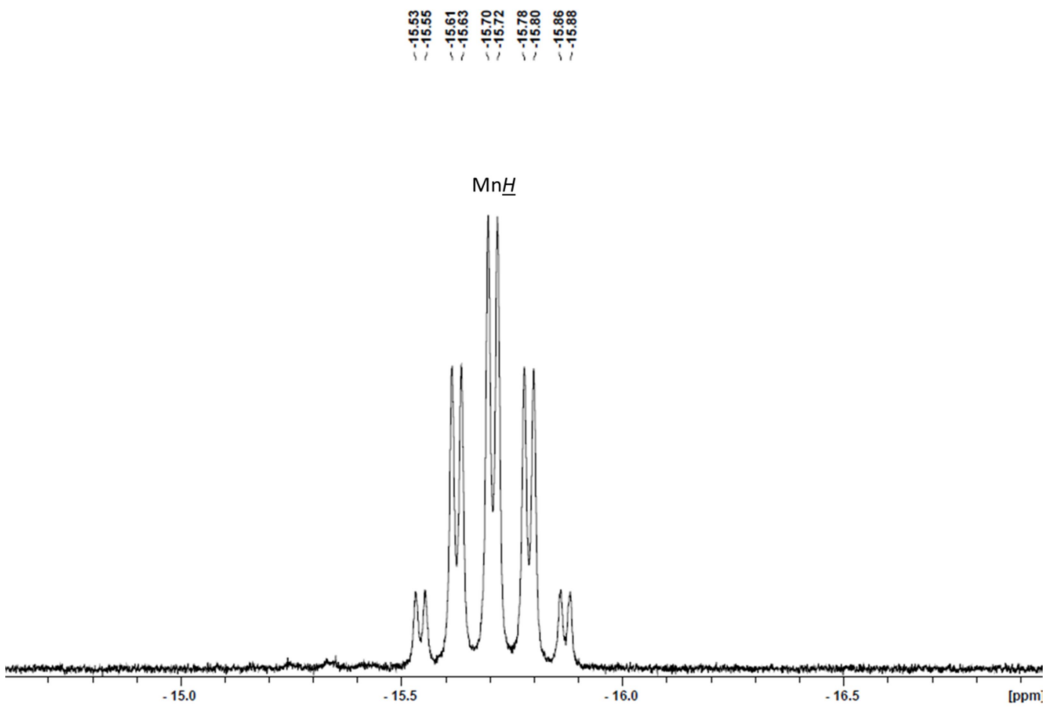

Figure S49. Expanded Mn*H* region of the ^{1}H NMR spectrum of *trans*-[(dmpe)$_2$MnH(κ$_1$-dmpe)] (***trans*-7**) in C_6D_6 (600 MHz, 298 K).

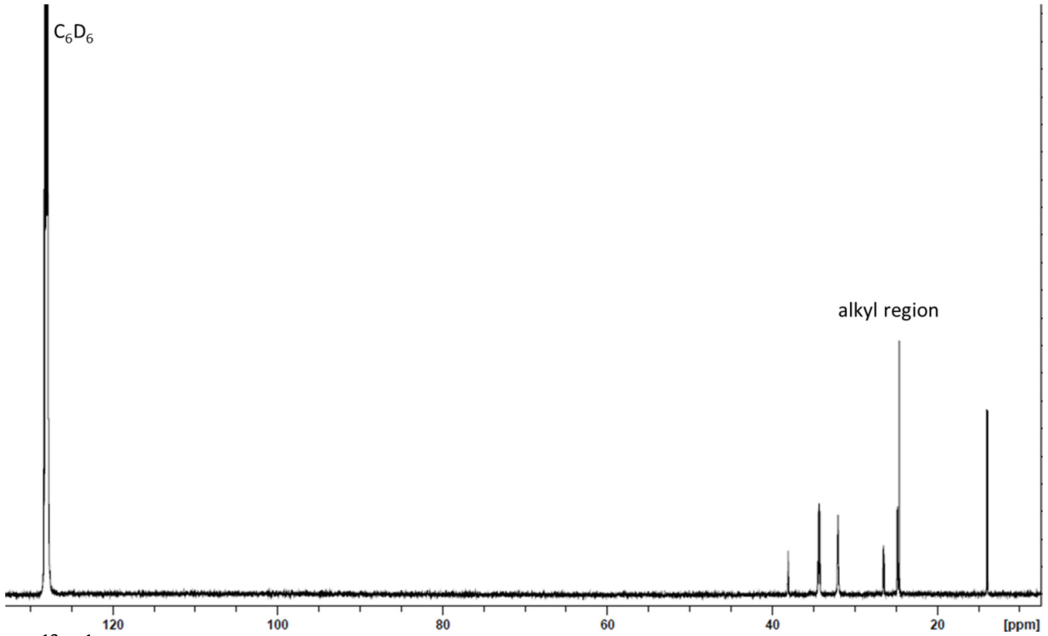

Figure S50. ^{13}C{^{1}H} NMR spectrum of *trans*-[(dmpe)$_2$MnH(κ$_1$-dmpe)] (***trans*-7**) in C_6D_6 (151 MHz, 298 K).

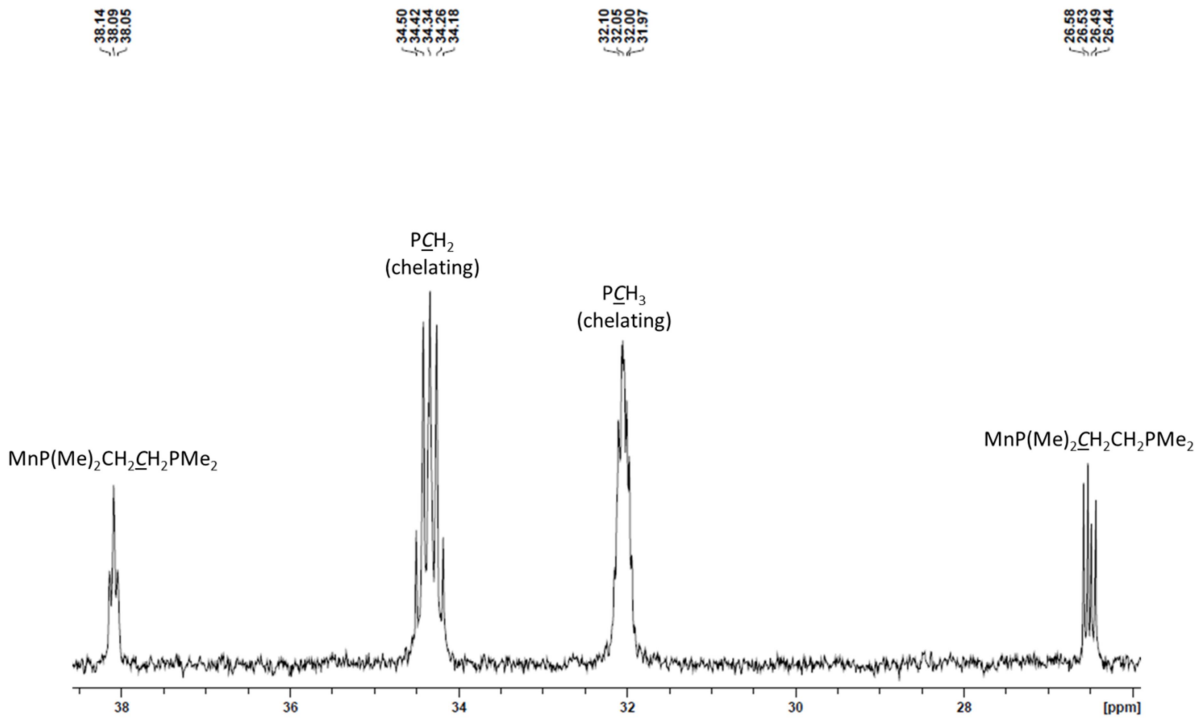

Figure S51. Expanded high frequency portion of the alkyl region of the $^{13}C\{^{1}H\}$ NMR spectrum of *trans*-[(dmpe)$_2$MnH(κ$_1$-dmpe)] (***trans*-7**) in C_6D_6 (151 MHz, 298 K).

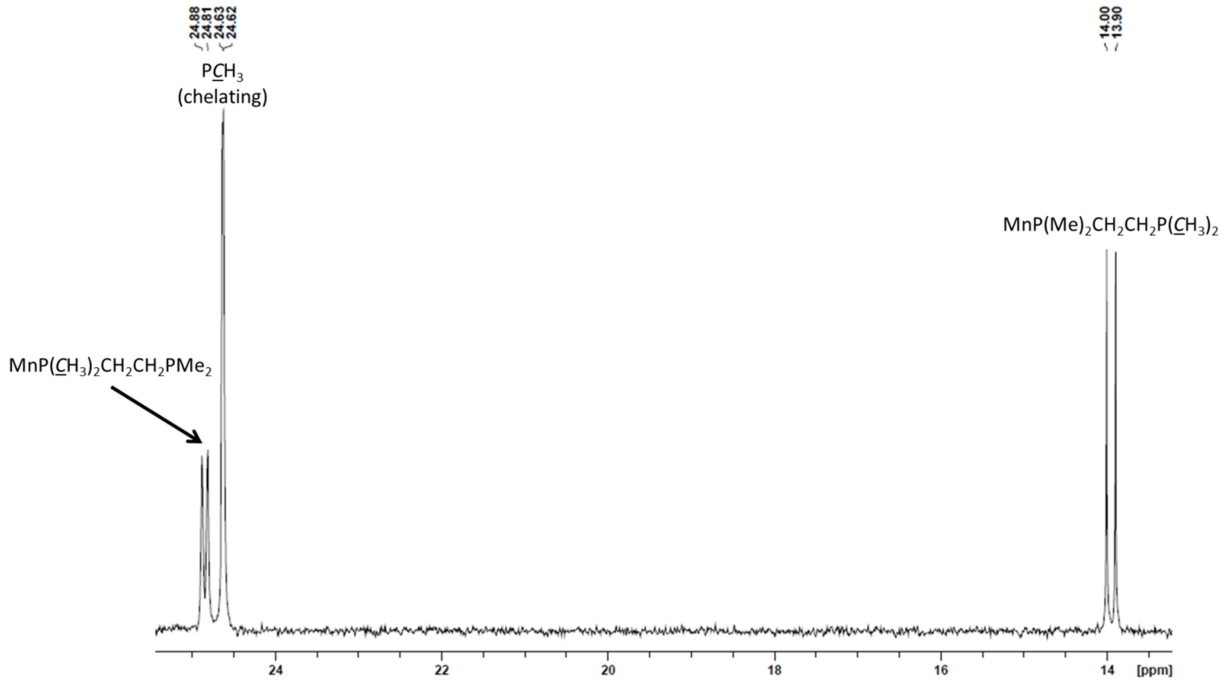

Figure S52. Expanded low frequency portion of the alkyl region of the $^{13}C\{^{1}H\}$ NMR spectrum of *trans*-[(dmpe)$_2$MnH(κ$_1$-dmpe)] (***trans*-7**) in C_6D_6 (151 MHz, 298 K).

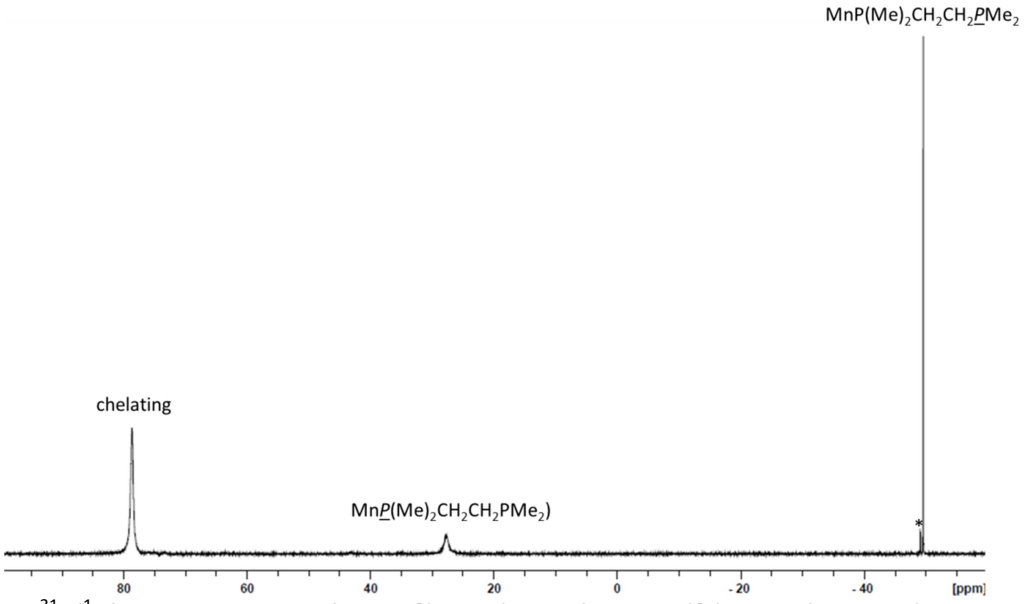

Figure S53. $^{31}P\{^{1}H\}$ NMR spectrum of *trans*-[(dmpe)$_2$MnH(κ$_1$-dmpe)] (***trans*-7**) in C_6D_6 (243 MHz, 298 K).

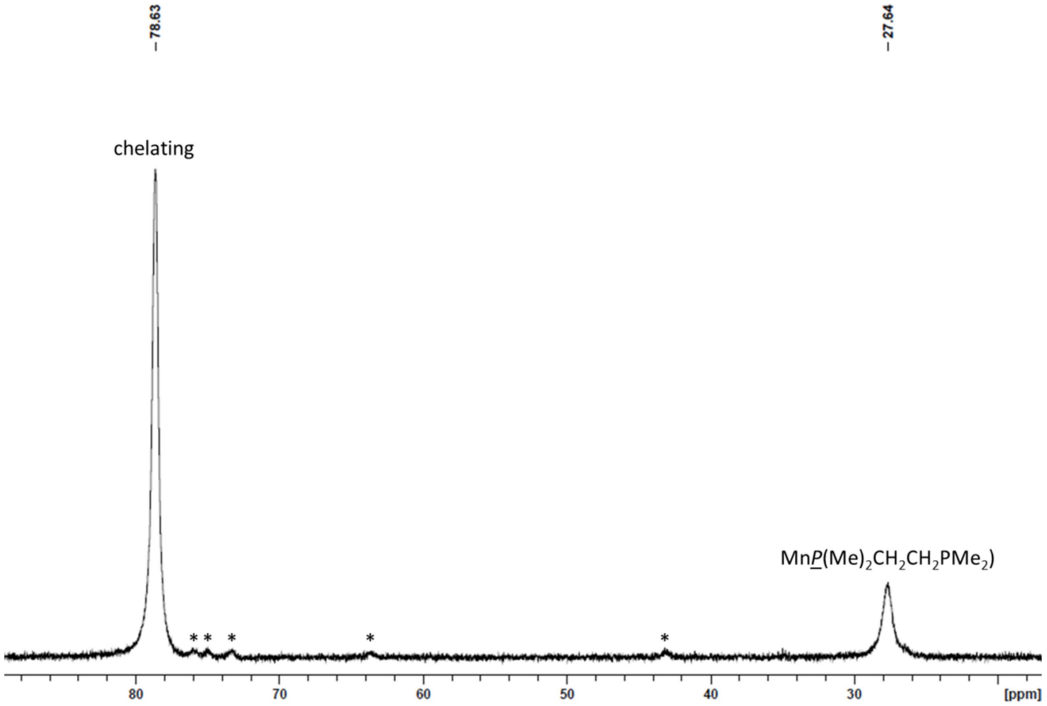

Figure S54. Expanded Mn*P* region of the $^{31}P\{^{1}H\}$ NMR spectrum of *trans*-[(dmpe)$_2$MnH(κ$_1$-dmpe)] (***trans*-7**) in C_6D_6 (243 MHz, 298 K). * indicates peaks from an impurity of *cis*-[(dmpe)$_2$MnH(κ$_1$-dmpe)] (***cis*-7**).

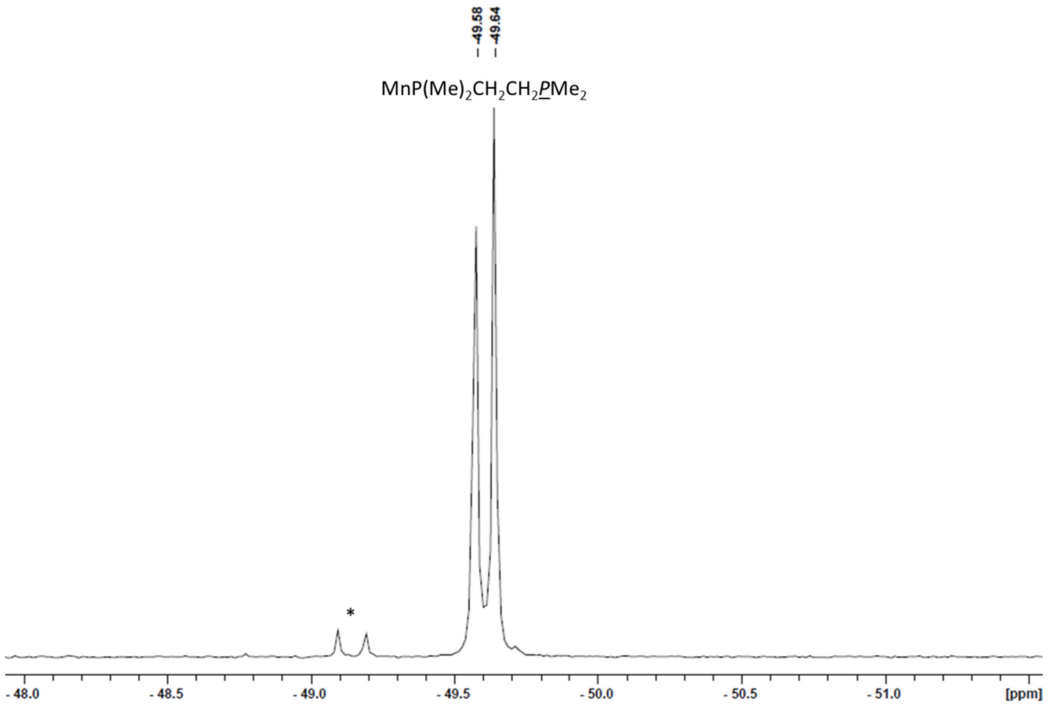

Figure S55. Expanded free phosphine region of the $^{31}P\{^{1}H\}$ NMR spectrum of *trans*-[(dmpe)$_2$MnH(κ$_1$-dmpe)] (***trans*-7**) in C_6D_6 (243 MHz, 298 K). * indicates a peak from an impurity of *cis*-[(dmpe)$_2$MnH(κ$_1$-dmpe)] (***cis*-7**).

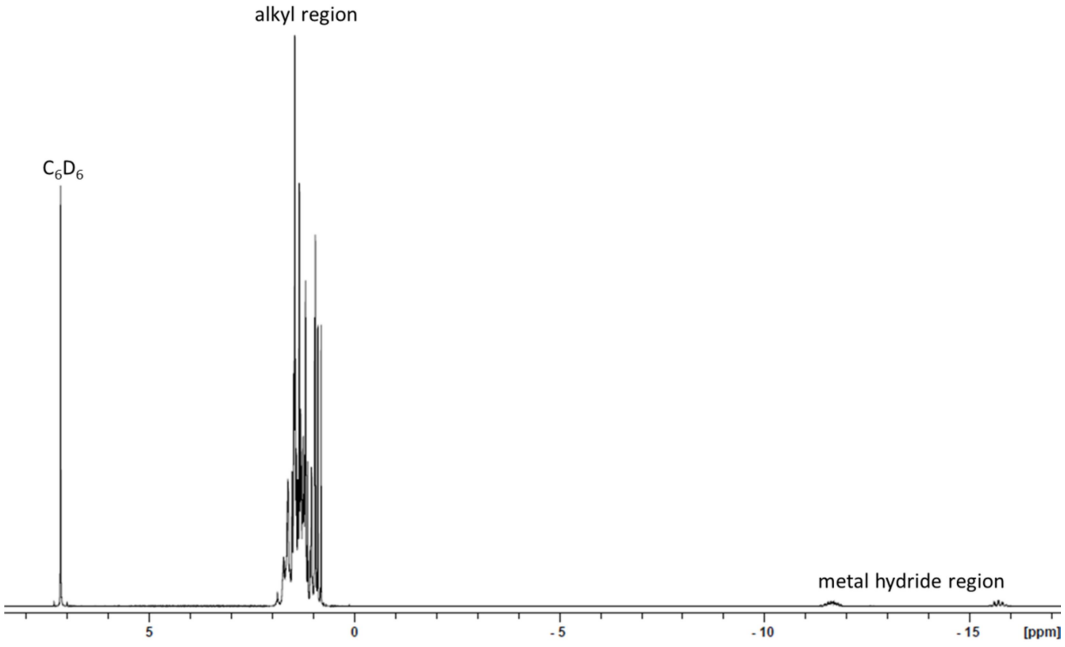

Figure S56. ^{1}H NMR spectrum of a solution containing *cis*-[(dmpe)$_2$MnH(κ$_1$-dmpe)] (***cis*-7**) generated by exposing a solution of *trans*-[(dmpe)$_2$MnH(κ$_1$-dmpe)] (***trans*-7**) in C_6D_6 to light at room temperature for 25 hours (500 MHz, 298 K).

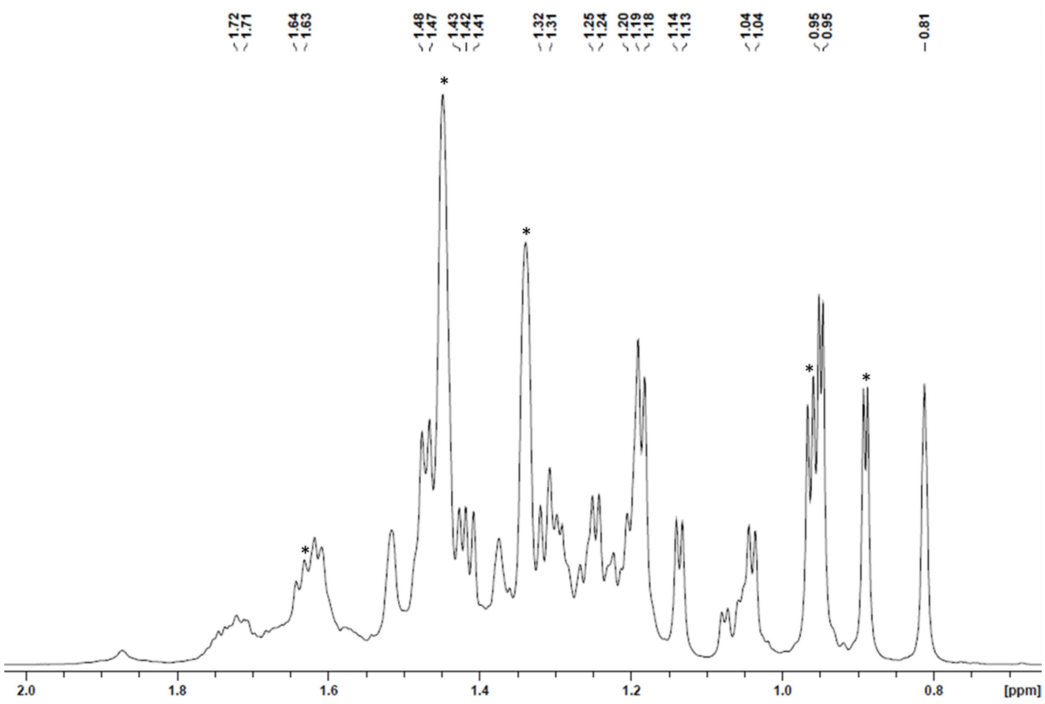

Figure S57. Expanded alkyl region of the ^{1}H NMR spectrum of a solution containing *cis*-[(dmpe)$_2$MnH(κ$_1$-dmpe)] (***cis*-7**) generated by exposing a solution of *trans*-[(dmpe)$_2$MnH(κ$_1$-dmpe)] (***trans*-7**) in C_6D_6 to light at room temperature for 25 hours (500 MHz, 298 K). * indicates peaks from ***trans*-7**.

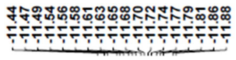

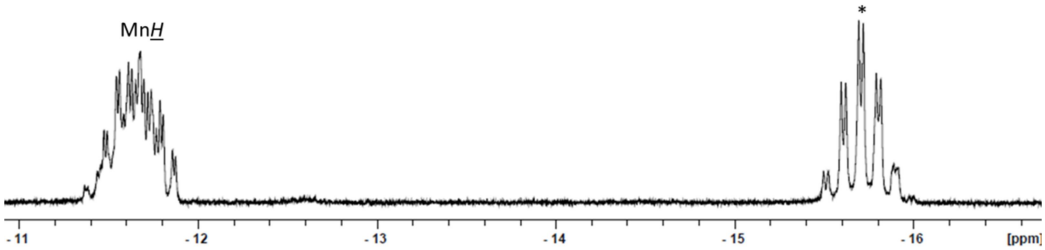

Figure S58. Expanded Mn*H* region of the ^{1}H NMR spectrum of a solution containing *cis*-[(dmpe)$_2$MnH(κ$_1$-dmpe)] (***cis*-7**) generated by exposing a solution of *trans*-[(dmpe)$_2$MnH(κ$_1$-dmpe)] (***trans*-7**) in C_6D_6 to light at room temperature for 25 hours (500 MHz, 298 K). * indicates a peak from ***trans*-7**.

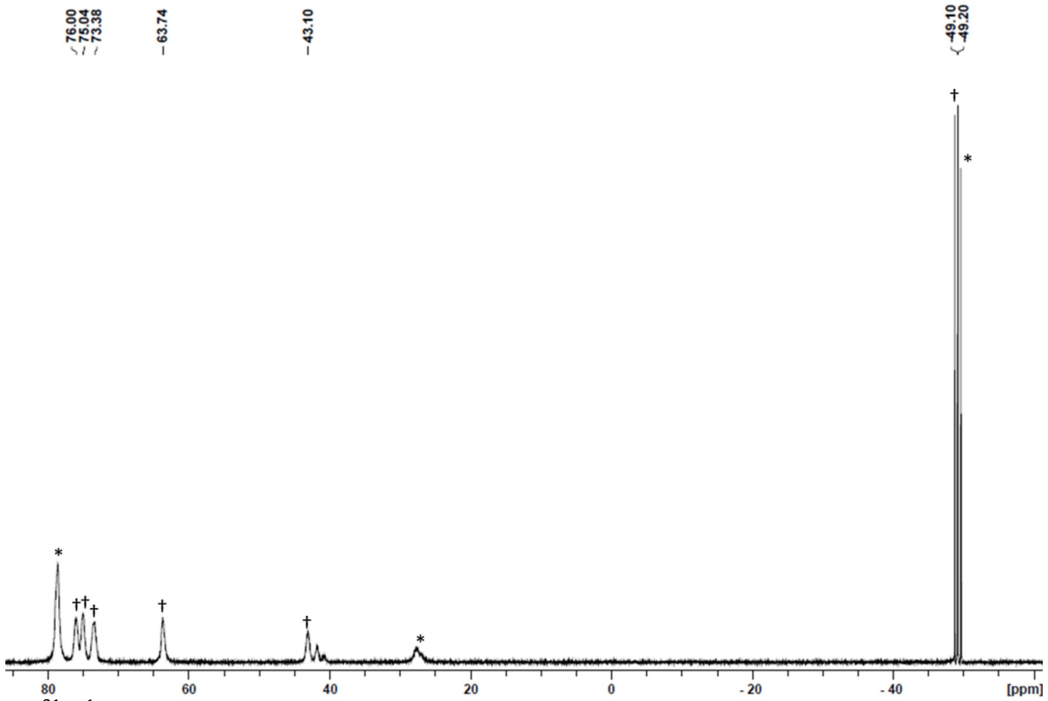

Figure S59. $^{31}P\{^{1}H\}$ NMR spectrum of a solution containing *cis*-[(dmpe)$_2$MnH(κ_1-dmpe)] (***cis*-7**) generated by exposing a solution of *trans*-[(dmpe)$_2$MnH(κ_1-dmpe)] (***trans*-7**) in C_6D_6 to light at room temperature for 25 hours (202 MHz, 298 K). † indicates peaks from ***cis*-7**, and * indicates peaks from ***trans*-7**.

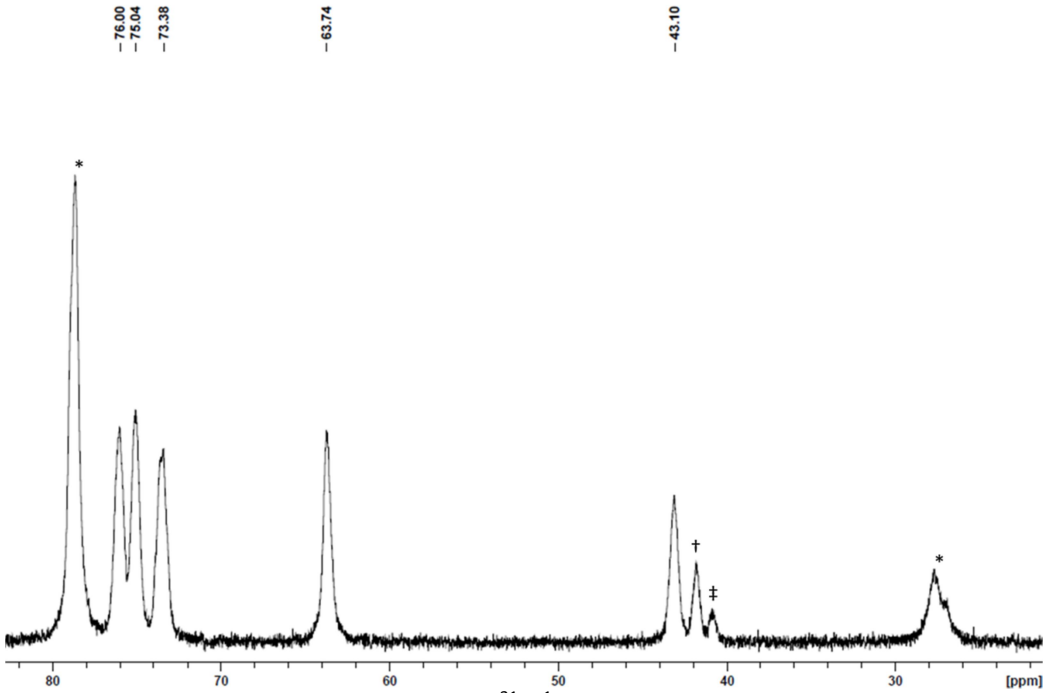

Figure S60. Expanded Mn*P* region of the $^{31}P\{^{1}H\}$ NMR spectrum of a solution containing *cis*-[(dmpe)$_2$MnH(κ_1-dmpe)] (***cis*-7**) generated by exposing a solution of *trans*-[(dmpe)$_2$MnH(κ_1-dmpe)] (***trans*-7**) in C_6D_6 to light at room temperature for 25 hours (202 MHz, 298 K). * indicates peaks from ***trans*-7**, † indicates a peak from ***cis*-containing 6**, and ‡ indicates a peak from an unidentified impurity.

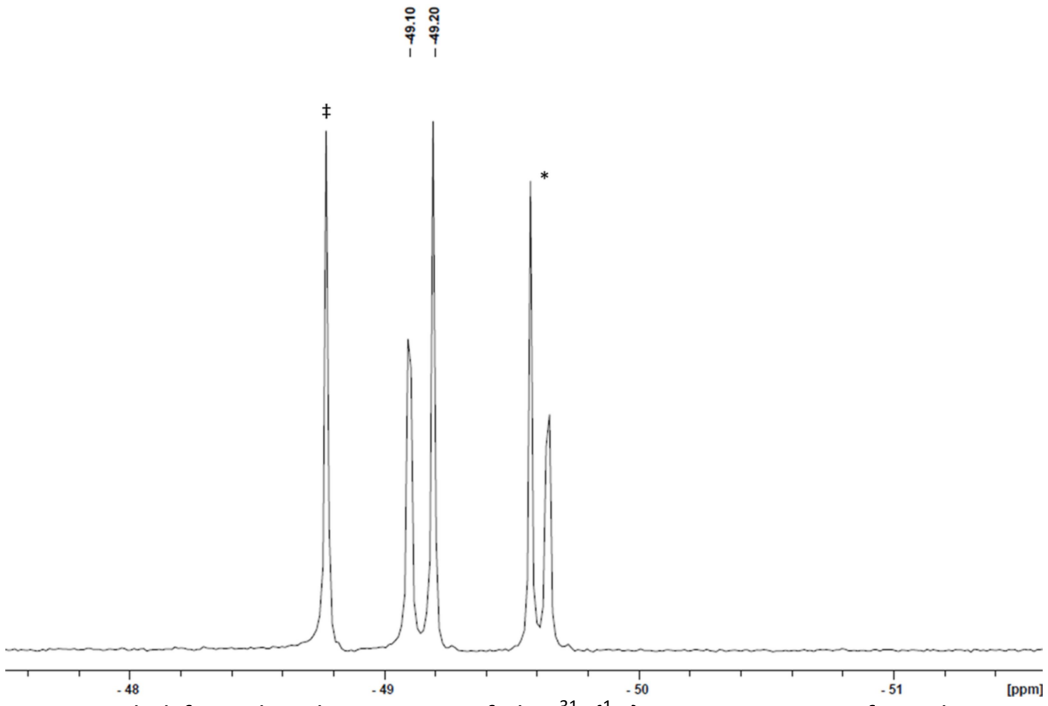

Figure S61. Expanded free phosphine region of the $^{31}P\{^{1}H\}$ NMR spectrum of a solution containing *cis*-[(dmpe)$_2$MnH(κ$_1$-dmpe)] (***cis*-7**) generated by exposing a solution of *trans*-[(dmpe)$_2$MnH(κ$_1$-dmpe)] (***trans*-7**) in C_6D_6 to light at room temperature for 25 hours (202 MHz, 298 K). * indicates a peak from ***trans*-7** and ‡ indicates a peak from an unidentified impurity.

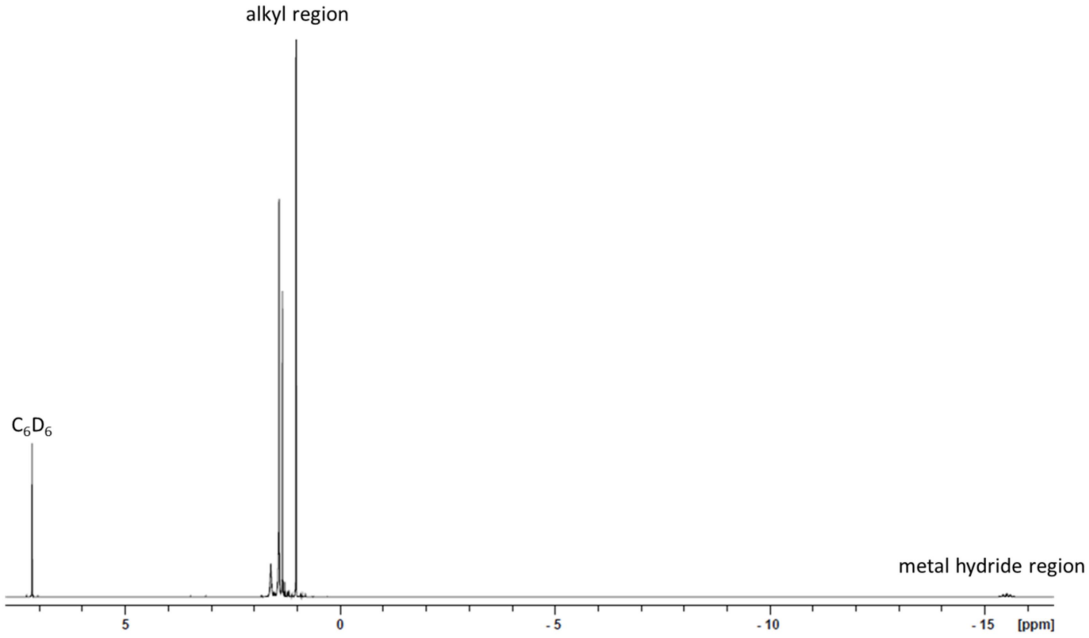

Figure S62. ^{1}H NMR spectrum of *trans*-[(dmpe)$_2$MnH(PMe$_3$)] (***trans*-8**) in C_6D_6 (600 MHz, 298 K).

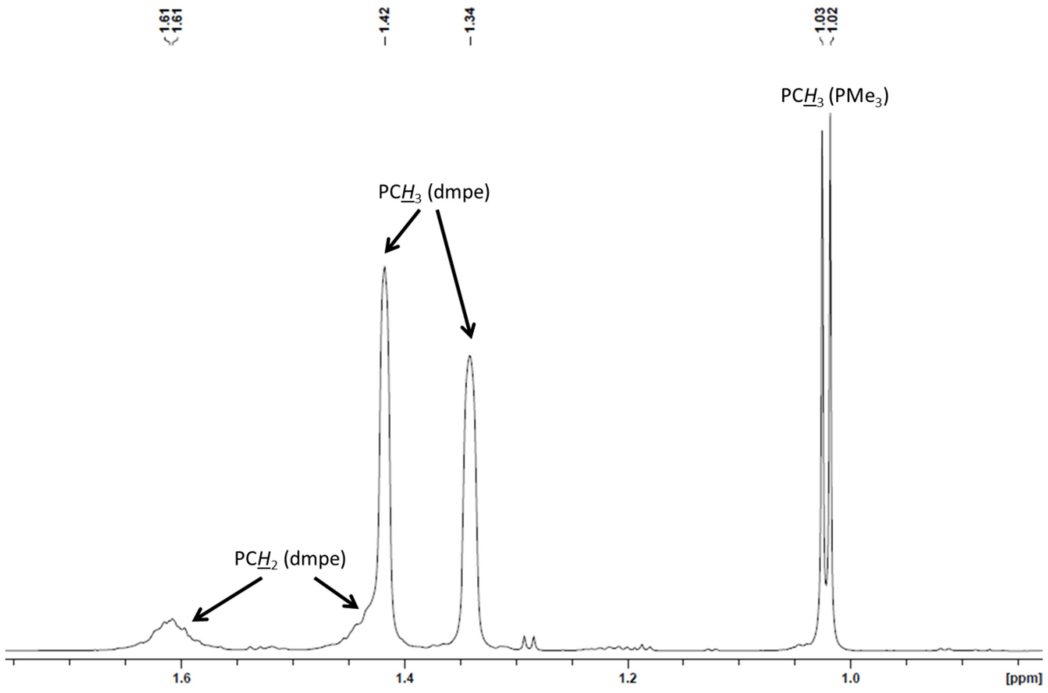

Figure S63. Expanded alkyl region of the ^{1}H NMR spectrum of *trans*-[(dmpe)$_2$MnH(PMe$_3$)] (***trans*-8**) in C_6D_6 (600 MHz, 298 K).

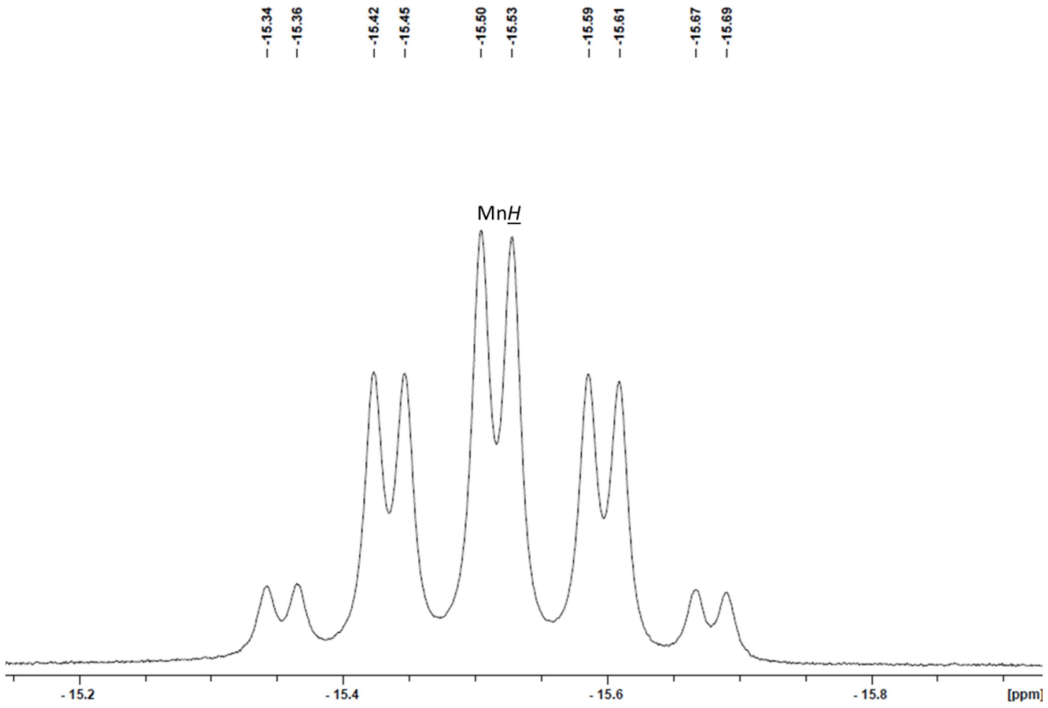

Figure S64. Expanded Mn*H* region of the ^{1}H NMR spectrum of *trans*-[(dmpe)$_2$MnH(PMe$_3$)] (***trans*-8**) in C_6D_6 (600 MHz, 298 K).

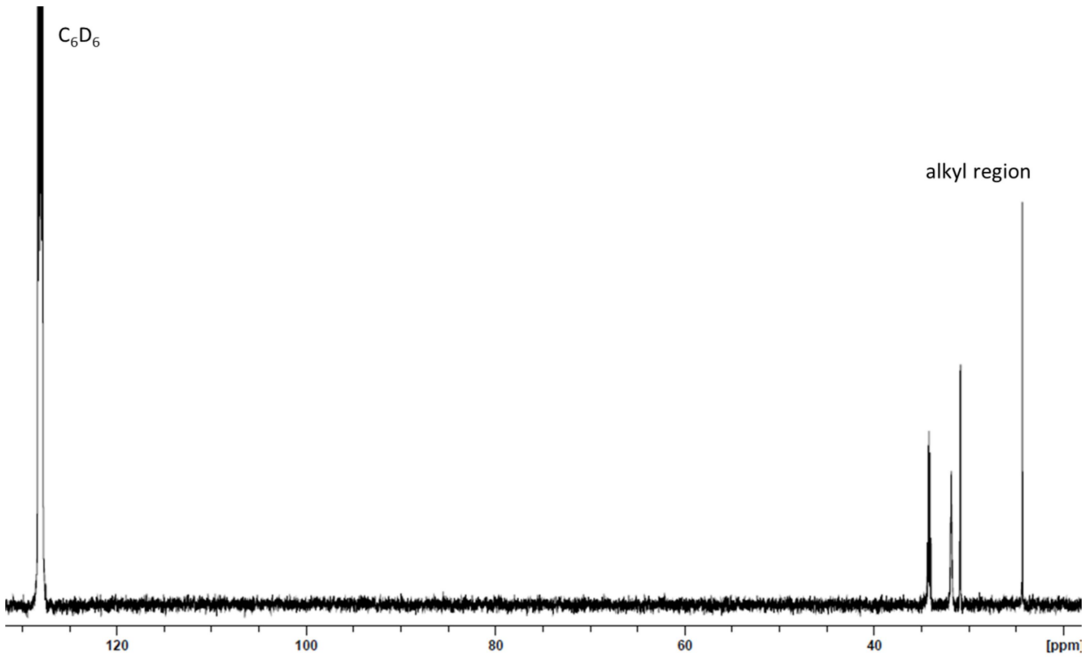

Figure S65. $^{13}C\{^{1}H\}$ NMR spectrum of *trans*-[(dmpe)$_2$MnH(PMe$_3$)] (***trans*-8**) in C_6D_6 (126 MHz, 298 K).

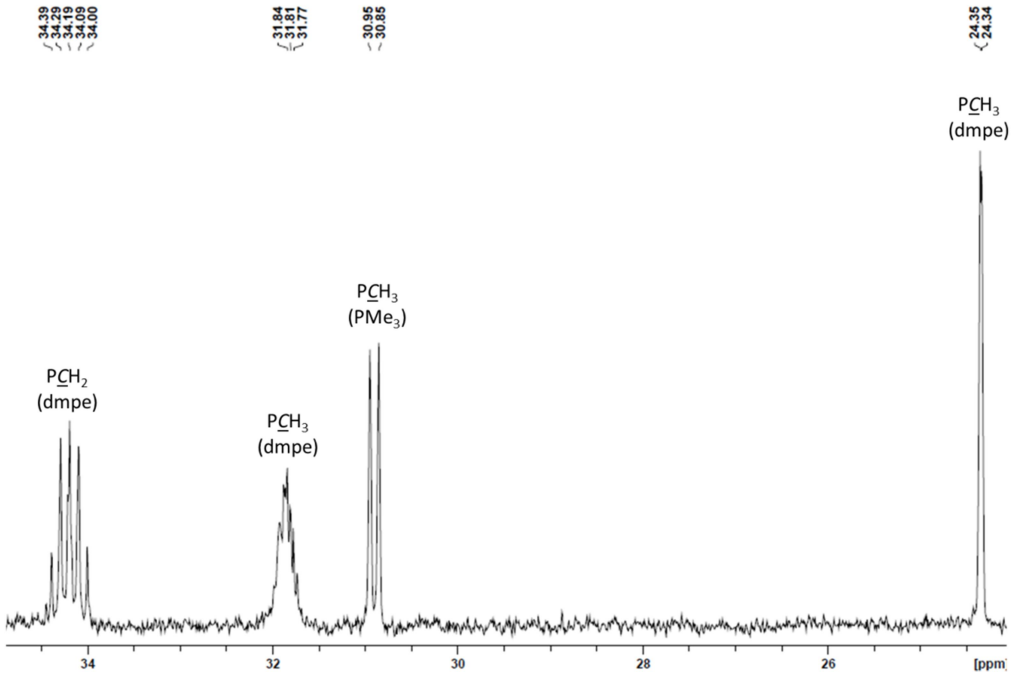

Figure S66. Expanded alkyl region of the $^{13}C\{^{1}H\}$ NMR spectrum of *trans*-[(dmpe)$_2$MnH(PMe$_3$)] (***trans*-8**) in C_6D_6 (126 MHz, 298 K).

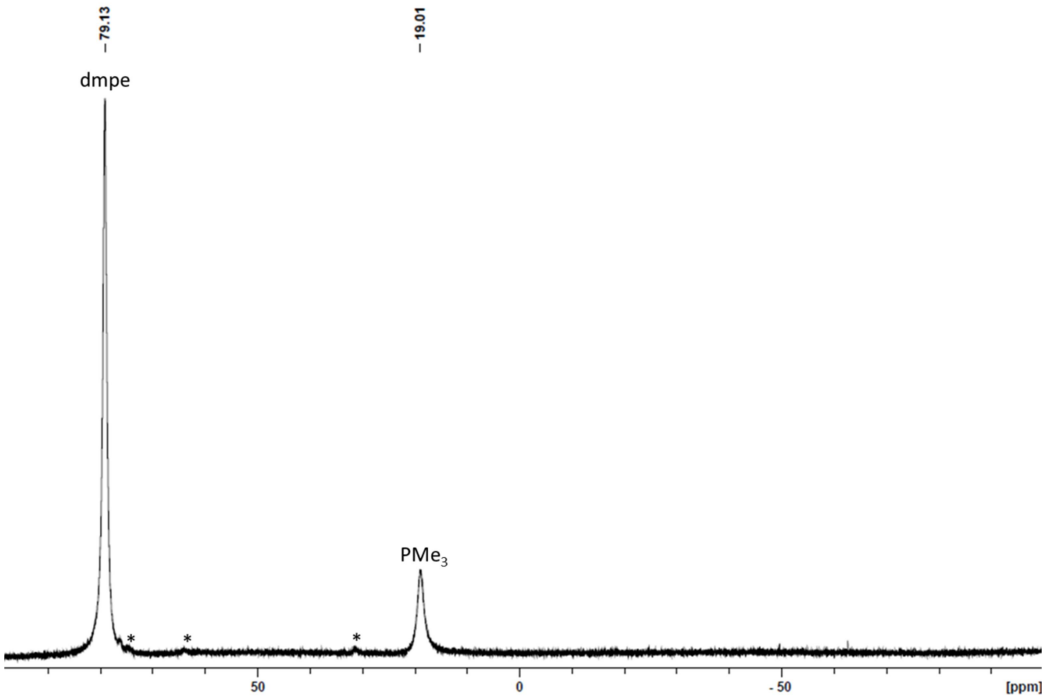

Figure S67. $^{31}P\{^{1}H\}$ NMR spectrum of *trans*-[(dmpe)$_2$MnH(PMe$_3$)] (***trans*-8**) in C_6D_6 (243 MHz, 298 K). * indicates peaks from an impurity of *cis*-[(dmpe)$_2$MnH(PMe$_3$)] (***cis*-8**).

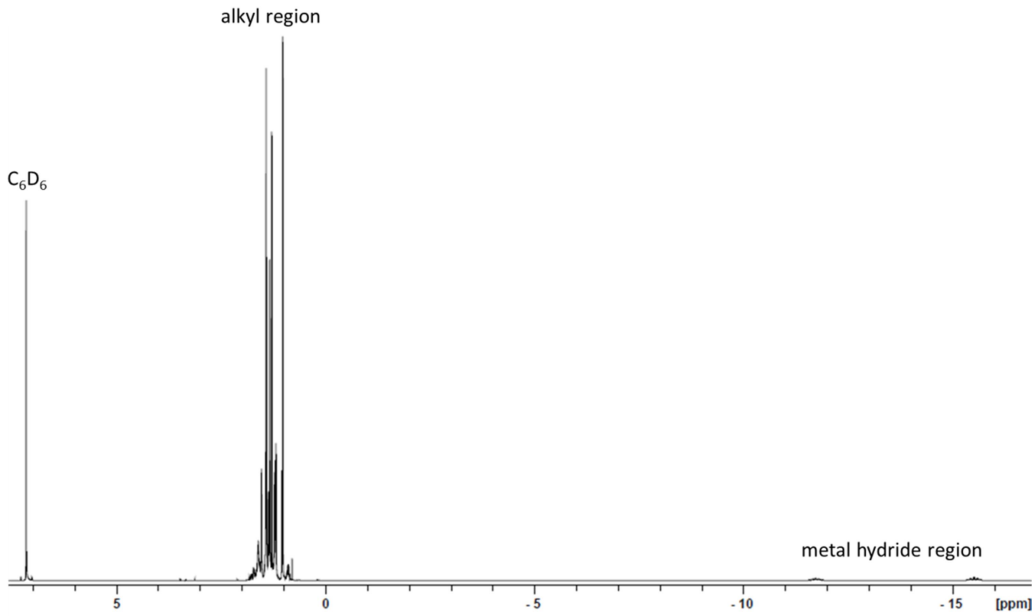

Figure S68. ^{1}H NMR spectrum of a solution containing *cis*-[(dmpe)$_2$MnH(PMe$_3$)] (***cis*-8**) generated from leaving a solution of *trans*-[(dmpe)$_2$MnH(PMe$_3$)] (***trans*-8**) in C_6D_6 at room temperature (mix of light and dark) for 11 days (600 MHz, 298 K).

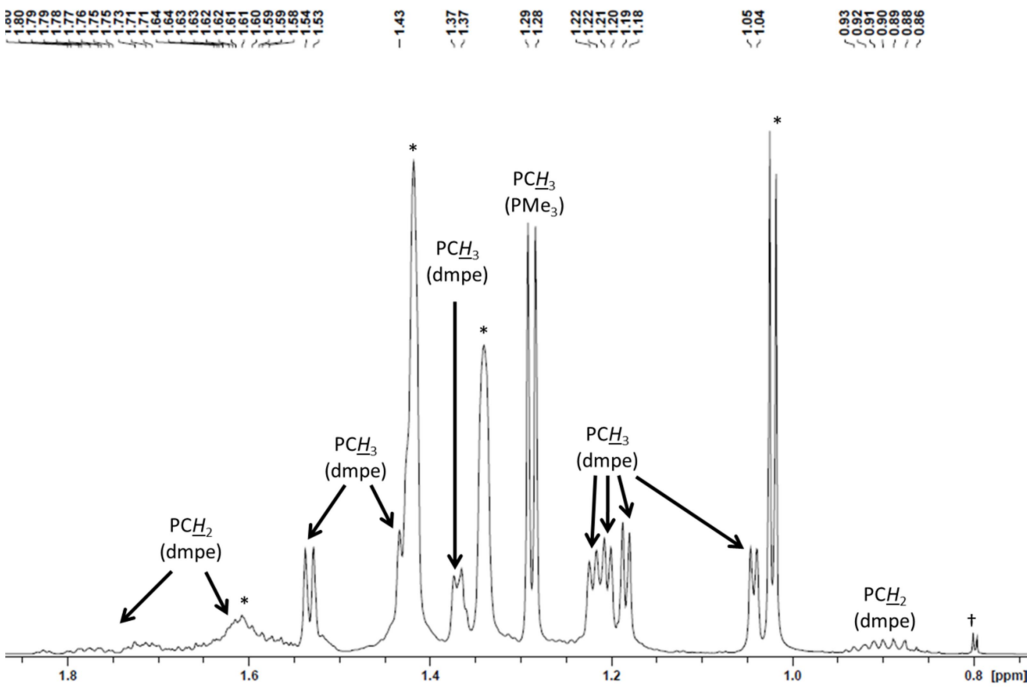

Figure S69. Expanded alkyl region of the ^{1}H NMR spectrum of a solution containing *cis*-[(dmpe)$_2$MnH(PMe$_3$)] (***cis*-8**) generated from leaving a solution of *trans*-[(dmpe)$_2$MnH(PMe$_3$)] (***trans*-8**) in C_6D_6 at room temperature (mix of light and dark) for 11 days (600 MHz, 298 K). * indicates peaks from ***trans*-8** and † indicates a peak from PMe$_3$.

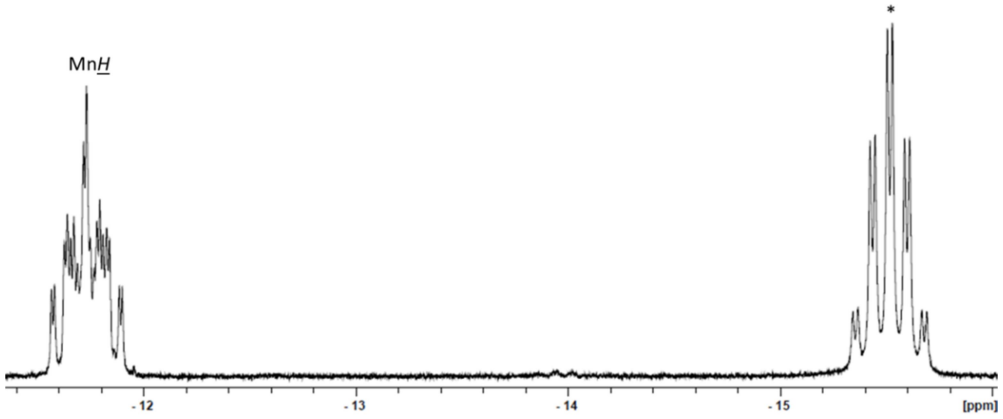

Figure S70. Expanded Mn$\underline{H}$ region of the ^{1}H NMR spectrum of a solution containing *cis*-[(dmpe)$_2$MnH(PMe$_3$)] (***cis*-8**) generated from leaving a solution of *trans*-[(dmpe)$_2$MnH(PMe$_3$)] (***trans*-8**) in C_6D_6 at room temperature (mix of light and dark) for 11 days (600 MHz, 298 K). * indicates a peak from ***trans*-8**.

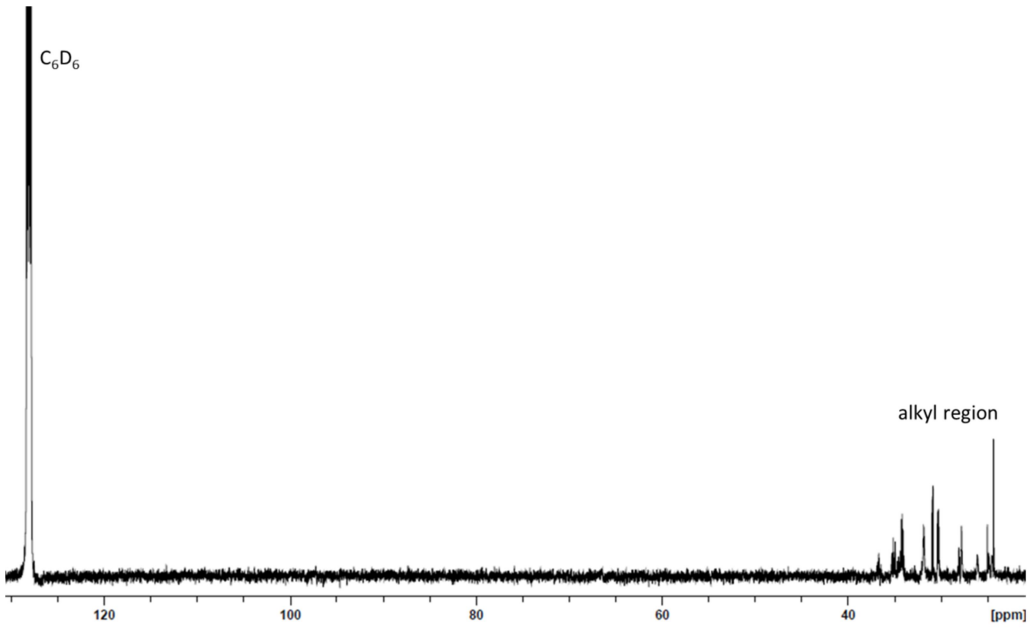

Figure S71. $^{13}C\{^{1}H\}$ NMR spectrum of a solution containing *cis*-[(dmpe)$_2$MnH(PMe$_3$)] (***cis*-8**) generated from leaving a solution of *trans*-[(dmpe)$_2$MnH(PMe$_3$)] (***trans*-8**) in C_6D_6 at room temperature (mix of light and dark) for 10 days (126 MHz, 298 K).

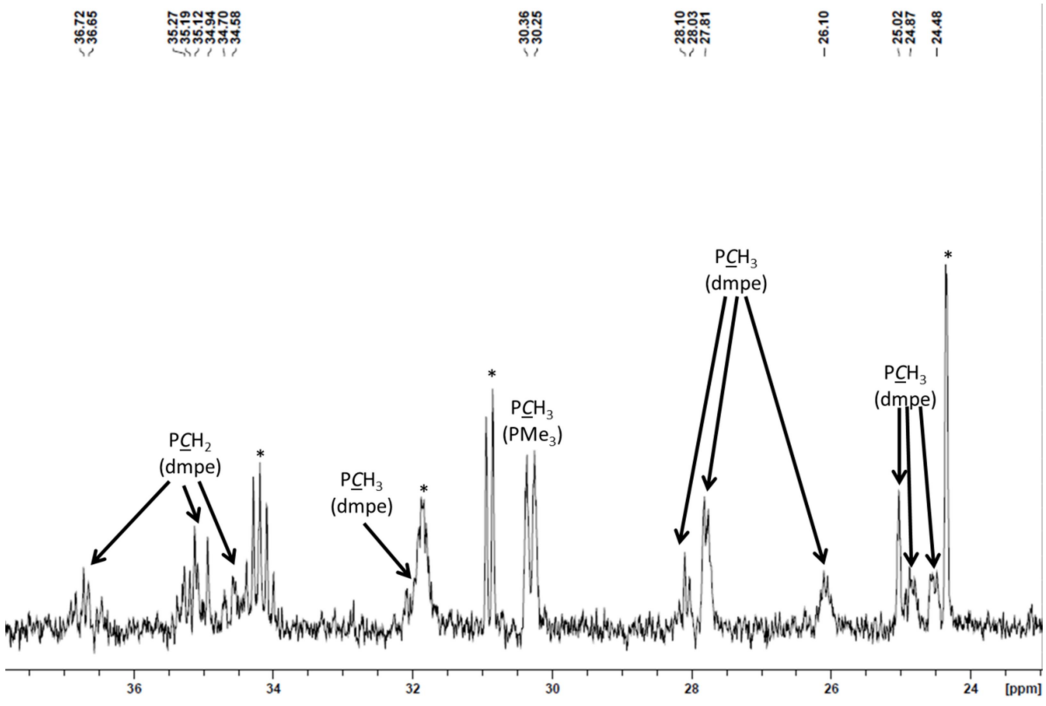

Figure S72. Expanded alkyl region of the $^{13}C\{^{1}H\}$ NMR spectrum of a solution containing *cis*-[(dmpe)$_2$MnH(PMe$_3$)] (***cis*-8**) generated from leaving a solution of *trans*-[(dmpe)$_2$MnH(PMe$_3$)] (***trans*-8**) in C_6D_6 at room temperature (mix of light and dark) for 10 days (126 MHz, 298 K). * indicates peaks from ***trans*-8**.

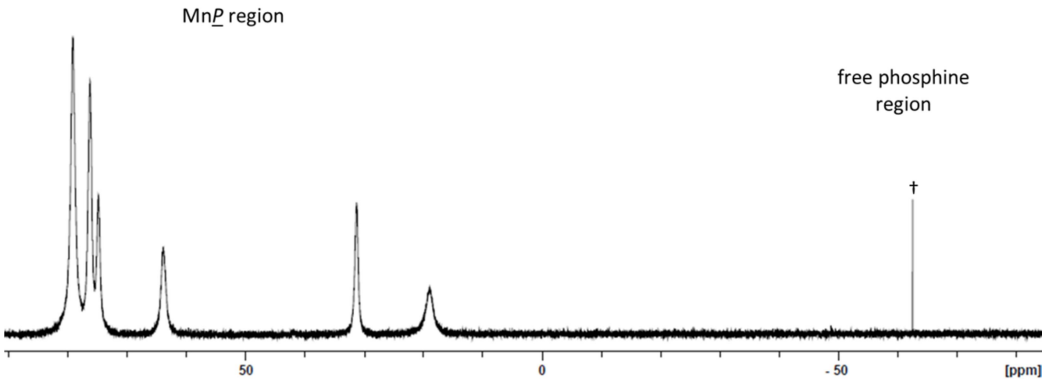

Figure S73. $^{31}P\{^{1}H\}$ NMR spectrum of a solution containing *cis*-[(dmpe)$_2$MnH(PMe$_3$)] (***cis*-8**) generated from leaving a solution of *trans*-[(dmpe)$_2$MnH(PMe$_3$)] (***trans*-8**) in C_6D_6 at room temperature (mix of light and dark) for 11 days (243 MHz, 298 K). † indicates a peaks from PMe$_3$.

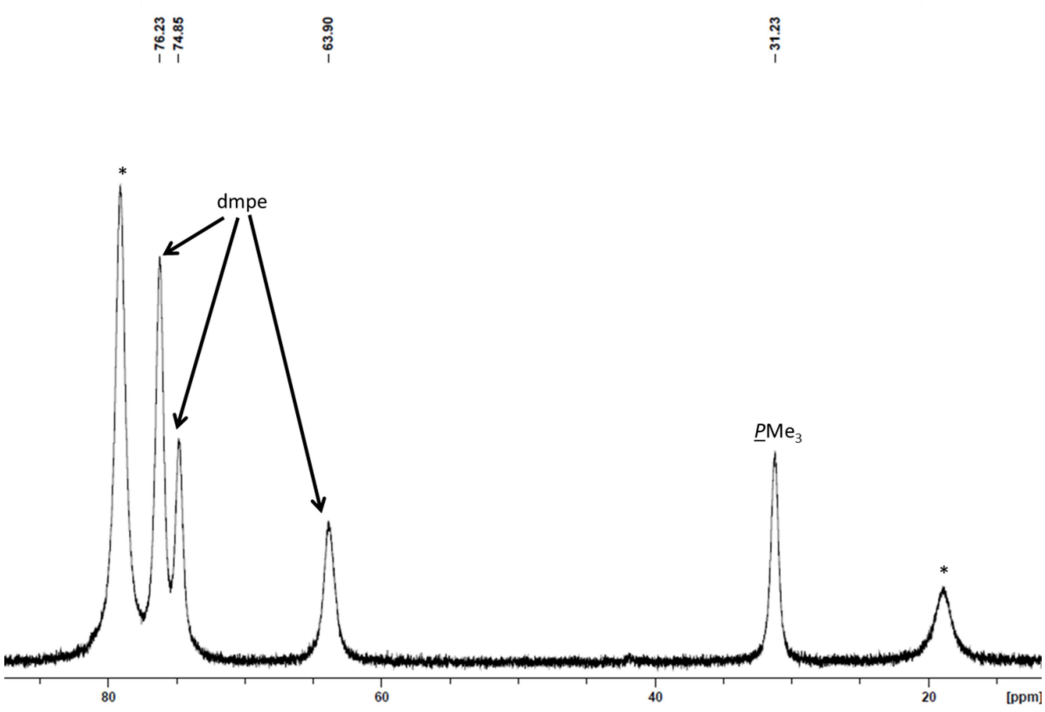

Figure S74. Expanded MnP region of the $^{31}P\{^{1}H\}$ NMR spectrum of a solution containing *cis*-[(dmpe)$_2$MnH(PMe$_3$)] (***cis*-8**) generated from leaving a solution of *trans*-[(dmpe)$_2$MnH(PMe$_3$)] (***trans*-8**) in C_6D_6 at room temperature (mix of light and dark) for 11 days (243 MHz, 298 K). * indicates peaks from ***trans*-8**.

Selected NMR Spectra for Deuteration of [(dmpe)$_2$Mn(μ-H)$_2$BH$_2$] (3)

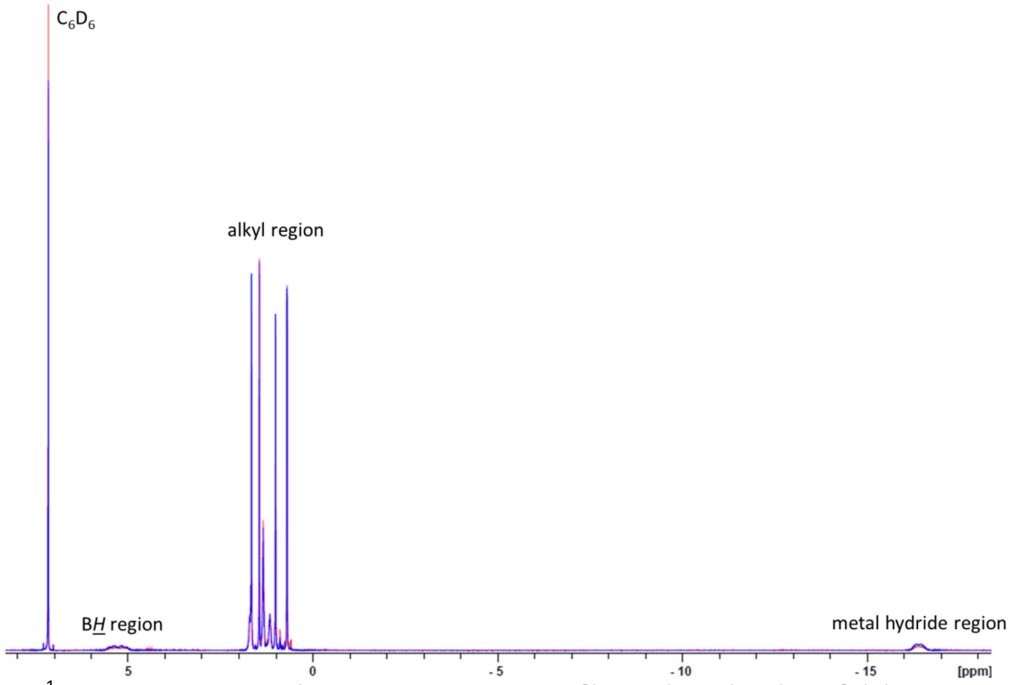

Figure S75. ^{1}H NMR spectrum of a solution containing [(dmpe)$_2$Mn(μ-H)$_2$BH$_2$] (**3**) and D_2 immediately (blue) and after 12 h at 90 °C (red) in C_6D_6 (600 MHz, 298 K).

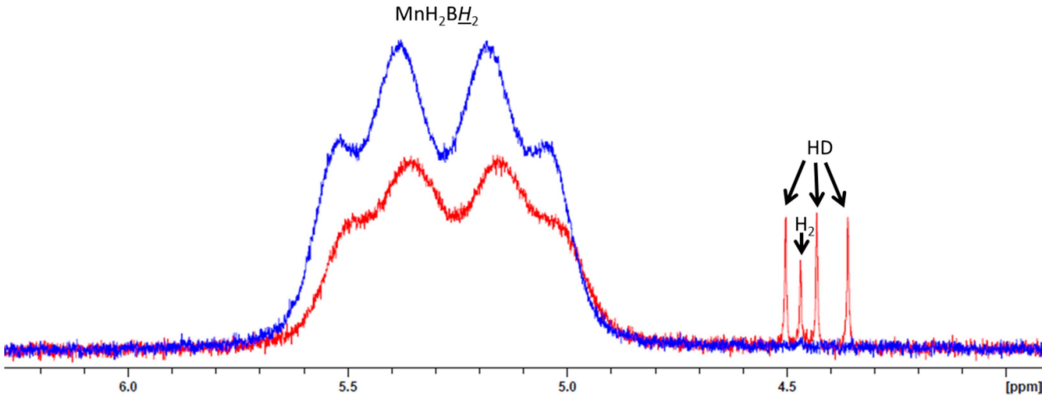

Figure S76. Expanded B*H* region of the ^{1}H NMR spectrum of a solution containing [(dmpe)$_2$Mn(μ-H)$_2$BH$_2$] (**3**) and D_2 immediately (blue) and after 12 h at 90 °C (red) in C_6D_6 (600 MHz, 298 K).

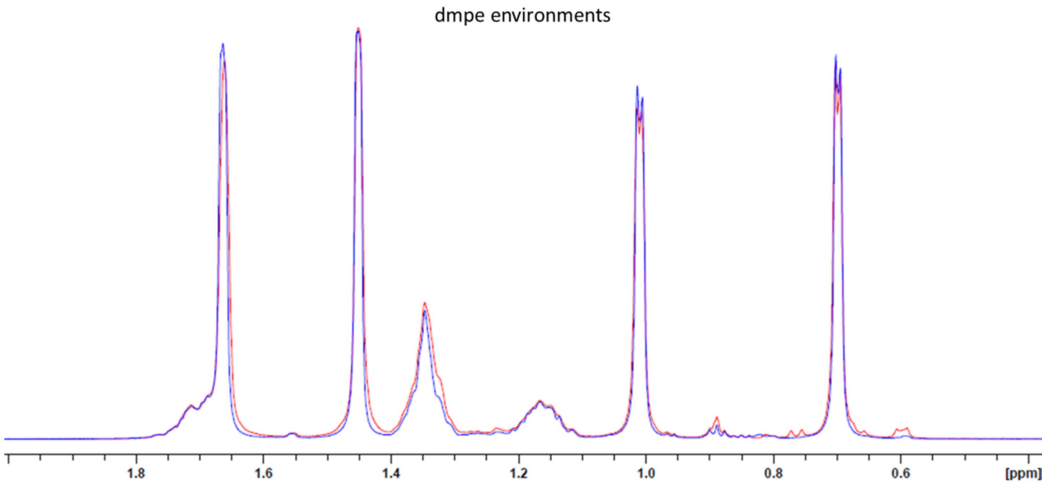

Figure S77. Expanded alkyl region of the ^{1}H NMR spectrum of a solution containing [(dmpe)$_2$Mn(μ-H)$_2$BH$_2$] (**3**) and D_2 immediately (blue) and after 12 h at 90 °C (red) in C_6D_6 (600 MHz, 298 K).

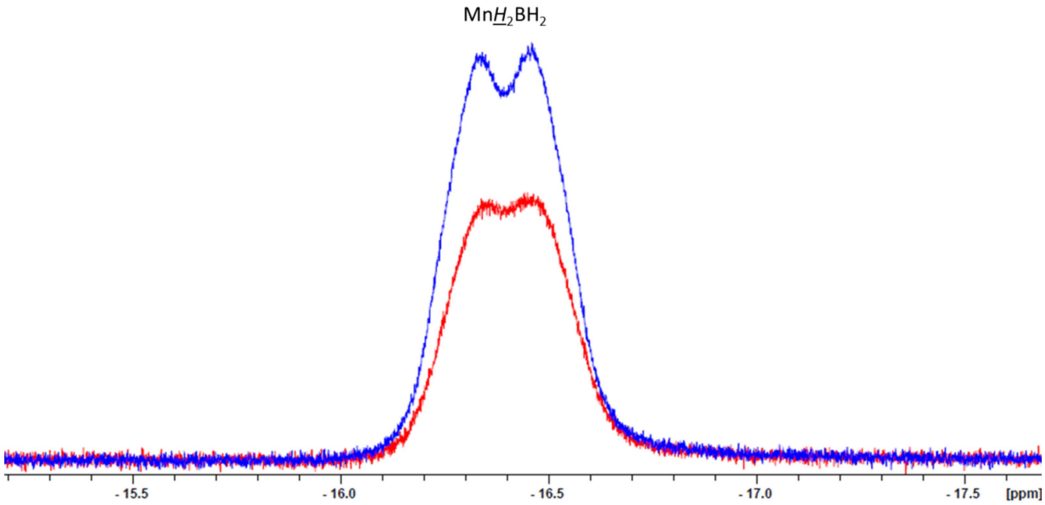

Figure S78. Expanded Mn$\underline{H}$ region of the ^{1}H NMR spectrum of a solution containing [(dmpe)$_2$Mn(μ-H)$_2$BH$_2$] (**3**) and D_2 immediately (blue) and after 12 h at 90 °C (red) in C_6D_6 (600 MHz, 298 K).

Experimental Details and Selected NMR Spectra of Intermediates in the Reactions of [(dmpe)$_2$MnH(C$_2$H$_4$)] (1) with 9-BBN or HBMes$_2$

Reactions to generate the intermediates in the synthesis of 4. a) 3.6 mg (0.030 mmol) of 9-BBN and 11.3 mg (0.029 mmol) of [(dmpe)$_2$MnH(C$_2$H$_4$)] (**1**) were dissolved in approx. 0.6 mL of C$_6$D$_6$ and the resulting mixture was left for 7 days at room temperature and analyzed *in situ* by NMR spectroscopy indicating a 1.3 : 1.0 : 2.1 ratio of **1** : **4** : intermediates. b) 6.5 mg (0.05 mmol) of 9-BBN and 10.3 mg (0.27 mmol) of [(dmpe)$_2$MnH(C$_2$H$_4$)] (**1**) were dissolved in approx. 0.6 mL of C$_6$D$_6$ and the resulting mixture was left for 3 days at room temperature and analyzed *in situ* by ^{1}H NMR spectroscopy indicating a 1.0 : 2.5 : 1.5 ratio of **1** : **4** : intermediates. A major (>95 %) and minor (<5 %) intermediate were both observed in solution. Selected NMR data for the major species: **^{1}H NMR (C$_6$D$_6$, 600 MHz, 298 K):** δ 2.68, 2.60, 2.05, 0.53, 0.31 (5 × m, 1H), 2.46 (m, 4H), –1.44 (br. s, 1H), –13.14 (br. s, 1H, Mn*H*). **^{11}B{^{1}H} NMR (C$_6$D$_6$, 192 MHz, 298 K):** δ –15.49 (s). **^{31}P{^{1}H} NMR (C$_6$D$_6$, 243 MHz, 298 K):** δ 85.83, 76.47, 64.94, 57.83 (4 × s, 1P). Selected NMR data for the minor species: **^{31}P{^{1}H} NMR (C$_6$D$_6$, 243 MHz, 298 K):** δ –5.64 (s).

Reactions to generate the intermediates in the synthesis of 5. 13.0 mg (0.052 mmol) of HBMes$_2$ and 10.0 mg (0.026 mmol) of [(dmpe)$_2$MnH(C$_2$H$_4$)] (**1**) were dissolved in approx. 0.6 mL of C$_6$D$_6$, and the resulting mixture was heated for 1.5 h at 60 °C. The resulting solution was analyzed *in situ* by NMR spectroscopy, indicating a 2.3 : 1.7 : 1.0 ratio of **1** : **5** : intermediates. A major (>95 %) and minor (<5 %) intermediate were both observed in solution. Selected NMR data for the major species: **^{1}H NMR (C$_6$D$_6$, 600 MHz, 298 K):** 4.12 (app. t, 2H, *J* 2.2 Hz), 1.96 (q, 2H, $^3J_{H,H}$ 7.1 Hz), –13.03 (t, 1H, $J_{H,P}$ 73.7 Hz, Mn*H*). **^{31}P{^{1}H} NMR (C$_6$D$_6$, 243 MHz, 298 K):** δ –4.01 (s). Selected NMR data for the minor species: **^{31}P{^{1}H} NMR (C$_6$D$_6$, 243 MHz, 298 K):** δ 73.27 (br. s).

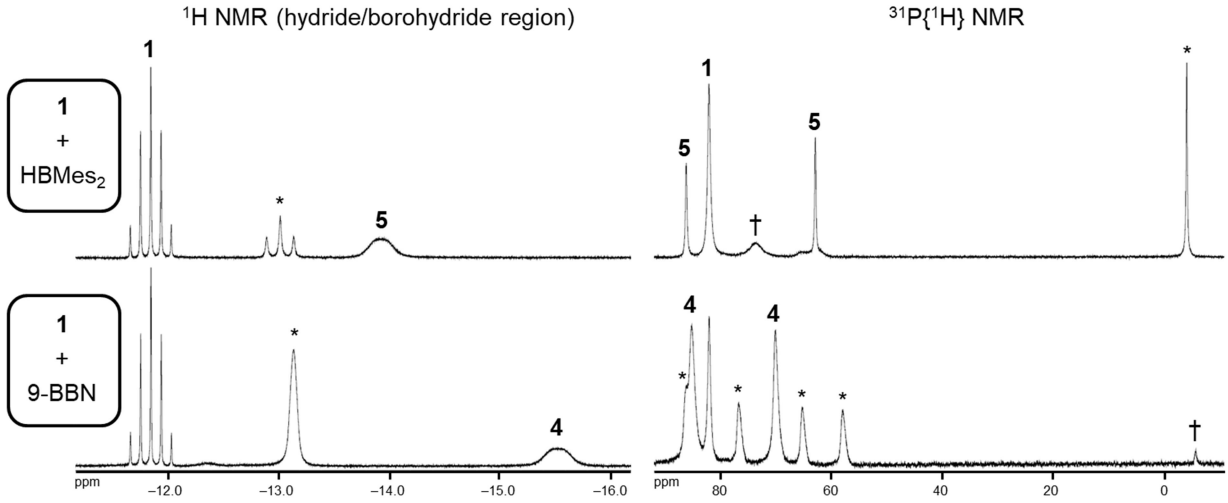

Figure S79. Left: (boro)hydride region of the ^{1}H NMR spectra, and right: ^{31}P{^{1}H} NMR spectra, for reactions of *trans*-[(dmpe)$_2$MnH(C$_2$H$_4$)] (**1**) with (bottom) 9-BBN or (top) HBMes$_2$ before completion. * = peaks attributed to the dominant intermediate isomer, and † = peaks attributed to the minor intermediate isomer. C$_6$D$_6$, 600 MHz, 298 K.

Experimental Details and Selected NMR Spectra of Solutions Generated by Hydroboration of Ethylene by HBR_2

Hydroboration of ethylene by 9-BBN and $HBMes_2$ (in order to determine whether this reaction will take place under the conditions used to synthesize **3** and **4**, and to allow conclusive identification of the reaction byproducts $EtBC_8H_{14}$ and $EtBMes_2$). (a) Approximately 10 mg of 9-BBN was dissolved in roughly 0.6 mL of C_6D_6. The reaction mixture was freeze/pump/thaw cycled in a J. Young NMR tube three times and then was placed under 1 atm of ethylene at –95 °C, sealed, and warmed to room temperature. 90 % conversion of HBC_8H_{14} to $EtBC_8H_{14}$ was observed by NMR spectroscopy after heating at 60 °C for 1 h, and the resulting solution of $EtBC_8H_{14}$ was analyzed by NMR spectroscopy *in situ*. **^{1}H NMR (C_6D_6, 600 MHz, 298 K):** δ 1.84 (m, 6H, $C_8\underline{H}_{14}$), 1.76 (br. s, 2H, $C_8\underline{H}_{14}$), 1.65 (m, 4H, $C_8\underline{H}_{14}$), 1.35 (q, 2H, $^3J_{H,H}$ 7.6 Hz, $C\underline{H}_2CH_3$), 1.17 (m, 2H, $C_8\underline{H}_{14}$) 1.08 (t, 3H, $^3J_{H,H}$ 7.6 Hz, $CH_2C\underline{H}_3$). **^{11}B{^{1}H} NMR (C_6D_6, 192 MHz, 298 K):** δ 87.41 (s). **^{13}C{^{1}H} NMR (C_6D_6, 151 MHz, 298 K):** δ 33.39, 23.63, 8.41 (3 × s), 31.13, 20.23 (2 × br. s). (b) Approximately 10 mg of $BHMes_2$ was dissolved in roughly 0.6 mL of C_6D_6. The reaction mixture was freeze/pump/thaw cycled in a J. Young NMR tube three times and then was placed under 1 atm of ethylene at –95 °C, sealed, and warmed to room temperature. 99 % conversion of $HBMes_2$ to $EtBMes_2$ was observed by NMR spectroscopy after heating at 60 °C for 1 h, and the resulting solution of $EtBMes_2$ was analyzed by NMR spectroscopy *in situ*. **^{1}H NMR (C_6D_6, 600 MHz, 298 K):** δ 6.74 (s, 4H, *m*), 2.23 (s, 12H, *o*-$C\underline{H}_3$), 2.15 (s, 6H, *p*-$C\underline{H}_3$), 1.93 (q, 2H, $^3J_{H,H}$ 7.5 Hz, $C\underline{H}_2CH_3$), 1.15 (t, 3H, $^3J_{H,H}$ 7.5 Hz, $CH_2C\underline{H}_3$). **^{11}B{^{1}H} NMR (C_6D_6, 192 MHz, 298 K):** δ 84.02 (br. s). **^{13}C{^{1}H} NMR (C_6D_6, 151 MHz, 298 K):** δ 139.13, 138.34, 128.98, 22.91, 21.18, 9.38 (6 × s), 26.55 (br. s).

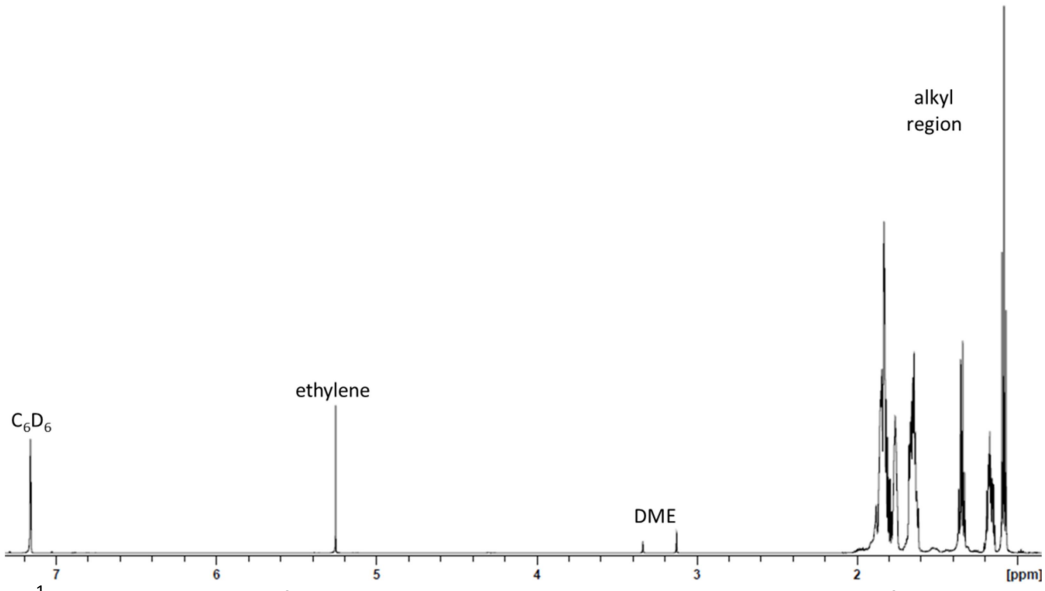

Figure S80. ^{1}H NMR spectrum of a solution containing $EtBC_8H_{14}$, observed *in situ* from the reaction of 9-BBN with ethylene for 1 h in C_6D_6 at 60 °C (600 MHz, 298 K).

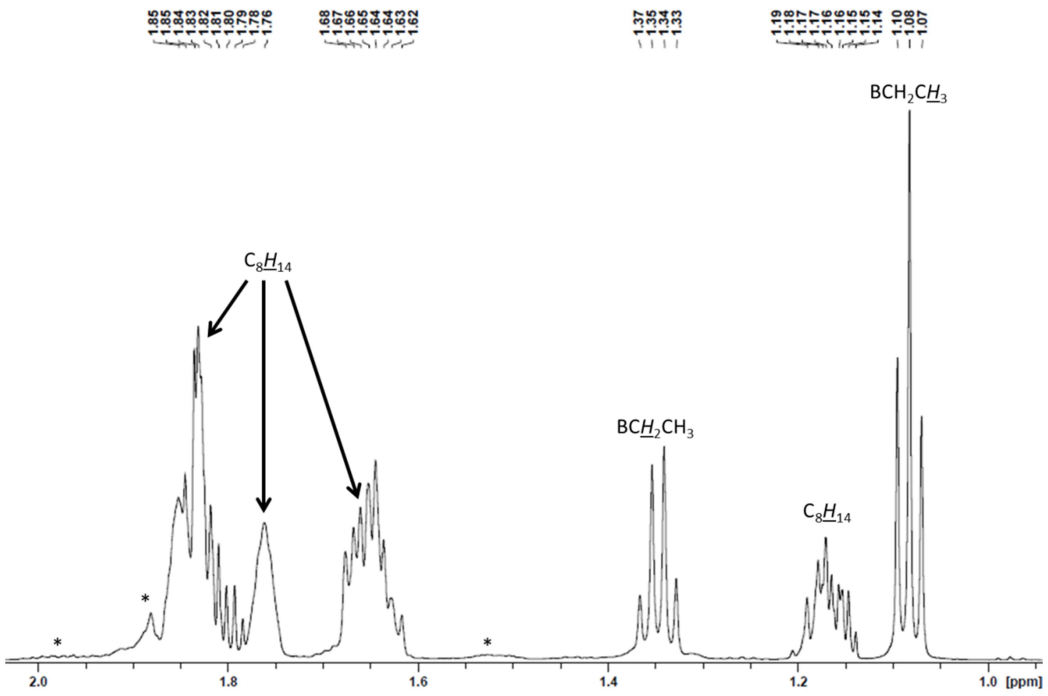

Figure S81. Expanded alkyl region of the ^{1}H NMR spectrum of a solution containing $EtBC_8H_{14}$, observed *in situ* from the reaction of 9-BBN ethylene for 1 h in C_6D_6 at 60 °C (600 MHz, 298 K). * indicates peaks from residual 9-BBN.

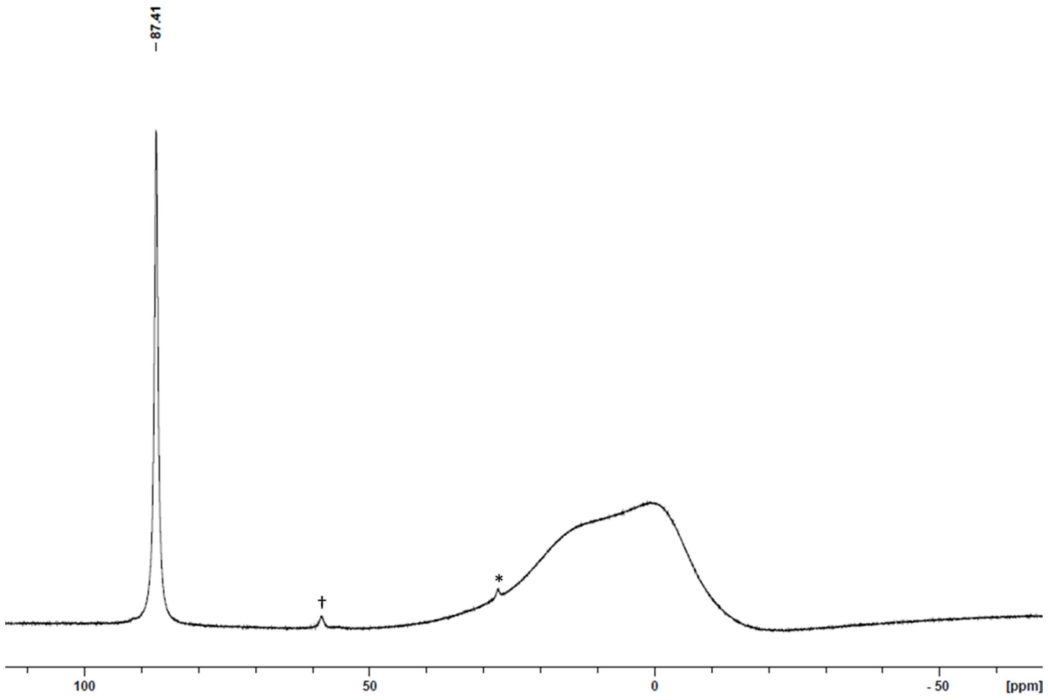

Figure S82. $^{11}B\{^{1}H\}$ NMR spectrum of a solution containing $EtBC_8H_{14}$, observed *in situ* from the reaction of 9-BBN with ethylene for 1 h in C_6D_6 at 60 °C (192 MHz, 298 K). * indicates a peak from residual 9-BBN, and † indicates a peak from an impurity present in the 9-BBN starting material.

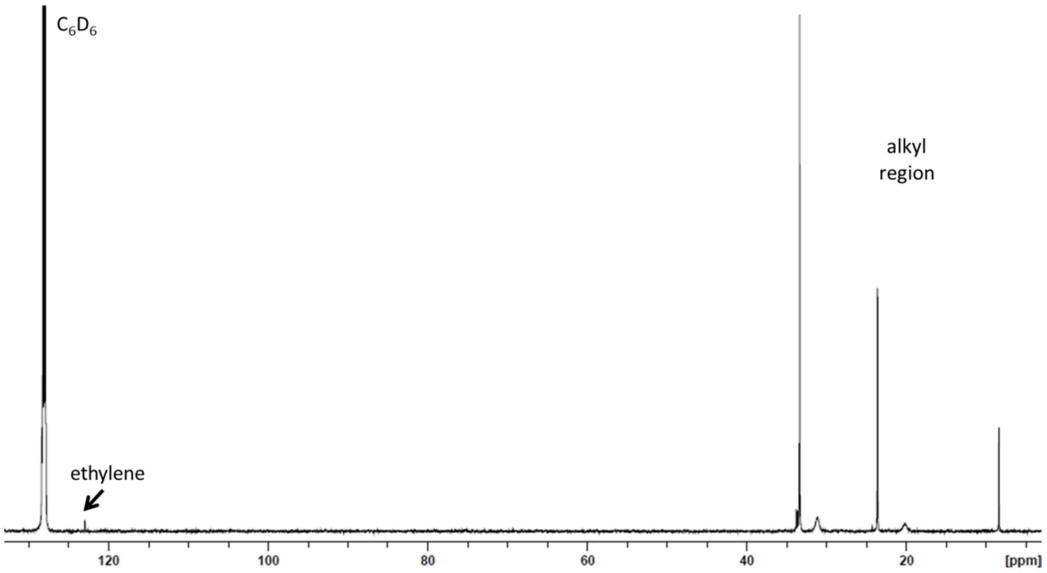

Figure S83. $^{13}C\{^{1}H\}$ NMR spectrum of a solution containing $EtBC_8H_{14}$, observed *in situ* from the reaction of 9-BBN with ethylene for 1 h in C_6D_6 at 60 °C (151 MHz, 298 K).

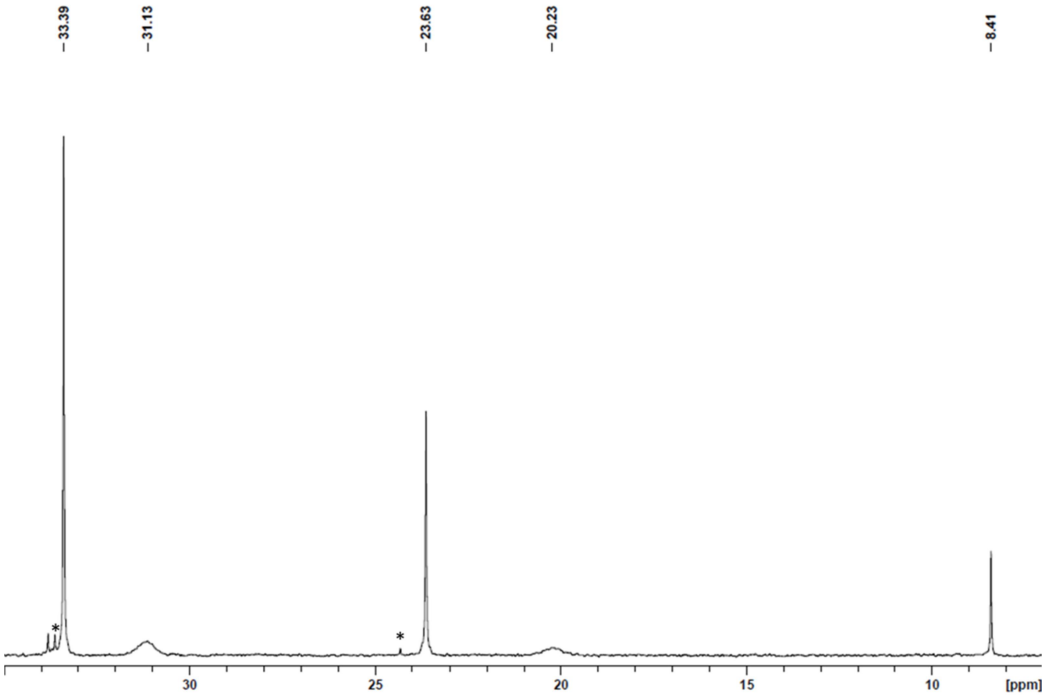

Figure S84. Expanded alkyl region of the $^{13}C\{^{1}H\}$ NMR spectrum of a solution containing $EtBC_8H_{14}$, observed *in situ* from the reaction of 9-BBN with ethylene for 1 h in C_6D_6 at 60 °C (151 MHz, 298 K). * indicates peaks from residual 9-BBN.

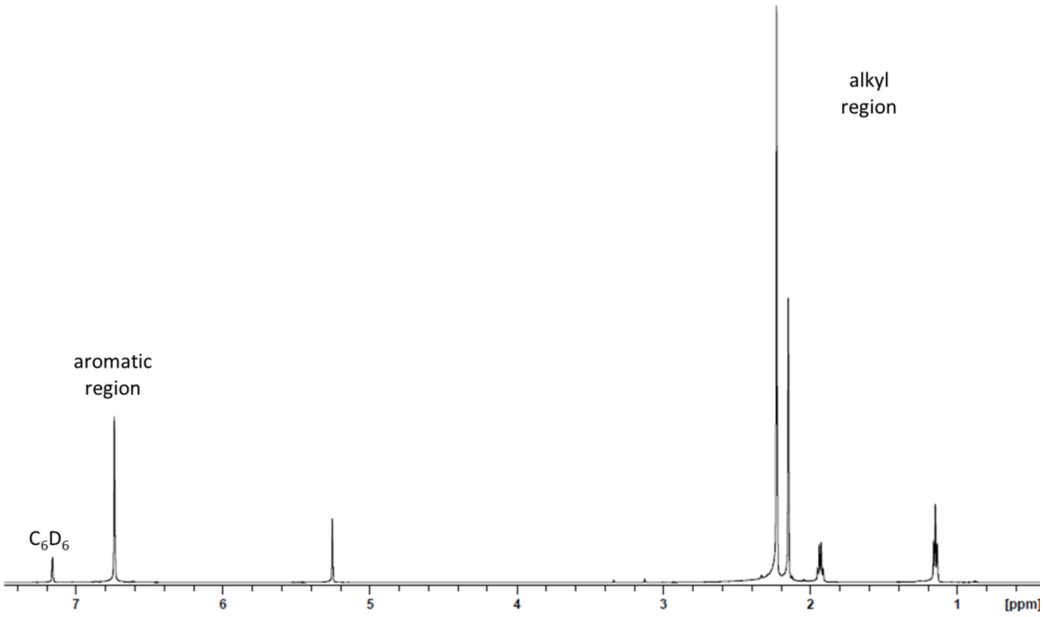

Figure S85. ^{1}H NMR spectrum of a solution containing $EtBMes_2$, observed *in situ* from the reaction of $HBMes_2$ with ethylene for 1 h in C_6D_6 at 60 °C (600 MHz, 298 K).

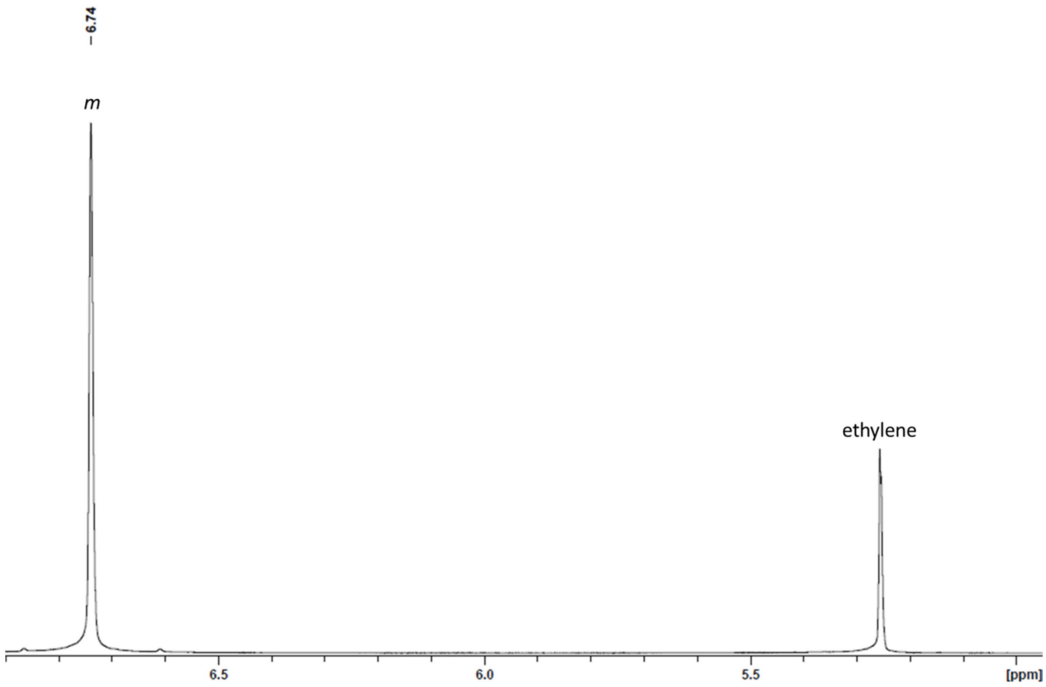

Figure S86. Expanded aromatic region of the ^{1}H NMR spectrum of a solution containing $EtBMes_2$, observed *in situ* from the reaction of $HBMes_2$ with ethylene for 1 h in C_6D_6 at 60 °C (600 MHz, 298 K).

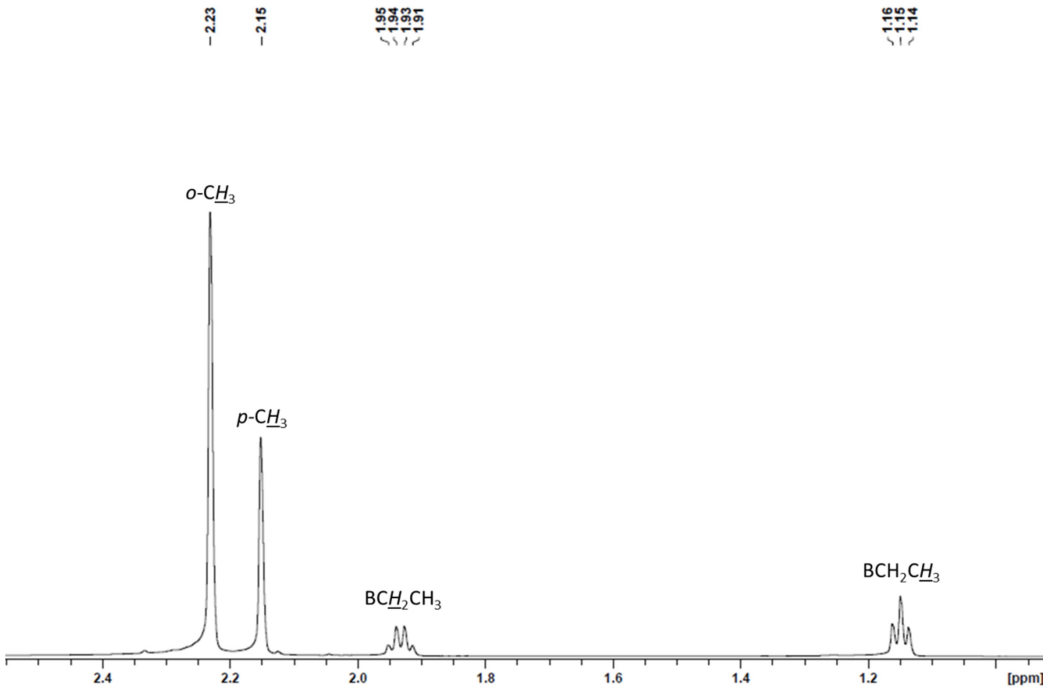

Figure S87. Expanded alkyl region of the ^{1}H NMR spectrum of a solution containing EtBMes$_2$, observed *in situ* from the reaction of HBMes$_2$ with ethylene for 1 h in C_6D_6 at 60 °C (600 MHz, 298 K).

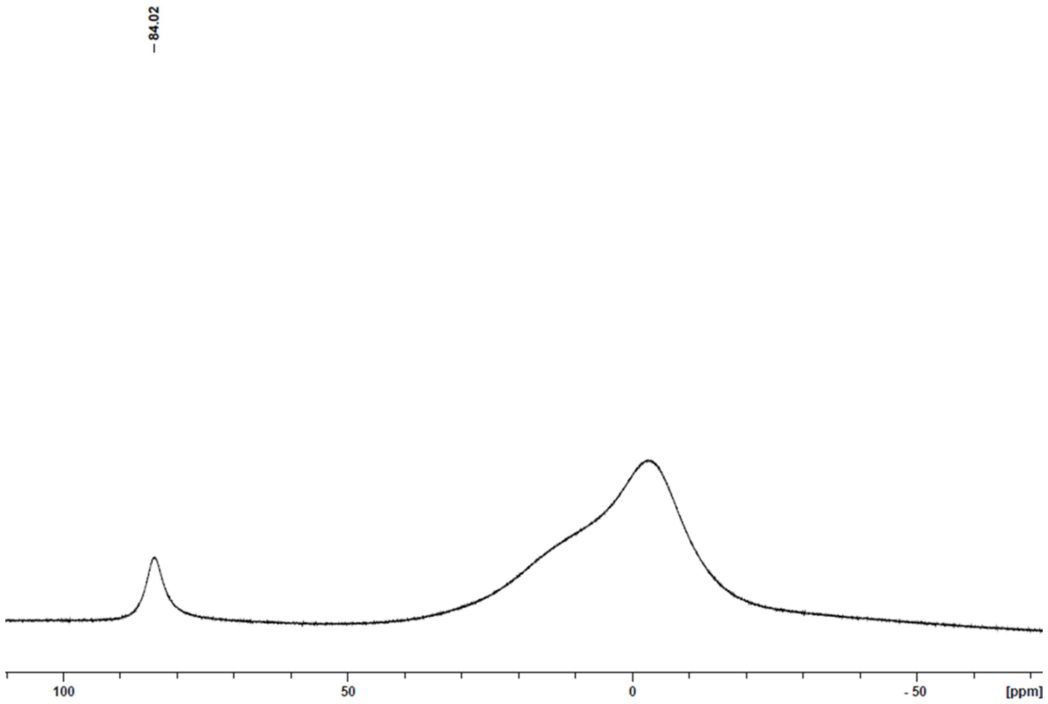

Figure S88. ^{11}B{^{1}H} NMR spectrum of a solution containing EtBMes$_2$, observed *in situ* from the reaction of HBMes$_2$ with ethylene for 1 h in C_6D_6 at 60 °C (192 MHz, 298 K).

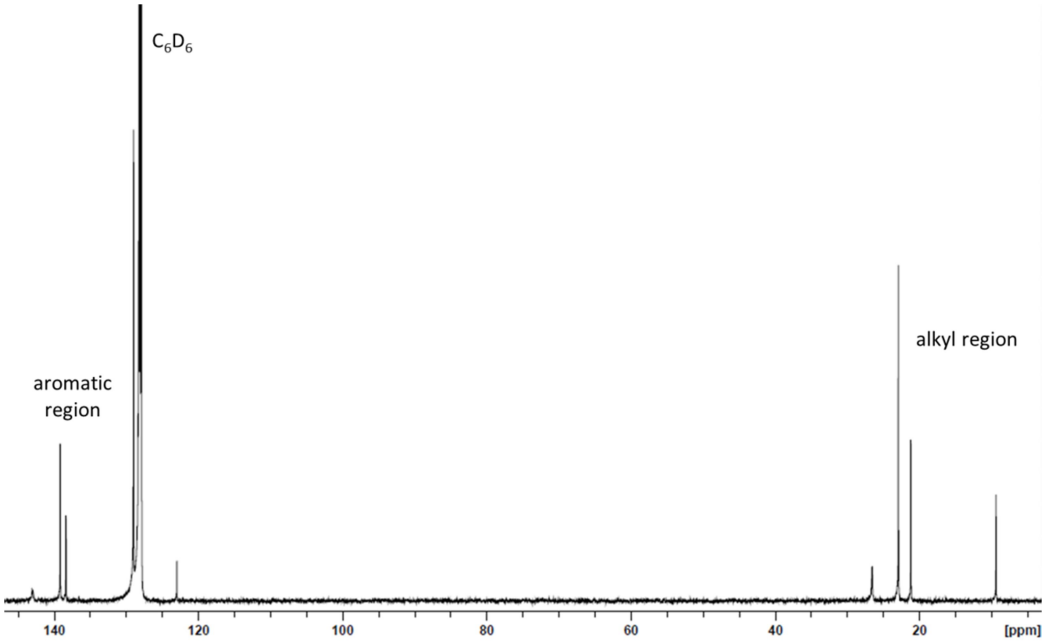

Figure S89. $^{13}C\{^{1}H\}$ NMR spectrum of a solution containing $EtBMes_2$, observed *in situ* from the reaction of $HBMes_2$ with ethylene for 1 h in C_6D_6 at 60 °C (151 MHz, 298 K).

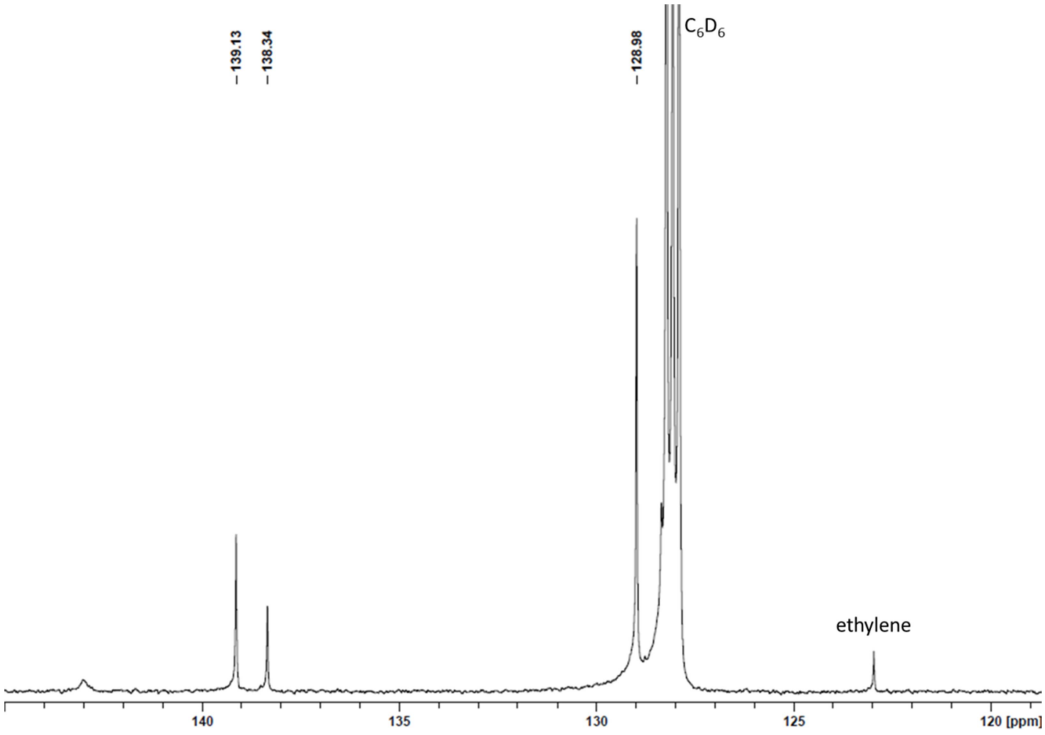

Figure S90. Expanded aromatic region of the $^{13}C\{^{1}H\}$ NMR spectrum of a solution containing $EtBMes_2$, observed *in situ* from the reaction of $HBMes_2$ with ethylene for 1 h in C_6D_6 at 60 °C (151 MHz, 298 K).

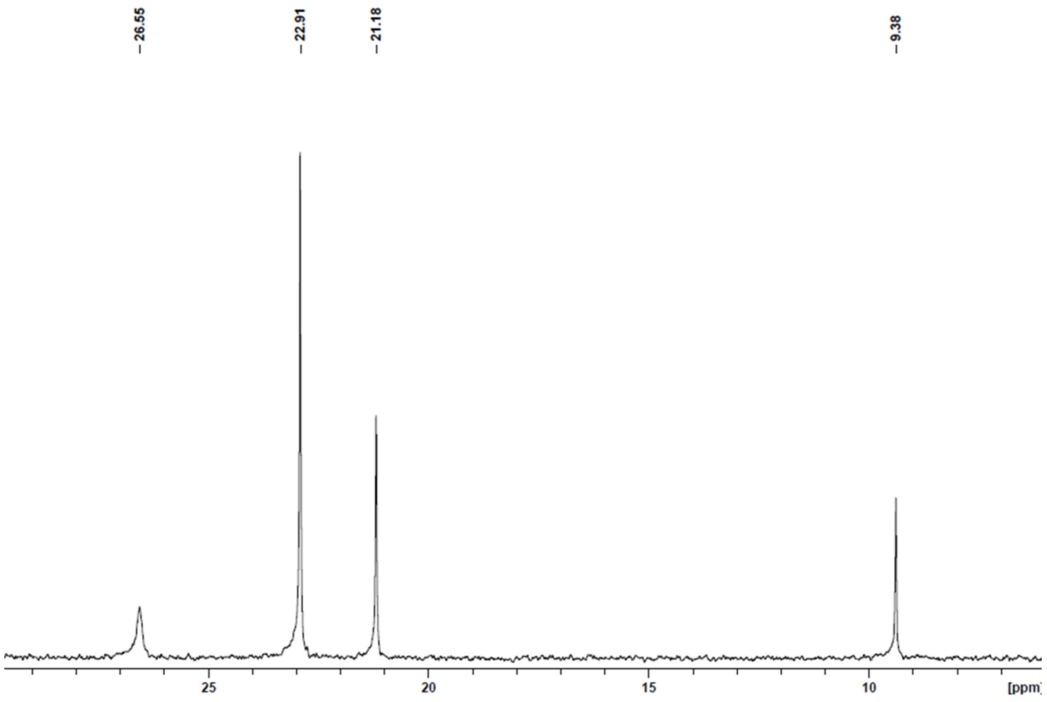

Figure S91. Expanded alkyl region of the $^{13}C\{^{1}H\}$ NMR spectrum of a solution containing $EtBMes_2$, observed *in situ* from the reaction of $HBMes_2$ with ethylene for 1 h in C_6D_6 at 60 °C (151 MHz, 298 K).

Selected NMR Spectra for Determining the Mechanism of the Reaction of [(dmpe)$_2$MnH(C$_2$H$_4$)] (1) with HBMes$_2$

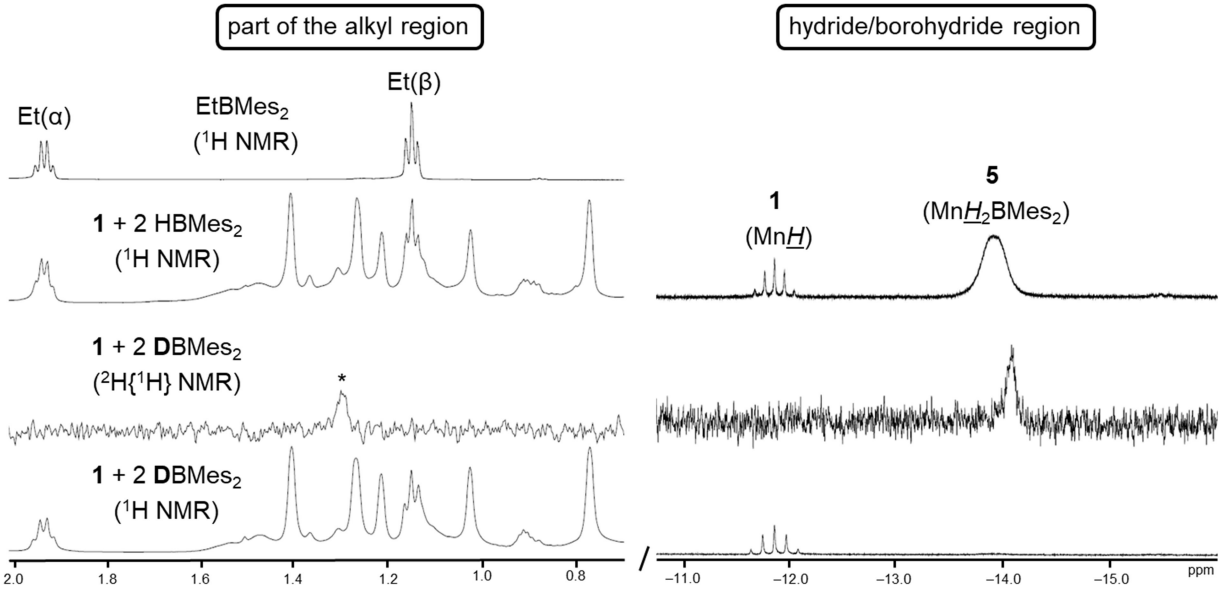

Figure S92. Regions of the ^{n}H NMR spectra (n = 1; 500 or 600 MHz, n= 2; 77 MHz) in C_6D_6 at 298 K containing the *Et*BMes$_2$ (left) and metal hydride/borohydride (right) environments for, from bottom to top, ^{1}H NMR for the reaction of 2 DBMes$_2$ with [(dmpe)$_2$MnH(C$_2$H$_4$)] (**1**) after heating overnight at 60 °C, ^{2}H NMR for the reaction of 2 DBMes$_2$ with **1** after heating overnight at 60 °C, ^{1}H NMR for the reaction of 2 HBMes$_2$ with **1** after heating overnight at 60 °C, and ^{1}H NMR for EtBMes$_2$. * is from an impurity in the C_6D_6 used. Spectra indicate that the products of the reaction of **1** with two equivalents of DBMes$_2$ are fully protonated EtBMes$_2$ and [(dmpe)$_2$Mn(μ-D)$_2$BMes$_2$] (***d*$_2$-5**).

References

1. (a) ADF2010, SCM, Theoretical Chemistry, Vrije Universiteit, Amsterdam, The Netherlands, http://www.scm.com; C. F. Guerra, J. G. Snijders, G. te Velde and E. J. Baerends, *Theor. Chem. Acc.*, 1998, **99**, 391-403; (b) G. te Velde, F. M. Bickelhaupt, E. J. Baerends, C. Fonseca Guerra, S. J. A. Van Gisbergen, J. G. Snijders and T. Ziegler, *J. Comput. Chem.*, 2001, **22**, 931-967.
2. J. P. Perdew, K. Burke and M. Ernzerhof, *Phys. Rev. Lett.*, 1996, **77**, 3865-3868.
3. (a) E. van Lenthe, E. J. Baerends and J. G. Snijders, *J. Chem. Phys.*, 1993, **99**, 4597-4610; (b) E. van Lenthe, E. J. Baerends and J. G. Snijders, *J. Chem. Phys.*, 1994, **101**, 9783-9792; (c) E. van Lenthe, J. G. Snijders and E. J. Baerends, *J. Chem. Phys.*, 1996, **105**, 6505-6516; (d) E. van Lenthe, R. van Leeuwen, E. J. Baerends and J. G. Snijders, *Int. J. Quantum Chem.*, 1996, **57**, 281-293; (e) E. van Lenthe, A. Ehlers and E. J. Baerends, *J. Chem. Phys.*, 1999, **110**, 8943-8953.
4. (a) S. Grimme, J. Antony, S. Ehrlich and H. Krieg, *J. Chem. Phys.*, 2010, **132**, 154104; (b) S. Grimme, S. Ehrlich and L. Goerigk, *J. Comput. Chem.*, 2011, **32**, 1456-1465.
5. (a) A. D. Becke, *J. Chem. Phys.*, 1988, **88**, 2547-2553; (b) M. Franchini, P. H. T. Philipsen and L. Visscher, *J. Comput. Chem.*, 2013, **34**, 1819-1827.
6. (a) A. Bérces, R. M. Dickson, L. Fan, H. Jacobsen, D. Swerhone and T. Ziegler, *Comput. Phys. Commun.*, 1997, **100**, 247-262; (b) H. Jacobsen, A. Bérces, D. P. Swerhone and T. Ziegler, *Comput. Phys. Commun.*, 1997, **100**, 263-276; (c) S. K. Wolff, *Int. J. Quantum Chem.*, 2005, **104**, 645-659.
7. The SCANFREQ command rescans a specific range of frequencies along a normal mode numerically as described in the ADF manual: https://www.scm.com/doc/ADF/Input/Frequencies.html#scanning-a-range-of-frequencies. Reference for numeric frequency calculations is as follows; L. Fan and T. Ziegler, *J. Chem. Phys.*, 1992, **96**, 9005-9012.
8. R. F. W. Bader, *Atoms in Molecules: A Quantum Theory*, Clarendon Press, Oxford, 1990.
9. (a) J. I. Rodríguez, R. F. W. Bader, P. W. Ayers, C. Michel, A. W. Götz and C. Bo, *Chem. Phys. Lett.*, 2009, **472**, 149-152; (b) J. I. Rodríguez, A. M. Köster, P. W. Ayers, A. Santos-Valle, A. Vela and G. Merino, *J. Comput. Chem.*, 2009, **30**, 1082-1092; (c) J. I. Rodríguez, *J. Comput. Chem.*, 2013, **34**, 681-686; (d) P. W. Ayers and S. Jenkins, *Computational and Theoretical Chemistry*, 2015, **1053**, 112-122; (e) V. Tognetti and L. Joubert, *Physical Chemistry Chemical Physics*, 2014, **16**, 14539-14550; (f) Y. A. Abramov, *Acta Crystallogr., Sect. A: Found. Crystallogr.*, 1997, **A53**, 264-272; (g) X. Fradera, M. A. Austen and R. F. W. Bader, *The Journal of Physical Chemistry A*, 1999, **103**, 304-314; (h) J. Poater, M. Solà, M. Duran and X. Fradera, *Theoretical Chemistry Accounts*, 2002, **107**, 362-371.